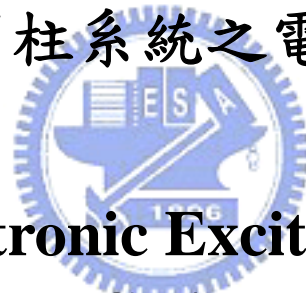


國立交通大學

電子工程學系電子研究所

博士論文

平面及圓柱系統之電子激發效應



**Electronic Excitations in
Planar and Cylindrical Systems**

研究生：杜宇軒 Yu-Hsuan Tu

指導教授：桂正楣 Cheng-May Kwei

中華民國九十五年六月

平面及圓柱系統之電子激發效應
Electronic Excitations in Planar and Cylindrical Systems

研究生：杜宇軒

Student: Yu-Hsuan Tu

指導教授：桂正楣

Advisor: Cheng-May Kwei

國立交通大學
電子工程學系電子研究所
博士論文



**A Dissertation
Submitted to
Department of Electronics Engineering & Institute of Electronics
College of Electrical and Computer Engineering
National Chiao Tung University
In Partial Fulfillment of the Requirements
For the Degree of
Doctor of Philosophy
In
Electronics Engineering**

**June 2006
Hsinchu, Taiwan, Republic of China**

中華民國 九十五年 六月

平面及圓柱系統之電子激發效應

研究生：杜宇軒

指導教授：桂正楣

國立交通大學電子工程學系電子研究所

摘要

本論文在探討運動之帶電粒子與固體間的非彈性交互作用，研究相關的理論模式，針對電子激發所產生的效應加以模擬與分析。

當帶電粒子在靠近固體表面移動時，其所產生的電子激發效應，對表面靈敏性散射能譜有很大的影響。根據電磁介電理論，這些激發效應可以用物質的介電函式來描述。在本論文中，所採用的是延伸式德魯特介電函式，在此函式中的所有參數是由實驗所量測到的光學數據及電子能量損失能譜來決定的。除此之外，建立介電函式時也考慮總和率的限制來確保精確性，並檢驗在能帶躍遷關鍵點之能量轉移及集體激發之電漿子能量以確認無誤。

在平面系統的電子激發效應方面，本研究推導之電子微分倒數非彈性平均自由行徑及非彈性平均自由行徑模式，可以適用在以任意入射角或出射角穿越固體表面並且離穿越點任意距離之電子。體及表面激發效應對於非彈性散射截面貢獻

甚大，體激發效應只在固體裡面發生，而表面激發效應則會在靠近固體表面的兩側發生。由於在固體內部的表面激發效應和體激發效應會互相抵消，所以在真空中之表面激發效應就變得格外重要，而此真空部分之表面電漿子總激發機率通常以表面激發參數來描述。本研究主要探討當電子穿越 III-V 半導體固體表面的表面激發參數，其與穿越角、電子能量之關係。結果顯示，表面激發參數滿足一個簡單的算式。更進一步地，本研究也建立了非彈性交互作用的記憶效應模式，此一記憶效應詮釋了前次的非彈性交互作用會影響到下次的非彈性交互作用之現象。對於帶電粒子沿固體表面平行移動時，其感生電位、阻擋本領、微分倒數非彈性平均自由行徑和非彈性平均自由行徑之模式均被建構，研究顯示對某特定粒子能量，其考慮記憶效應的結果會座落在不考慮記憶效應之此粒子能量及上次非彈性作用前粒子能量的結果之間，而記憶效應會隨前次非彈性交互作用能量損失增加而變大。

在圓柱系統的電子激發效應方面，本研究推導出可以適用在平行於一般或鍍層圓柱結構之軸運動的電子和系統間的非彈性交互作用之模式。利用電磁介電理論，微分倒數非彈性平均自由行徑及倒數非彈性平均自由行徑的模式均被推導，且被應用在矽圓柱、矽空腔、矽圓柱管、長有二氧化矽膜之矽圓柱…等情況。結果顯示，表面激發效應會在表面兩側發生，而體激發效應只會在固體內部發生。且靠近表面時，表面激發效應會增加而體激發效應會減少，而能互補抵消。對於矽空腔來說，除了在極靠近表面的地方以外，其他地方的倒數非彈性平均自由行

徑幾乎是固定值，大概等於無限大矽塊材之倒數非彈性平均自由行徑。對於長有二氧化矽膜之矽圓柱來說，非彈性交互作用則包含了體、表面和介面激發效應。而這些激發效應與電子跟表面或介面之距離、矽圓柱之半徑、二氧化矽膜之厚度…等有關。



ELECTRONIC EXCITATIONS IN PLANAR AND CYLINDRICAL SYSTEMS

Student : Yu-Hsuan Tu

Advisor : Cheng-May Kwei

**Department of Electronics Engineering and Institute of Electronics
National Chiao Tung University**

ABSTRACT



In this dissertation, the models dealing with the inelastic interactions between a charged particle and a solid were developed. Based on inelastic-scattering models, simulations and analyses of electronic excitations were made.

The electronic excitations produced by a charged particle moving near a solid surface play a crucial role in surface-sensitive spectroscopies. By the use of the dielectric response theory, these excitations can be described in terms of the dielectric functions of the materials. The dielectric functions employed in this dissertation were the extended Drude dielectric functions. All parameters in such function were determined by fits to the corresponding experimental optical data and electron

energy-loss spectra. In addition, this function was constrained by sum-rules to assure the accuracy and examined to confirm critical-point energies in the interband transitions and plasmon energies in the collective excitations.

In the work for the electronic excitations in planar systems, theoretical derivations of the differential inverse inelastic mean free path (DIIMFP) and inelastic mean free path (IMFP) for electrons crossing solid surfaces were made for different crossing angles and electron distances relative to the crossing point at the surface. Such inelastic cross-sections comprise mainly the contributions from volume and surface excitations. Volume and surface excitations occur when electrons travel, respectively, inside the bulk of the material and near the surface inside or outside the solid. Due to the rough compensation of surface and volume excitations inside the solid, one may pay attention to surface excitations in vacuum. The surface excitation parameters (SEPs) which describe the total probabilities of surface plasmon excitations by electrons traveling in vacuum before impinging on or after escaping from several semiconducting III-V compounds have also been calculated for electrons crossing the compound surfaces with various crossing angles and with various energies. The SEPs were then found to follow to a simple formula. Moreover, the model accounting for the memory effect, which describes the influence of the previous inelastic interaction on the succeeding inelastic interaction, of a charge

particle between two successive inelastic interactions was established. Formulas of the induced potential, stopping power, DIIMFP and IMFP considering the memory effect were derived for a charged particle moving parallel to a solid surface. It was found that those with the memory effect for energy E lay between the corresponding values without the memory effect for energy E and previous energy E_0 . The memory effect increased with increasing energy loss, $E_0 - E$, in the previous inelastic interaction.

In the work for the electronic excitations in cylindrical systems, the theories were developed to deal with inelastic interactions for an electron moving parallel to the axis of a cylindrical structure and a clad cylindrical structure. Formulas for the DIIMFP and inverse IMFP (IIMFP) were derived using dielectric response theory. The DIIMFPs and IIMFPs were calculated for a Si wire, a cavity in Si, a Si cylindrical tube, or a Si cylinder clad in a SiO₂ film. The calculated results showed that surface excitations occurred as the electron moved near the boundary either inside or outside the solid, whereas volume excitations arose only for electron moving inside the solid. It was found that the probability for surface excitations increases and that for volume excitations decreases for an electron moving close to the surface. Near the surface, the decrease in volume excitations is compensated by the increase in surface excitations. For a cavity in Si, the IIMFP inside the solid can be approximated by a

constant value equal to the IIMFP for the infinite Si, except in the immediate vicinity of the cavity boundary. For the Si cylinder clad in the SiO₂ film, inelastic interactions were contributed from volume, surface and interface excitations. Calculated results showed that the relative importance of these excitations depended on the electron distance from the surface or interface of the cylindrical system, the radius of the Si cylinder, and the thickness of the SiO₂ film.

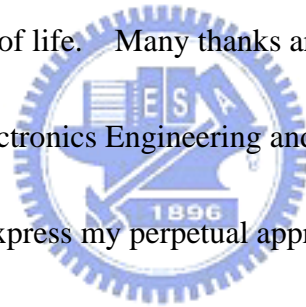


ACKNOWLEDGEMENTS

I would like to express my sincere gratitude to my advisor, Prof. C. M. Kwei, for her guidance and encouragement during the course of the study. I would also like to appreciate Prof. C. J. Tung for his invaluable comments and suggestions. In addition, this dissertation has benefited from the contributions of the members working in Solid State Physics Laboratory. Special thanks are given to them.

From my undergraduate to graduate study, many professors have influenced and encouraged me in philosophy of life. Many thanks are devoted here to all the teachers of Department of Electronics Engineering and Institute of Electronics.

Finally, I would like to express my perpetual appreciations to my family. Their love is always the most important support for me. This dissertation is dedicated to them.



CONTENTS

ABSTARCT (CHINESE)	i
ABSTARCT (ENGLISH)	iv
ACKNOWLEDGEMENTS	viii
CONTENTS	ix
TABLE CAPTIONS	xiii
FIGURE CAPTIONS	xiv
CHAPTER 1 INTRODUCTION	1
1.1 Dielectric Function	1
1.2 Electronic Excitations in Planar Systems	2
1.3 Electronic Excitations in Cylindrical Systems	5
CHAPTER 2 DIELECTRIC FUNCTION	8
2.1 Drude Dielectric Function	8
2.2 Extended Drude Dielectric Function	10
2.3 Optical Data	12
2.4 Parameters in Extended Drude Dielectric Function	14



CHAPTER 3 ELECTRONIC EXCITATIONS IN PLANAR SYSTEMS 20

3.1 Inelastic Interactions of Electrons with Planar Systems 20

3.1.1 Induced Potential 22

3.1.2 Differential Inverse Inelastic Mean Free Path 25

3.1.2.1 Electrons Moving from Solid to Vacuum 25

3.1.2.2 Electrons Moving from Vacuum to Solid 27

3.1.3 Surface Excitation Parameter 27

3.2 Memory Effect 36

3.2.1 Induced Potential 36

3.2.2 Stopping Power 48

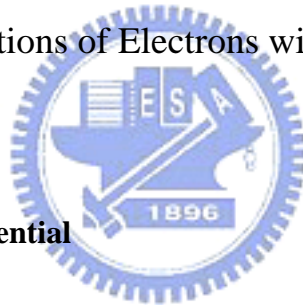
3.2.3 Differential Inverse Inelastic Mean Free Path 52

3.2.4 Inelastic Mean Free Path 56

CHAPTER 4 ELECTRONIC EXCITATIONS IN CYLINDRICAL SYSTEMS 59

4.1 Inelastic Interactions of Electrons with Cylindrical Systems 59

4.1.1	Induced Potential	60
4.1.1.1	Case I. Electrons Moving in Medium 1 (i.e. $\rho_0 < a$)	62
4.1.1.2	Case II. Electrons Moving in Medium 2 (i.e. $\rho_0 > a$)	63
4.1.2	Stopping Power	64
4.1.2.1	Case I. Electrons Moving in Medium 1 (i.e. $\rho_0 < a$)	64
4.1.2.2	Case II. Electrons Moving in Medium 2 (i.e. $\rho_0 > a$)	65
4.1.3	Differential Inverse Inelastic Mean Free Path	66
4.1.4	Inverse Inelastic Mean Free Path	72
4.2	Inelastic Interactions of Electrons with Clad Cylindrical Systems	75
4.2.1	Induced Potential	75
4.2.1.1	Case I. Electrons Moving in Medium 1 (i.e. $\rho_0 < a$)	78
4.2.1.2	Case II. Electrons Moving in Medium 2 (i.e. $a < \rho_0 < b$)	80
4.2.1.3	Case III. Electrons Moving in Medium 3 (i.e. $\rho_0 > b$)	82
4.2.2	Stopping Power	83
4.2.2.1	Case I. Electrons Moving in Medium 1 (i.e. $\rho_0 < a$)	83
4.2.2.2	Case II. Electrons Moving in Medium 2 (i.e. $a < \rho_0 < b$)	84
4.2.2.3	Case III. Electrons Moving in Medium 3 (i.e. $\rho_0 > b$)	84
4.2.2.4	Limiting Cases	85



4.2.3 Differential Inverse Inelastic Mean Free Path	85
CHAPTER 5 SUMMARY	95
REFENENCES	97
VITA	101
PUBLICATION LIST	102



TABLE CAPTIONS

CHAPTER 2

Table 2.1 Parameters in the dielectric function of Eq. (2.8) for semiconducting III-V compounds.

CHAPTER 3

Table 3.1 Fitted values of parameters a , b and c in Eq. (3.15) for semiconducting III-V compounds.



FIGURE CAPTIONS

CHAPTER 2

Fig. 2.1 A plot of the dielectric functions, $\epsilon_R(0, \omega)$, $\epsilon_I(0, \omega)$, $\text{Im}[-1/\epsilon(0, \omega)]$ and $\text{Im}[-1/(\epsilon(0, \omega)+1)]$, for GaN. Solid curves are results of the present work. The experimental data (Brockett 2000) (dotted curves) are also plotted for comparison.

Fig. 2.2 A plot of the dielectric functions, $\epsilon_R(0, \omega)$, $\epsilon_I(0, \omega)$, $\text{Im}[-1/\epsilon(0, \omega)]$ and $\text{Im}[-1/(\epsilon(0, \omega)+1)]$, for InSb. Solid curves are results of the present work. Other calculated results (Kwei 1986) (dotted curves) and the experimental data (Festenberg 1969; Palik 1985) (dashed curves) are also plotted for comparison.

CHAPTER 3

Fig. 3.1 A sketch of the problem studied in this work. An electron of velocity \vec{v} moves across the interface at time $t = 0$ from medium 1 of dielectric function $\epsilon_1(\vec{k}, \omega)$ to medium 2 of dielectric function $\epsilon_2(\vec{k}, \omega)$ with crossing angle α . The instant position of the electron is $\vec{r} = \vec{v}t$, relative to the crossing point at interface.

Fig. 3.2 A plot of crossing-angle-dependent SEPs for 800 eV electrons moving from GaAs to vacuum. Solid circles are the results calculated using Eq. (3.12). The solid and dashed curves are, respectively, a fit of the calculated results using Eq. (3.15) and the previous work (Kwei 1998).

Fig. 3.3 A plot of crossing-angle-dependent SEPs for 800 eV electrons moving from vacuum to GaSb. Solid circles are the results calculated using Eq. (3.14). The solid and dashed curves are, respectively, a fit of the calculated results using Eq. (3.15) and the previous work (Kwei 1998).

Fig. 3.4 A plot of energy-dependent total SEPs for electrons moving from vacuum to GaP with incident angle 50° and then moving from GaP to vacuum with escaping angle 0° . Solid circles are the results calculated using Eqs. (3.12) and (3.14). The solid and dashed curves are, respectively, a fit of the calculated results using Eq. (3.15) and the previous work (Kwei 1998). Open circles are the experimental data measured by Orosz *et al.*

(Orosz 2003).

Fig. 3.5 A sketch of the problem studied in the present work. A particle of charge q , velocity \bar{v}_0 moves parallel to the interface of two media of dielectric functions $\epsilon_1(\bar{k}, \omega)$ and $\epsilon_2(\bar{k}, \omega)$. The interface is located at $z = 0$ and the particle is moving along y -direction at a distance D above the interface. At time $t = 0$, the particle experiences an inelastic interaction which changes particle velocity to \bar{v} . Special interest is on the induced potential and the stopping power at $t > 0$.

Fig. 3.6 The induced potential for a proton moving parallel to the surface of Si. Results (solid curve) are plotted at proton position for $y_p = 5$ a.u., $v_0 = 10$ a.u. and $D = 1$ a.u. as a function of proton velocity v . Corresponding results without the memory effect are plotted (dotted curve) for a comparison.

Fig. 3.7 The induced potential at a distance $y - y_p$ from the proton with $y_p = 5$ a.u. and $D = 1$ a.u. from Si surface. The solid curve is results with the memory effect for $v_0 = 5$ a.u. and $v = 3$ a.u. The dotted and dashed curves are results without the memory effect for $v = v_0 = 3$ a.u. and 5 a.u., respectively.

Fig. 3.8 The induced potential at a distance $y - y_p$ from the proton with $D = 1$

(solid curve), 2 (dotted curve) and 3 a.u. (dashed curve) from Si surface.

Here $y_p = 5$ a.u., $v_0 = 5$ a.u. and $v = 3$ a.u.

Fig. 3.9 Results of the stopping power for a proton moving parallel to with a distance $D = 2$ a.u. from the Si surface. Solid and dotted curves are for $v_0 = 10$ a.u. (with memory effect) and $v_0 = v$ (without memory effect), respectively.

Fig. 3.10 A comparison of the DIIMFPs with (solid curve) and without (dotted curves) the memory effect for electrons moving parallel to the Cu surface

at a distance $D = 1$ a.u. The DIIMFP with the memory effect is calculated for preceding and succeeding electron energies $E_0 = 800$ eV and $E = 500$ eV. The DIIMFPs without the memory effect are calculated for constant electron energies $E_0 = E = 500$ eV and

$E_0 = E = 800$ eV.

Fig. 3.11 A plot of the DIIMFPs with the memory effect for electrons of preceding and succeeding energies $E_0 = 500$ eV and $E = 300$ eV. These electrons are moving at various distances D from the Cu surface.

Fig. 3.12 A comparison of the IMFPs with (solid curve) and without (dotted curve) the memory effect for electrons moving parallel to the Cu surface at a distance $D = 1$ a.u. The IMFP with the memory effect is calculated for

a preceding electron energy $E_0 = 800$ eV as a function of succeeding electron energy E . The IMFP without the memory effect is calculated for constant electron energy $E_0 = E$.

CHAPTER 4

Fig. 4.1 A sketch of the configuration studied in the present work. An electron of velocity \vec{v} moves parallel to and at a distance ρ_0 from the axis of an infinitely long cylinder of radius a . The media inside and outside the cylinder have dielectric functions $\varepsilon_1(k, \omega)$ and $\varepsilon_2(k, \omega)$, respectively.

Fig. 4.2 Calculated DIIMFPs for a 500 eV electron moving parallel to the axis of a Si cylinder (radius $a = 20$ a.u.) in vacuum for several electron distances ρ_0 from the axis.

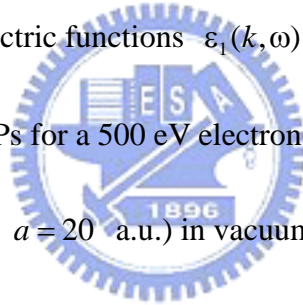


Fig. 4.3 Calculated DIIMFPs for a 500 eV electron moving parallel to the axis of a cylindrical cavity (radius $a = 20$ a.u.) in Si for several electron distances ρ_0 from the axis.

Fig. 4.4 Calculated results of the DIIMFP for an electron moving parallel to and at a distance $\rho_0 = 21$ a.u. from the axis of a Si cylinder (radius $a = 20$ a.u.) in vacuum for several electron energies.

Fig. 4.5 Calculated results of the IIMFP for an electron moving parallel to the axis of a cylindrical cavity (radius $a = 20$ a.u.) in Si for several electron energies.

Fig. 4.6 A sketch of the problem studied in the present work. An electron of velocity \vec{v} moves parallel to and at a distance ρ_0 from the axis of an infinitely long clad cylindrical system with inner radius a and outer radius b . The media in the regions $\rho < a$, $a < \rho < b$ and $\rho > b$ have dielectric functions $\epsilon_1(k, \omega)$, $\epsilon_2(k, \omega)$ and $\epsilon_3(k, \omega)$, respectively.

Fig. 4.7 Calculated DIIMFP for a 500 eV electron moving parallel to and at a distance $\rho_0 < 15 \text{ \AA}$ from the axis of a Si tube of inner radius $a = 15 \text{ \AA}$ and outer radius $b = 25 \text{ \AA}$.

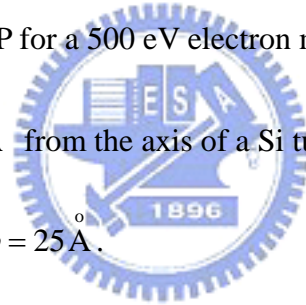


Fig. 4.8 Calculated DIIMFP for a 500 eV electron moving parallel to and at a distance $15 \text{ \AA} < \rho_0 < 25 \text{ \AA}$ from the axis of a Si tube of inner radius $a = 15 \text{ \AA}$ and outer radius $b = 25 \text{ \AA}$.

Fig. 4.9 Calculated DIIMFP for a 500 eV electron moving parallel to and at a distance $\rho_0 > 25 \text{ \AA}$ from the axis of a Si tube of inner radius $a = 15 \text{ \AA}$ and outer radius $b = 25 \text{ \AA}$.

Fig. 4.10 Calculated DIIMFP for an electron moving parallel to and at a distance $\rho_0 = 26 \text{ \AA}$ from the axis of a Si tube of inner radius $a = 15 \text{ \AA}$ and outer

radius $b = 25 \text{ \AA}$ for several electron energies.

Fig. 4.11 Calculated DIIMFP for a 500 eV electron moving parallel to and at a distance $\rho_0 = 26 \text{ \AA}$ from the axis of a Si cylinder clad in a SiO_2 film, having outer radius $b = 25 \text{ \AA}$ and inner radius $a = 0, 15, 22, 24$ or 25 \AA . Results of $a = 0$ and 25 \AA correspond to the SiO_2 and the Si cylindrical wires.



CHAPTER 1

INTRODUCTION

Quantitative information on inelastic interactions between electrons and solids is important in the surface-sensitive spectroscopies. In these spectroscopies, electron inelastic cross-sections comprise mainly the contributions from volume, surface and interface excitations. Thus, the study of electronic excitations is necessary in the analyses of electron spectroscopies. Note that all quantities are expressed in atomic units (a.u.) unless otherwise specified.



1.1 Dielectric Function

Electronic excitations can be described using the dielectric response theory. In this theory, the excitations are characterized in terms of the dielectric function of the materials. The experimental optical and electron energy-loss measured data and their extrapolation from the optical limit to other momentum transfers are frequently used to obtain the full spectrum of the dielectric function (Ritchie 1977; Yubero 1996; Ding 1998). Previously, an extended Drude dielectric function with spatial dispersion (Kwei 1993) was established with parameters determined from

experimental data. This function was constrained by sum-rules to assure the accuracy. In addition, a background dielectric constant was included to account for the influence of polarized ion cores (Smith 1978).

In this dissertation, the extended Drude dielectric function with spatial dispersion was adopted to calculate the electronic excitations. The process of determining the parameters in such function was depicted in chapter 2. Due to the strong overlapping of oscillator strengths between electrons in the valence band and the outermost inner shells, fits of parameters in the extended Drude dielectric function were performed to include the contribution from outermost inner shells. Measured optical data were taken from ellipsometric measurements in the infrared spectral region and from energy loss measurements in the ultraviolet spectral region. Such a combination of data provided detailed information on the interband transitions and the plasmon excitations. In all fits, the real- and imaginary-parts of the dielectric function and the volume and surface energy-loss functions were in good agreement with experimental data.

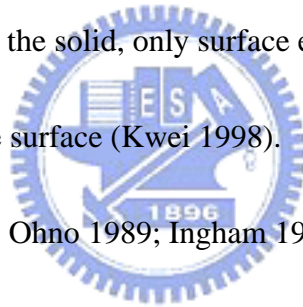
1.2 Electronic Excitations in Planar Systems

In the research of the inelastic interactions between a charged particle and a

planar solid surface, much attention have been paid to inelastic cross-sections. Such cross-sections contain the combined effects arisen from volume and surface plasmon excitations. Volume excitations occur for electrons traveling inside the solid.

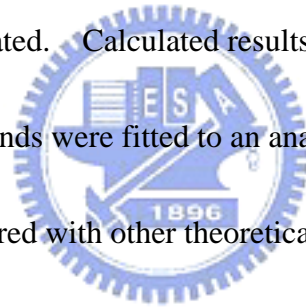
Surface excitations originate from electrons, either inside or outside the solid, moving at a distance in the order of angstroms from the surface. Within the solid, the decrease in volume excitations as electrons move close to the surface is compensated by the increase in surface excitations. This makes the total inelastic cross-sections at any position inside the solid nearly independent of depth (Chen 1996; Kwei 1998).

For electrons traveling outside the solid, only surface excitations are attainable over an effective region close to the surface (Kwei 1998). Many theoretical approaches (Ritchie 1957; Chiarello 1984; Ohno 1989; Ingham 1990; Yubero 1990, 1992;



Vicanek 1999) have been proposed to describe surface excitations in inelastic interactions. Such surface excitations are most conveniently characterized by the so-called surface excitation parameter (SEP), defined as the average number of surface excitations by an electron crossing through the solid surface (Chen 1996; Kwei 1998). For other tilted crossing angle α , the SEP values were approximated by multiplying the results on SEP for normally crossing angle with $(\cos\alpha)^{-1}$ (Kwei 1998; Chen 2002). In their works, however, conservations of energy and momentum were not completely satisfied due to the treatment of momentum transfer in

cylindrical coordinates that carried no restriction on the normal component (Kwei 2006). Later, Werner *et al.* (Werner 2001) rescaled the electron momentum in Oswald's free electron theory (Oswald 1992) by a material-dependent parameter to estimate the SEP for arbitrary material. In their model, however, they assumed a cosine dependence which works only approximately. In section 3.1, the model of SEP was developed for electrons incident into or escaping from solids. Spherical coordinates were employed in the momentum integration to satisfy the energy and momentum conservations. The dependences of SEP on the crossing angle and the electron energy were investigated. Calculated results of SEPs for several semiconducting III-V compounds were fitted to an analytical formula. The calculated results were compared with other theoretical results and measured data.



When a charged particle moves close and parallel to the surface of a solid, an induced potential is produced due to the interaction of the particle and solid. This potential is then acted on the particle resulting to a stopping power. Theoretical derivations of the induced potential and stopping power were previously made (de Abajo 1992, 1993; Kwei 2003; Arista 1994) for a constant velocity, v_0 , of the particle until it experienced an inelastic interaction. After the interaction, the particle changed its velocity to v and continued to interact with the solid. For a second inelastic interaction, it was generally assumed that a new induced potential, dependent

only on v but not on v_0 , was generated. This new potential then determined the stopping power acting on the particle of velocity v . In section 3.2, the induced potential and stopping power for the second inelastic interaction were derived using image charges and dielectric response functions. It was found that the particle previous velocity v_0 had also an effect on the second inelastic interaction. Another words, the particle kept a memory on its previous velocity, v_0 , in determining the stopping power for the particle of velocity v . Calculations were made for a proton moving parallel to Si surface and for an electron moving parallel to Cu surface.

Results were analyzed for the dependences of the induced potential, stopping power, differential inverse inelastic mean free path (DIIMFP) and inelastic mean free path (IMFP) on particle velocities before and after the last inelastic interaction, the distance from surface, and the distance from previous inelastic interaction. Finally, the calculated results with memory effect were compared with the corresponding results without memory effect.

1.3 Electronic Excitations in Cylindrical Systems

In the past few years, new developments in fabrications have allowed the production of miniaturized devices with typical sizes ranging in the nanometer scale.

The study of the inelastic interactions in these devices has become an active field of research. In the research of this interaction between an electron and a cylindrical solid surface, much attention has been paid to inelastic cross-sections. Several theoretical approaches have been developed to evaluate these cross-sections in cylindrical wires and cavities (Chu 1984; Rivacoba 1995; Tökési 1999, 2000; Arista 2001; Zabala 2001; Gervasoni 2003). Of these treatments, the single plasma resonance dielectric model was often used. Although this model is a good approximation for materials that exhibit single pole energy-loss peak, it is not so well for solids that have complex band structures. In section 4.1, the extended Drude dielectric function with spatial dispersion was used to calculate the differential inverse inelastic mean free path and the total inverse inelastic mean free path (IIMFP) in a cylindrical system. These calculations were made for an electron moving parallel to the axis of the cylinder (Si wire and cavity in Si). The dependences of DIIMFP and IIMFP on electron position and energy were then analyzed.

Besides cylindrical systems, clad cylindrical systems have also attracted some attentions. Expressions of inelastic cross-sections for electrons in such systems (Walsh 1989; Zabala 1989) were derived based on the frequency dependent dielectric function, i.e. neglecting spatial dispersion. The inclusion of spatial dispersion may be important at short distances from the surface and the interface, where electrons

might couple to short-wavelength modes (de Abajo 1992). In section 4.2, a general expression for the DIIMFP was derived for electrons moving parallel to the axis of an infinitely long clad cylindrical system. The extended Drude dielectric function with spatial dispersion was used to calculate the DIIMFP in this clad cylindrical system. The present calculations were made for electrons moving parallel to the axis of either a Si cylindrical tube or a Si cylinder clad in a SiO₂ film. The dependences of the DIIMFP on the electron position and energy were analyzed.



CHAPTER 2

DIELECTRIC FUNCTION

When a charged particle moves inside a solid, the inelastic interaction between the charged particle and the solid occurs. This interaction results in the energy loss due to plasmon excitations and interband transitions. The collective excitations are characterized by the dielectric function. Therefore, the improvement in the analysis of inelastic interactions is significant when an applicable dielectric function is considered. In this chapter, the extended Drude dielectric function for semiconducting III-V compounds will be constructed.



2.1 Drude Dielectric Function

The Drude model work quite well for the conduction band of a free-electron-like metal (Daniels 1970). In this model, conduction electrons are described by a free-electron gas constrained by the Fermi-Dirac statistics. The Drude dielectric function in the optical limit, i.e. momentum $k \rightarrow 0$, is given by

$$\varepsilon(0, \omega) = \varepsilon_R(0, \omega) + i\varepsilon_I(0, \omega) \quad , \quad (2.1)$$

where ω is the energy transfer. Here, $\varepsilon_1(0, \omega)$ is the imaginary part of the dielectric function given as

$$\varepsilon_1(0, \omega) = \frac{\omega_p^2 \gamma \omega}{\omega^4 + \omega^2 \gamma^2} \quad (2.2)$$

and $\varepsilon_R(0, \omega)$ is the real part of the dielectric function given by the Kramers-Kronig analysis as

$$\varepsilon_R(0, \omega) = 1 - \frac{\omega_p^2 \omega^2}{\omega^4 + \omega^2 \gamma^2} \quad , \quad (2.3)$$


where ω_p is the free-electron plasmon energy and γ is the damping constant.

For a valence band of n_i bound electrons per volume adding to the conduction band of n_0 free electrons per volume, the imaginary part of the dielectric function is given by (Raether 1980)

$$\varepsilon_1(0, \omega) = \frac{\omega_p^2 \gamma \omega}{\omega^4 + \omega^2 \gamma^2} + \frac{\frac{n_i}{n_0} \omega_p^2 \gamma_i \omega}{(\omega^2 - \omega_i^2)^2 + \omega^2 \gamma_i^2} \quad , \quad (2.4)$$

where γ_i is the damping constant associated with the valence band, and ω_i is the

gap-energy between conduction and valence bands or the critical-point energy for interband transitions. The real part of the dielectric function is then given by the Kramers-Kronig analysis as

$$\varepsilon_{\text{R}}(0, \omega) = 1 - \frac{\omega_p^2 \omega^2}{\omega^4 + \omega^2 \gamma^2} - \frac{\frac{n_i}{n_0} \omega_p^2 (\omega^2 - \omega_i^2)}{(\omega^2 - \omega_i^2)^2 + \omega^2 \gamma_i^2} \quad (2.5)$$

2.2 Extended Drude Dielectric Function

For a solid having a complex structure, the valence band may be composed of several subbands. Each i th subband is characterized by its own oscillator strength A_i , damping constant γ_i , and critical-point energy ω_i . Based on the superposition of damped linear oscillators, the imaginary part of the extended Drude dielectric function in the optical limit, is given by (Kwei 1993)

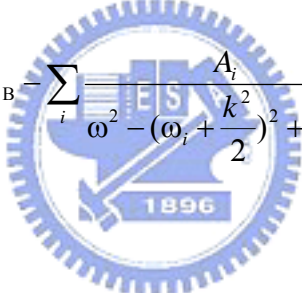
$$\varepsilon_{\text{I}}(0, \omega) = \sum_i \frac{A_i \gamma_i \omega}{(\omega^2 - \omega_i^2)^2 + \omega^2 \gamma_i^2} \quad (2.6)$$

The real part of the extended Drude dielectric function is therefore given by

$$\varepsilon_R(0, \omega) = \varepsilon_B - \sum_i \frac{A_i(\omega^2 - \omega_i^2)}{(\omega^2 - \omega_i^2)^2 + \omega^2 \gamma_i^2}, \quad (2.7)$$

where ε_B is the background dielectric constant to account for the influence of polarizable ion cores (Smith 1978).

To extend the dielectric function into $k \neq 0$ region of the $k - \omega$ plane, one can replace ω_i in Eq. (2.7) to $\omega_i + \frac{k^2}{2}$ (Ritchie 1977, 1991). Thus, the extended Drude dielectric function is given by

$$\varepsilon(k, \omega) = \varepsilon_R(k, \omega) + i\varepsilon_I(k, \omega) = \varepsilon_B - \sum_i \frac{A_i}{\omega^2 - (\omega_i + \frac{k^2}{2})^2 + i\omega\gamma_i}. \quad (2.8)$$


The volume and surface energy-loss function may then be calculated from

$$\text{Im} \left[\frac{-1}{\varepsilon(k, \omega)} \right] = \frac{\varepsilon_I(k, \omega)}{[\varepsilon_R(k, \omega)]^2 + [\varepsilon_I(k, \omega)]^2} \quad (2.9)$$

and

$$\text{Im} \left[\frac{-1}{\varepsilon(k, \omega) + 1} \right] = \frac{\varepsilon_I(k, \omega)}{[\varepsilon_R(k, \omega) + 1]^2 + [\varepsilon_I(k, \omega)]^2}, \quad (2.10)$$

respectively.

2.3 Optical Data

The experimental optical data and the extrapolation of these data from the optical limit to other momentum transfers are frequently used to obtain the full spectrum of the dielectric function (Ritchie 1977; Yubero 1996; Ding 1998). The information on the optical data will be helpful for obtaining the dielectric function due to

$$\varepsilon_R(0, \omega) = n^2(\omega) - \kappa^2(\omega) \quad (2.11)$$



and

$$\varepsilon_I(0, \omega) = 2n(\omega)\kappa(\omega) \quad (2.12)$$

However, optical data are only available for the extinction coefficient, κ , in a limited energy transfer range $\omega_1 \leq \omega \leq \omega_2$ and for the refraction index, n , in $\omega_3 \leq \omega \leq \omega_4$. Due to the lack of information on κ in $\omega < \omega_1$ and $\omega > \omega_2$,

extrapolations are applied as

$$\kappa(\omega) = \begin{cases} \kappa(\omega_1) \frac{\omega}{\omega_1} & \text{for } \omega < \omega_1 \\ \kappa(\omega_2) \left(\frac{\omega_2}{\omega} \right)^p & \text{for } \omega > \omega_2 \end{cases}, \quad (2.13)$$

where the parameter p is determined from the f-sum rule

$$\int_0^{\infty} \omega \kappa(\omega) d\omega = \frac{\pi}{4} \omega_p^2, \quad (2.14)$$

$\omega_p = (4\pi NZ)^{1/2}$ is the plasma energy, N is the molecular density, and Z is the total number of electrons per molecule. Further, the Kramers-Kronig relation is applied to obtain the refraction index at any ω in the range of $\omega < \omega_3$ and $\omega > \omega_4$.

The validity of the inertial sum rule

$$\int_0^{\infty} [n(\omega) - 1] d\omega = 0. \quad (2.15)$$

is also checked.

2.4 Parameters in Extended Drude Dielectric Function

All parameters (ϵ_B , A_i , γ_i and ω_i) of the extended Drude dielectric function in Eq. (2.8) are determined by fits of $\epsilon_R(0, \omega)$, $\epsilon_I(0, \omega)$, $\text{Im}[-1/\epsilon(0, \omega)]$ and $\text{Im}[-1/(\epsilon(0, \omega)+1)]$ to the experimental data of the semiconducting III-V compounds. For small energy transfers ($\omega < 6$ eV), the experimental data are taken from the optical ellipsometry (Palik 1985, 1991, 1998). For large energy transfers ($\omega \geq 6$ eV), the experimental data are taken from the electron energy-loss measurement (Festenberg 1969; Brockt 2000).

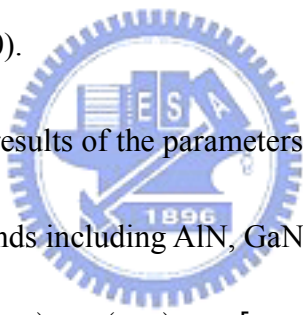


Table 2.1 lists the fitting results of the parameters in Eq. (2.8) for several semiconducting III-V compounds including AlN, GaN, GaP, GaAs, GaSb, InAs and InSb. A comparison on $\epsilon_R(0, \omega)$, $\epsilon_I(0, \omega)$, $\text{Im}[-1/\epsilon(0, \omega)]$ and $\text{Im}[-1/(\epsilon(0, \omega)+1)]$ for GaN is shown in Fig. 2.1 among the present fittings (solid curves) and the experimental data (dotted curves). It reveals that the present fittings are in good agreement as compared to the experimental data for all dielectric functions plotted. A similar plot for InSb is shown among the present fittings (solid curves), the previous fittings (Kwei 1986) (dotted curves), and the experimental data (Festenberg 1969; Palik 1985) (dashed curves). It reveals that the present fittings are in better agreement than the previous ones as compared to the experimental data for

all dielectric functions plotted. The better agreement is due to the considerations of the polarizable ion cores and partial $4d$ inner shell electrons in the dielectric functions. The previous fittings without such considerations produce poor agreement with optical data on ϵ_R and ϵ_I at small ω and on the volume and surface energy-loss functions at large ω . Further, the positions and the heights of the resonant plasmon peaks in the previous fittings are different from experimental data. It should be noted that care is taken in the present fittings of these dielectric functions against errors in ϵ_R near energy transfers corresponding to $\epsilon_R = -1$, where any small difference in ϵ_R could generate a large deviation in the surface energy-loss function.



Table 2.1 Parameters in the dielectric function of Eq. (2.8) for semiconducting III-V compounds.

AlN ($\epsilon_B=1.25$)			GaN ($\epsilon_B=1.35$)			GaP ($\epsilon_B=1.05$)			GaAs ($\epsilon_B=1.01$)		
$A_i(\text{eV}^2)$	$\gamma_i(\text{eV})$	$\omega_i(\text{eV})$	$A_i(\text{eV}^2)$	$\gamma_i(\text{eV})$	$\omega_i(\text{eV})$	$A_i(\text{eV}^2)$	$\gamma_i(\text{eV})$	$\omega_i(\text{eV})$	$A_i(\text{eV}^2)$	$\gamma_i(\text{eV})$	$\omega_i(\text{eV})$
2.30	1.20	5.00	3.90	0.90	3.98	3.40	2.00	2.89	2.08	0.10	2.92
13.00	0.90	8.00	87.00	2.20	6.98	12.50	0.20	3.73	25.97	0.61	3.16
60.00	1.80	8.20	33.00	6.00	7.00	34.00	0.90	4.02	31.90	1.20	3.84
6.00	3.00	9.00	25.00	1.60	8.70	40.90	0.80	4.80	58.80	0.70	4.60
95.00	2.20	9.10	56.00	3.00	9.80	58.70	0.70	5.10	17.00	0.35	4.90
75.00	3.00	11.50	13.00	3.00	10.50	10.00	2.00	5.45	10.00	1.00	5.60
90.00	5.00	13.00	28.00	1.80	11.20	40.00	1.70	6.80	43.44	2.42	6.70
10.00	1.92	14.00	79.00	2.50	12.80	45.00	4.00	9.80	48.00	10.30	11.10
80.00	7.00	15.00	33.00	3.00	13.20	15.00	5.00	13.20	5.60	2.80	11.50
22.00	6.30	17.00	30.00	3.00	14.80	3.00	3.00	22.00	1.50	2.00	21.00
70.00	14.11	17.10	49.00	4.40	17.30	4.50	3.00	24.00	5.00	3.20	21.80
3.00	6.40	20.50	1.20	3.20	19.90	16.00	25.20	26.00	15.00	29.30	30.00
190.00	28.00	34.60	3.60	1.80	21.30	19.00	29.40	30.00	25.00	36.70	37.00
			23.00	2.00	22.80	102.00	39.00	40.00	40.00	38.20	39.00
			12.00	3.00	25.00						
			160.00	4.10	29.00						

Table 2.1 (continued) Parameters in the dielectric function of Eq. (2.8) for semiconducting III-V compounds.

GaSb ($\epsilon_B=1.02$)			InAs ($\epsilon_B=1.05$)			InSb ($\epsilon_B=1.02$)		
$A_i(\text{eV}^2)$	$\gamma_i(\text{eV})$	$\omega_i(\text{eV})$	$A_i(\text{eV}^2)$	$\gamma_i(\text{eV})$	$\omega_i(\text{eV})$	$A_i(\text{eV}^2)$	$\gamma_i(\text{eV})$	$\omega_i(\text{eV})$
3.40	0.20	2.10	2.30	0.20	2.50	6.00	0.34	1.89
23.70	0.68	2.50	22.50	0.76	2.80	21.50	0.77	2.40
38.90	1.15	3.30	85.00	2.60	4.15	42.00	1.50	3.35
28.70	0.70	3.80	28.70	0.46	4.48	34.70	0.68	3.85
27.00	0.48	4.11	5.00	0.90	4.85	5.00	0.90	4.18
7.50	0.80	4.80	4.00	0.60	5.40	7.00	2.00	4.53
8.00	0.70	5.20	5.00	0.60	6.10	16.00	1.20	5.23
5.00	0.80	5.80	8.00	2.00	6.90	8.00	1.20	5.96
15.00	1.80	7.00	45.00	5.90	8.80	20.00	3.30	8.50
28.00	3.00	8.50	10.00	5.50	19.50	4.20	7.50	9.50
3.50	2.50	10.50	23.00	5.00	23.00	3.60	3.00	10.20
1.30	1.50	11.20	30.00	35.00	32.00	6.00	2.50	19.80
10.10	5.50	12.00	40.00	36.80	38.00	5.00	3.00	21.00
1.80	1.50	20.20				2.00	2.00	23.50
1.20	1.50	21.30				3.00	2.00	24.50
6.50	3.60	24.00				10.00	29.60	30.00
30.00	30.00	31.00				16.00	33.00	34.00
40.00	35.00	36.00				130.00	35.00	36.00
50.00	38.00	40.00						

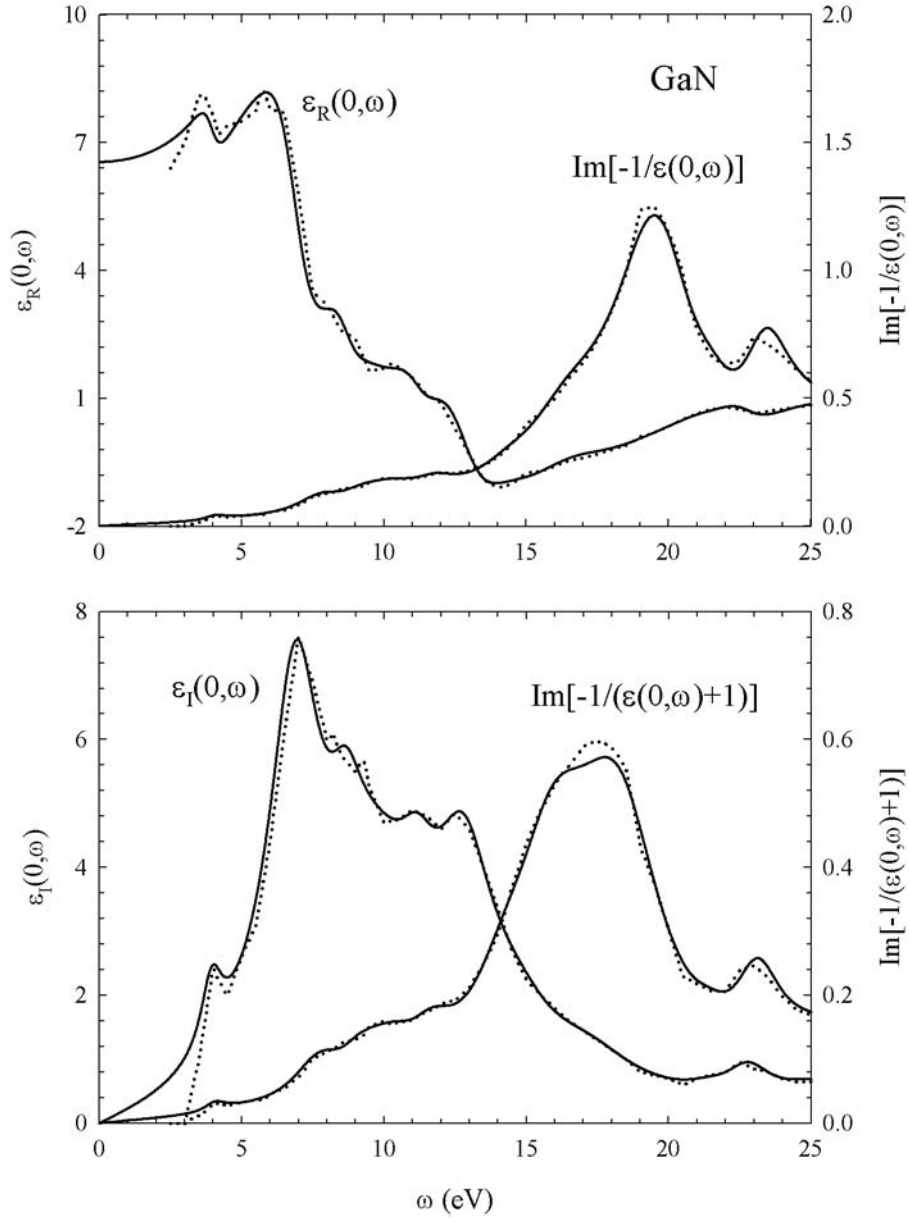


Fig. 2.1 A plot of the dielectric functions, $\epsilon_R(0, \omega)$, $\epsilon_I(0, \omega)$, $\text{Im}[-1/\epsilon(0, \omega)]$ and $\text{Im}[-1/(\epsilon(0, \omega)+1)]$, for GaN. Solid curves are results of the present work. The experimental data (Brockt 2000) (dotted curves) are also plotted for comparison.

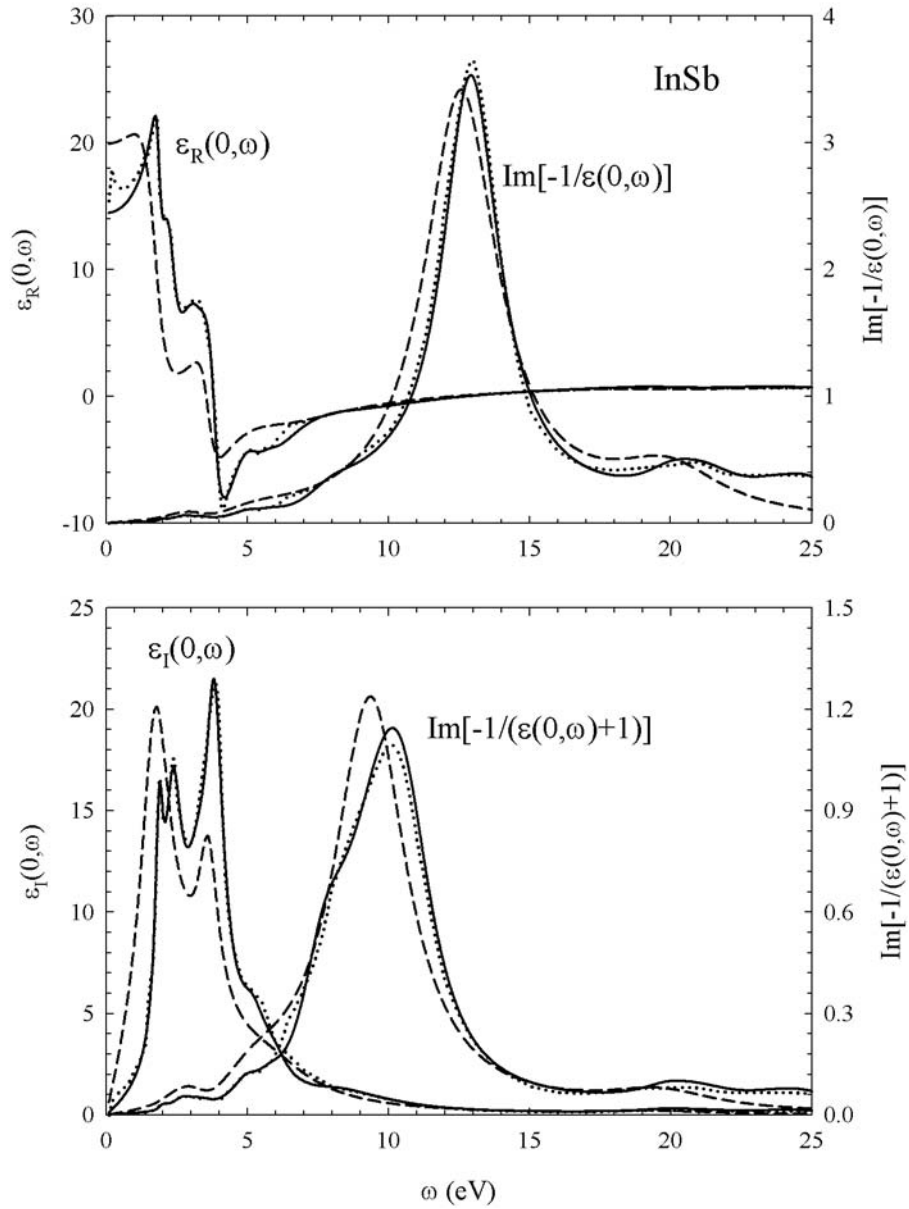


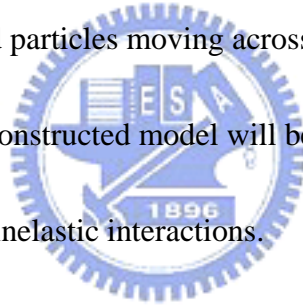
Fig. 2.2 A plot of the dielectric functions, $\epsilon_R(0, \omega)$, $\epsilon_I(0, \omega)$, $\text{Im}[-1/\epsilon(0, \omega)]$ and $\text{Im}[-1/(\epsilon(0, \omega)+1)]$, for InSb. Solid curves are results of the present work. Other calculated results (Kwei 1986) (dashed curves) and the experimental data (Festenberg 1969; Palik 1985) (dotted curves) are also plotted for comparison.

CHAPTER 3

ELECTRONIC EXCITATIONS

IN PLANAR SYSTEMS

The information on the electron inelastic interaction cross-sections plays an important role in the quantitative analysis of surface-sensitive electron spectroscopies. The most widely studied geometry for these interactions was planar (Yubero 1992; Jablonski 2000; Kwei 2004; Werner 2005). In this chapter, a theoretical model of inelastic scattering for charged particles moving across solid surfaces will be constructed. After that, the constructed model will be further modified to include the memory effect for successive inelastic interactions.



3.1 Inelastic Interactions of Electrons with Planar Systems

As illustrated in Fig. 3.1, an electron of velocity \vec{v} travels across an interface at time $t = 0$ from medium 1 of dielectric function $\epsilon_1(\vec{k}, \omega)$ to medium 2 of dielectric function $\epsilon_2(\vec{k}, \omega)$, where \vec{k} is the momentum transfer and ω is the energy transfer. The crossing angle α is defined as the angle between the interface normal and the

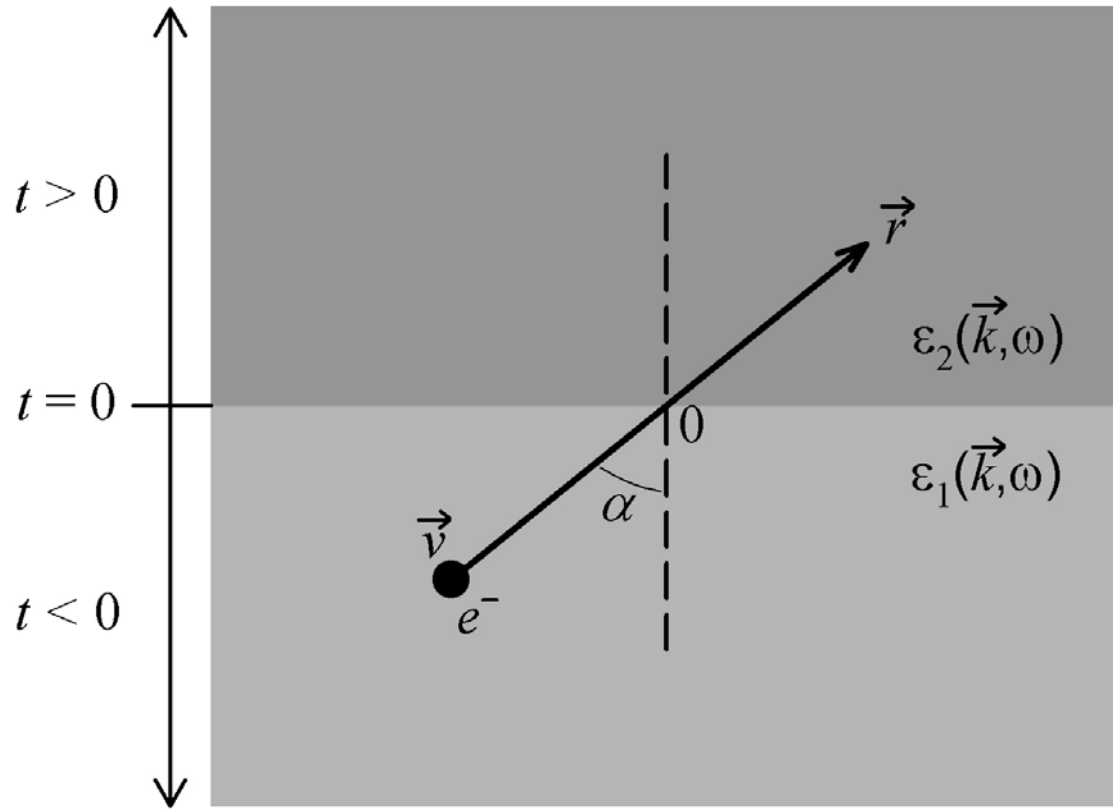


Fig. 3.1 A sketch of the problem studied in this work. An electron of velocity \vec{v} moves across the interface at time $t = 0$ from medium 1 of dielectric function $\epsilon_1(\vec{k}, \omega)$ to medium 2 of dielectric function $\epsilon_2(\vec{k}, \omega)$ with crossing angle α . The instant position of the electron is $\vec{r} = \vec{v}t$, relative to the crossing point at interface.

electron moving direction. The instant position of the electron is $\vec{r} = \vec{v}t$, relative to the crossing point at the interface.

3.1.1 Induced Potential

As the electron crosses the interface, volume and surface excitations are probable due to electron-solid interactions. Surface excitations occur when the electron travels near the interface, while volume excitations arise as the electron moves inside the media. These two excitations can be described using the dielectric response theory (Chen 1996; Kwei 1998). By solving the Poisson equation, the Fourier components of the scalar potentials in media 1 and 2 are given by (Kwei 1998, 1999)

$$\Phi_1(\vec{k}, \omega) = \frac{-8\pi^2}{k^2 \epsilon_1(\vec{k}, \omega)} [\delta(\omega - kv \cos \beta) + \rho_s(\vec{Q}, \omega)] \quad (3.1)$$

for $t < 0$, and

$$\Phi_2(\vec{k}, \omega) = \frac{-8\pi^2}{k^2 \epsilon_2(\vec{k}, \omega)} [\delta(\omega - kv \cos \beta) - \rho_s(\vec{Q}, \omega)] \quad (3.2)$$

for $t > 0$, where $\vec{k} = (\vec{Q}, k_z)$, \vec{Q} and k_z are the parallel and normal components of

\vec{k} with respect to the surface, β is the angle between \vec{k} and \vec{v} , and $\rho_s(\vec{Q}, \omega)$ is the induced surface charge density. The signs accompanying the induced surface charge density are opposite for $t < 0$ and for $t > 0$, which is due to the requirement for the continuity of the normal component of the electric displacement at the interface. The other boundary condition, i.e. the continuity of the tangential components of the electric field at the interface, requires that the induced surface charge density follows

$$\rho_s(\vec{Q}, \omega) = \frac{\int_{-\infty}^{+\infty} \frac{\delta(\omega - \vec{Q} \cdot \vec{v}_{\parallel} - k_z v_{\perp})}{q^2} \left[\frac{1}{\epsilon_2(\vec{k}, \omega)} - \frac{1}{\epsilon_1(\vec{k}, \omega)} \right] dk_z}{\int_{-\infty}^{+\infty} \frac{1}{k^2} \left[\frac{1}{\epsilon_2(\vec{k}, \omega)} + \frac{1}{\epsilon_1(\vec{k}, \omega)} \right] dk_z}, \quad (3.3)$$

where v_{\perp} and v_{\parallel} are the normal and parallel components of \vec{v} with respect to the surface.

Now the Fourier components of the scalar potentials, $\Phi_1(\vec{k}, \omega)$ and $\Phi_2(\vec{k}, \omega)$ on either side of the interface, can be obtained after substituting Eq. (3.3) into Eqs. (3.1) and (3.2). The induced potentials in real space can be derived by the inverse Fourier transforms of $\Phi_1(\vec{k}, \omega)$ and $\Phi_2(\vec{k}, \omega)$ after removing the potential of the electron in vacuum. Adopting spherical coordinates in the integration of momentum transfer, the induced potentials can be written as

$$\begin{aligned}\Phi_{1,ind}(\vec{r},t) = & -\frac{1}{\pi} \iiint \delta(\omega - kv\cos\beta) \left[\frac{1}{\varepsilon_1(\vec{k},\omega)} - 1 \right] e^{i(kv\cos\beta - \omega t)} \sin\beta d\beta dk d\omega \\ & - \frac{1}{2\pi^2} \iiint \iiint \frac{\rho_s(\vec{Q},\omega)}{\varepsilon_1(\vec{k},\omega)} e^{i(\vec{Q}\cdot\vec{R} - \omega t)} e^{ik_z z} \sin\theta d\phi d\theta dk d\omega\end{aligned}\quad (3.4)$$

for $t < 0$, and

$$\begin{aligned}\Phi_{2,ind}(\vec{r},t) = & -\frac{1}{\pi} \iiint \delta(\omega - kv\cos\beta) \left[\frac{1}{\varepsilon_2(\vec{k},\omega)} - 1 \right] e^{i(kv\cos\beta - \omega t)} \sin\beta d\beta dk d\omega \\ & + \frac{1}{2\pi^2} \iiint \iiint \frac{\rho_s(\vec{Q},\omega)}{\varepsilon_2(\vec{k},\omega)} e^{i(\vec{Q}\cdot\vec{R} - \omega t)} e^{ik_z z} \sin\theta d\phi d\theta dk d\omega\end{aligned}\quad (3.5)$$

for $t > 0$, where $\vec{r} = (\vec{R}, z)$, \vec{R} and z are the parallel and normal components of \vec{r} with respect to the surface, and

$$\frac{\rho_s(\vec{Q},\omega)}{\varepsilon_j(\vec{k},\omega)} = \frac{1}{\pi} \frac{Qv_{\perp}}{(\omega - \vec{Q}\cdot\vec{v}_{\parallel})^2 + Q^2v_{\perp}^2} \frac{\varepsilon_1(\vec{Q},\omega) - \varepsilon_2(\vec{Q},\omega)}{\varepsilon_j(\vec{Q},\omega)[\varepsilon_1(\vec{Q},\omega) + \varepsilon_2(\vec{Q},\omega)]}\quad (3.6)$$

for $j=1$ and 2 . Equation (3.6) was derived under the assumption that $\varepsilon(\vec{k},\omega) \approx \varepsilon(\vec{Q},\omega)$ (Yubero 1992, 1996). The integrations over ω in the second integrals of Eqs. (3.4) and (3.5) can be performed by closing the contour in the upper and lower half planes for $t < 0$ and $t > 0$, respectively. To carry out the contour

integration in the lower half plane, it is convenient to convert it into the upper half plane by replacing $e^{i(\vec{Q}\cdot\vec{R}-\omega t)}$ in Eq. (3.5) with $e^{i(\vec{Q}\cdot\vec{R}-\omega t)} = 2\cos(\omega t - \vec{Q}\cdot\vec{R}) - e^{-i(\vec{Q}\cdot\vec{R}-\omega t)}$.

3.1.2 Differential Inverse Inelastic Mean Free Path

The stopping power, F , can be related to the induced potential, $\Phi_{ind}(\vec{r}, t)$, by (Flores 1979)

$$F = \frac{1}{v} \left[\frac{\partial \Phi_{ind}(\vec{r}, t)}{\partial t} \right]_{t=\vec{r}/v}, \quad (3.7)$$



where the derivative of the induced potential is evaluated at the position of the electron. And the stopping power can be expressed in terms of the position-dependent DIIMFP, $\mu(\alpha, E, \omega, r)$, according to

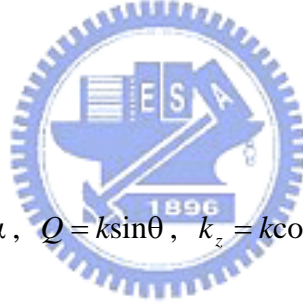
$$F = \int_0^E \omega \mu(\alpha, E, \omega, r) d\omega. \quad (3.8)$$

3.1.2.1 Electrons Moving from Solid to Vacuum

In the case of an electron traveling from solid to vacuum, i.e. $s \rightarrow v$, $\varepsilon_1(\vec{k}, \omega)$ and

$\varepsilon_2(\bar{k}, \omega)$ may be replaced by $\varepsilon(\bar{k}, \omega)$ and 1, respectively. The DIIMFP is therefore given by

$$\begin{aligned}
\mu^{s \rightarrow v}(\alpha, E, \omega, r) = & \frac{2}{\pi v^2} \int_{k_-}^{k_+} dk \frac{1}{k} \text{Im} \left[\frac{-1}{\varepsilon(\bar{k}, \omega)} \right] \Theta(-r) \\
& - \frac{2 \cos \alpha}{\pi^3} \int_{k_-}^{k_+} dk \int_0^{\pi/2} d\theta \int_0^{2\pi} d\phi \frac{k \sin^2 \theta \cos(k_z r \cos \alpha) \exp(-|r|Q \cos \alpha)}{\tilde{\omega}^2 + Q^2 v_\perp^2} \text{Im} \left[\frac{-1}{\varepsilon(\bar{Q}, \omega)} \right] \Theta(-r) \\
& + \frac{4 \cos \alpha}{\pi^3} \int_{k_-}^{k_+} dk \int_0^{\pi/2} d\theta \int_0^{2\pi} d\phi \frac{k \sin^2 \theta \cos(k_z r \cos \alpha) \exp(-|r|Q \cos \alpha)}{\tilde{\omega}^2 + Q^2 v_\perp^2} \text{Im} \left[\frac{-1}{\varepsilon(\bar{Q}, \omega) + 1} \right] \Theta(-r) \\
& + \frac{4 \cos \alpha}{\pi^3} \int_{k_-}^{k_+} dk \int_0^{\pi/2} d\theta \int_0^{2\pi} d\phi \frac{k \sin^2 \theta \exp(-|r|Q \cos \alpha)}{\tilde{\omega}^2 + Q^2 v_\perp^2} \text{Im} \left[\frac{-1}{\varepsilon(\bar{Q}, \omega) + 1} \right] \left[2 \cos \left(\frac{\tilde{\omega} r}{v} \right) - \exp(-|r|Q \cos \alpha) \right] \Theta(r)
\end{aligned} \tag{3.9}$$



where $\tilde{\omega} = \omega - kv \sin \theta \cos \phi \sin \alpha$, $Q = k \sin \theta$, $k_z = k \cos \theta$, $v_\perp = v \cos \alpha$, $E = \frac{v^2}{2}$, and

$\Theta(r)$ is the Heaviside step function. Applying the energy-momentum conservation

relations, the upper and lower limits of k are $k_\pm = \sqrt{2E} \pm \sqrt{2(E - \omega)}$. The terms

involving $\text{Im} \left(\frac{-1}{\varepsilon + 1} \right)$ are due to the contribution from surface excitations, whereas

those involving $\text{Im} \left(\frac{-1}{\varepsilon} \right)$ are contributed from volume excitations. Equation (3.9)

reveals that only surface excitations are possible for the electron traveling outside the

solid. However, both volume and surface excitations may occur for the electron

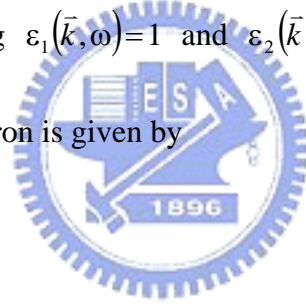
moving inside the solid. The term $\exp(-|r|Q \cos \alpha)$ in Eq. (3.9) indicates that the

contribution from surface excitations decreases exponentially with the increase in

distance from the surface. On the other hand, the reduction in the contribution from volume excitations increases rapidly as the electron moves near the surface. When electron moves deep inside the solid, i.e. $r \rightarrow -\infty$, Eq. (3.9) reduces to the same expression as that for an electron moving in the infinite solid.

3.1.2.2 Electrons Moving from Vacuum to Solid

Similar derivations can be performed for an electron traveling from solid to vacuum, i.e. $v \rightarrow s$, by taking $\varepsilon_1(\vec{k}, \omega) = 1$ and $\varepsilon_2(\vec{k}, \omega) = \varepsilon(\vec{k}, \omega)$. In this case, the DIIMFP for the incident electron is given by



$$\begin{aligned}
\mu^{v \rightarrow s}(\alpha, E, \omega, r) = & \frac{4\cos\alpha}{\pi^3} \int_{k_-}^{k_+} dk \int_0^{\pi/2} d\theta \int_0^{2\pi} d\phi \frac{k\sin^2\theta\cos(k_z r\cos\alpha)}{\tilde{\omega}^2 + Q^2 v_\perp^2} \exp(-|r|Q\cos\alpha) \operatorname{Im} \left[\frac{-1}{\varepsilon(\vec{Q}, \omega) + 1} \right] \Theta(-r) \\
& + \frac{2}{\pi v^2} \int_{k_-}^{k_+} dk \frac{1}{k} \operatorname{Im} \left[\frac{-1}{\varepsilon(\vec{k}, \omega)} \right] \Theta(r) \\
& - \frac{2\cos\alpha}{\pi^3} \int_{k_-}^{k_+} dk \int_0^{\pi/2} d\theta \int_0^{2\pi} d\phi \frac{k\sin^2\theta\exp(-|r|Q\cos\alpha)}{\tilde{\omega}^2 + Q^2 v_\perp^2} \operatorname{Im} \left[\frac{-1}{\varepsilon(\vec{Q}, \omega)} \right] \left[2\cos\left(\frac{\tilde{\omega}r}{v}\right) - \exp(-|r|Q\cos\alpha) \right] \Theta(r) \\
& + \frac{4\cos\alpha}{\pi^3} \int_{k_-}^{k_+} dk \int_0^{\pi/2} d\theta \int_0^{2\pi} d\phi \frac{k\sin^2\theta\exp(-|r|Q\cos\alpha)}{\tilde{\omega}^2 + Q^2 v_\perp^2} \operatorname{Im} \left[\frac{-1}{\varepsilon(\vec{Q}, \omega) + 1} \right] \left[2\cos\left(\frac{\tilde{\omega}r}{v}\right) - \exp(-|r|Q\cos\alpha) \right] \Theta(r)
\end{aligned} \tag{3.10}$$

3.1.3 Surface Excitation Parameter

Surface excitation parameters describe the total probability of surface excitations by crossing electrons traveling in vacuum. The SEP may be obtained by integrating the IIMFP over the whole path length of the electron outside the solid. The IIMFP for an escaping electron can be calculated using

$$\mu^{s \rightarrow v}(\alpha, E, r) = \int_0^E \mu^{s \rightarrow v}(\alpha, E, \omega, r) d\omega \quad (3.11)$$

The SEP for an escaping electron is therefore given by

$$P_s^{s \rightarrow v}(\alpha, E) = \int_0^\infty \mu^{s \rightarrow v}(\alpha, E, r) dr \quad (3.12)$$

Similarly, the IIMFP and SEP for an incident electron can be obtained from

$$\mu^{v \rightarrow s}(\alpha, E, r) = \int_0^E \mu^{v \rightarrow s}(\alpha, E, \omega, r) d\omega \quad (3.13)$$

and

$$P_s^{v \rightarrow s}(\alpha, E) = \int_{-\infty}^0 \mu^{v \rightarrow s}(\alpha, E, r) dr . \quad (3.14)$$

The angular dependence of SEP for III-V semiconducting compounds are then calculated for both escaping and incident electrons using Eqs. (3.12) and (3.14).

These calculated SEPs are found to follow a simple formula

$$P_s^{s \rightarrow v}(\alpha, E) \text{ or } P_s^{v \rightarrow s}(\alpha, E) = \frac{aE^{-b}}{\cos^c \alpha} , \quad (3.15)$$

where a , b and c are material dependent constants. With E in electron-volts, the best-fitted values of parameters a , b and c are listed in Table 3.1 for all solids studied.

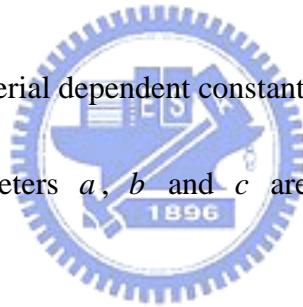
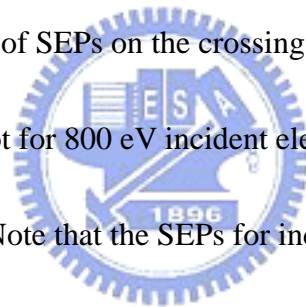


Table 3.1 Fitted values of parameters a , b and c in Eq. (3.15) for semiconducting III-V compounds.

	Escaping electrons			Incident electrons		
	a	b	c	a	b	c
AlN	1.2938	0.4491	0.9173	0.6617	0.4480	1.1551
GaN	1.3820	0.4596	0.9079	0.6996	0.4584	1.1533
GaP	2.4437	0.4938	0.8844	1.1731	0.4890	1.1541
GaAs	2.4981	0.4889	0.8762	1.2382	0.4894	1.1484
GaSb	3.0431	0.5153	0.8653	1.4387	0.5095	1.1442
InAs	2.9012	0.5152	0.8632	1.3759	0.5099	1.1418
InSb	3.2265	0.5241	0.8549	1.5213	0.5181	1.1360

Figure 3.2 shows the crossing-angle-dependent SEPs calculated for 800 eV escaping electrons moving from GaAs to vacuum. Solid circles represent the calculated data using Eq. (3.12). The results of fitted values using Eq. (3.15) (solid curve) and those calculated with the previous model (Kwei 1998) (dashed curve) are included in this figure for comparisons. It can be seen that the SEP is larger for larger crossing angle due to the longer time for electron-surface interaction. The SEP rises slowly with increasing crossing angle until about $\alpha = 70^\circ$, above which such a rise becomes rapidly. The present results show that the previous work, which assumed a cosine dependence of SEPs on the crossing angle, works only approximately. A similar plot for 800 eV incident electrons moving from vacuum to GaSb is shown in Fig. 3.3. Note that the SEPs for incident electrons exhibit similar energy and angular dependences as for escaping electrons. However, the SEPs for incident electrons have smaller values than for escaping electrons. This is because the attractive force acting on the incident electron (in vacuum) by the surface induced charges accelerates the electron. On the other hand, the attractive force on the escaping electron (in vacuum) decelerates the electron. Therefore, the time spent near the surface for incident electron is less than for escaping electron, thus leading to less surface excitations for incident electron.



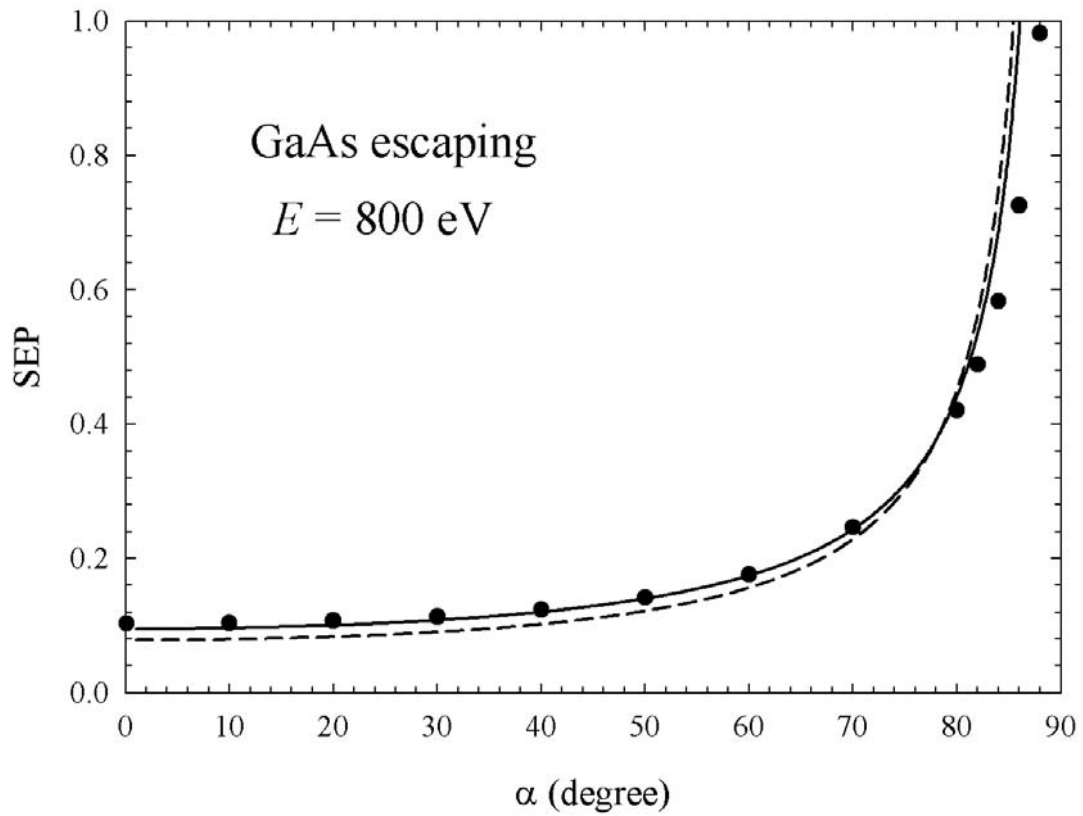


Fig. 3.2 A plot of crossing-angle-dependent SEPs for 800 eV electrons moving from GaAs to vacuum. Solid circles are the results calculated using Eq. (3.12). The solid and dashed curves are, respectively, a fit of the calculated results using Eq. (3.15) and the previous work (Kwei 1998).

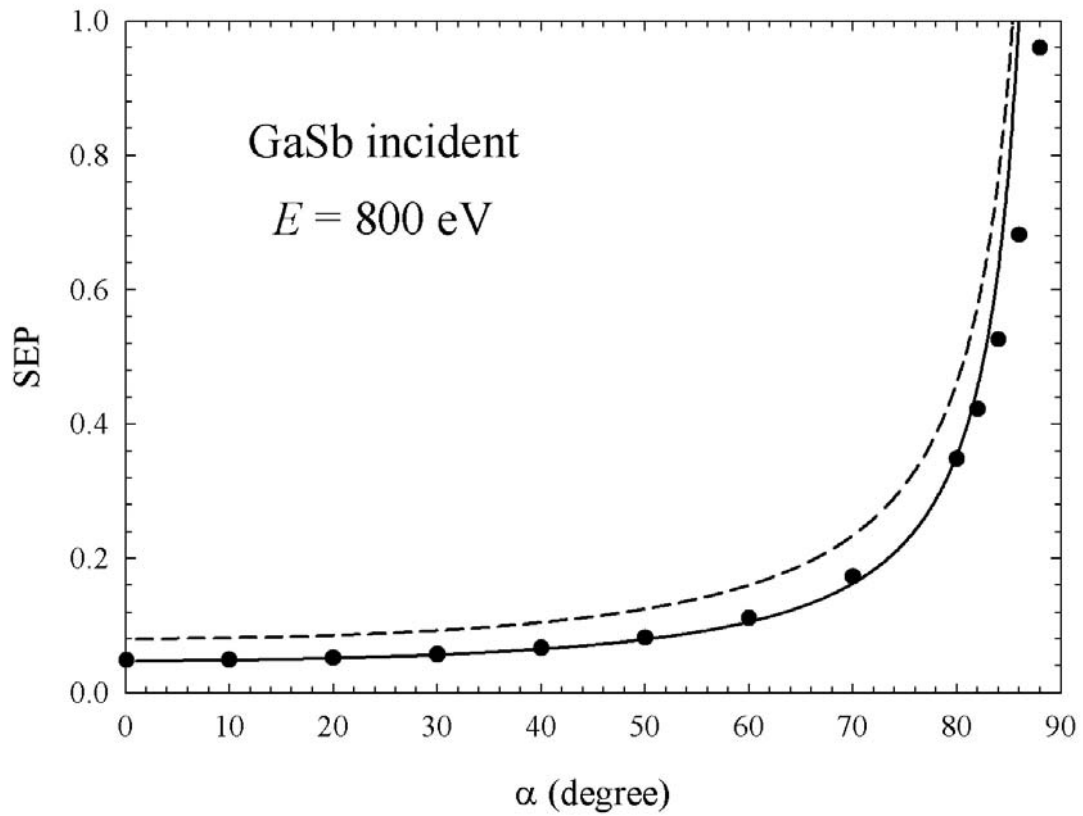


Fig. 3.3 A plot of crossing-angle-dependent SEPs for 800 eV electrons moving from vacuum to GaSb. Solid circles are the results calculated using Eq. (3.14). The solid and dashed curves are, respectively, a fit of the calculated results using Eq. (3.15) and the previous work (Kwei 1998).

The total electron SEPs of two surface crossings on GaP calculated using Eqs. (3.12) and (3.14) (solid circles) are plotted in Fig. 3.4 as a function of electron energy for a 50° incident angle and a 0° escaping angle. The fits using Eq. (3.15) (solid curve), the previous work (Kwei 1998) (dashed curve) and Orosz *et al.* (Orosz 2003) (open circles) are included in this figure for comparisons. It is seen that SEPs decrease with increasing electron energy because of the less interacting time for surface excitations. The difference in magnitude between the present work and the previous work for the SEP is due to the use of spherical coordinates in performing the momentum integration to satisfy the momentum and energy conservations. The results of Orosz *et al.* were deduced from a comparison of the experimental inelastic scattering cross-section spectra evaluated by the method of Tougaard *et al.* (Tougaard 1987, 1991) based on REELS measurements. The results from their procedure contain the contributions of surface excitations both inside and outside the solid (Gergely 2002). In the present work, however, the contribution of surface excitations outside the solid was dealt in the calculations of SEPs. This is because the approximate compensation of surface and volume excitations inside the solid (Kwei 1998). The different treatments result in the discrepancies between the results of the present work (solid circles) and Orosz *et al.* (open circles).

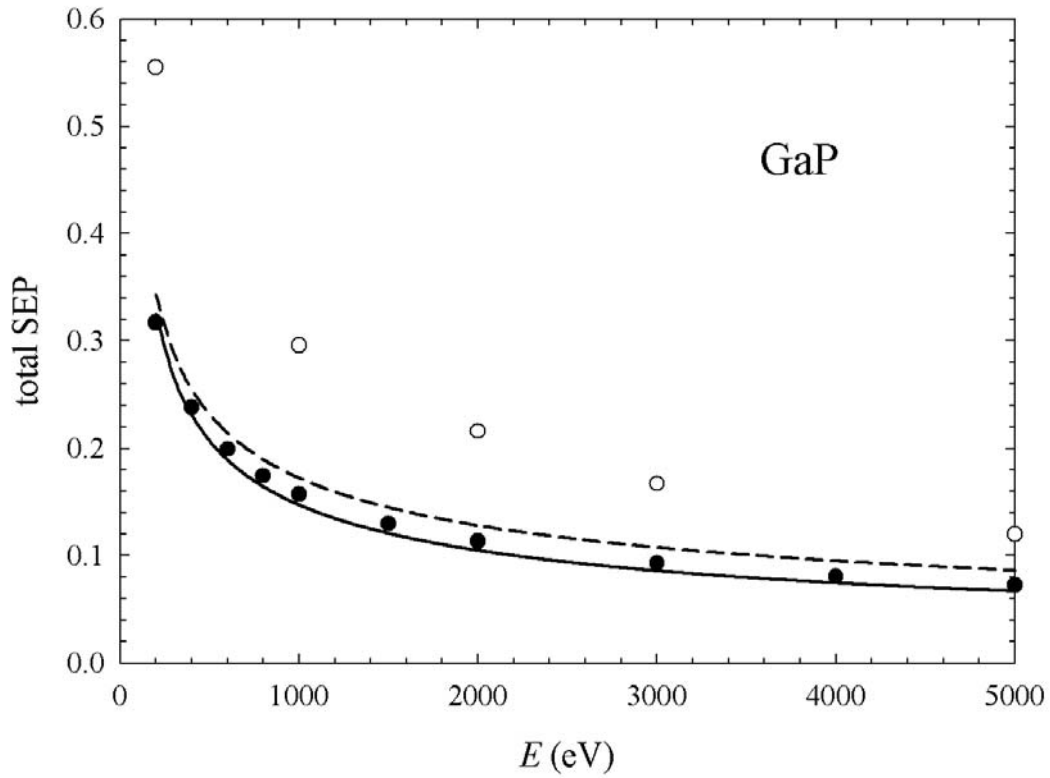
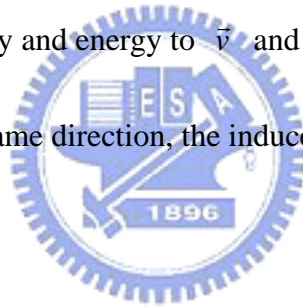


Fig. 3.4 A plot of energy-dependent total SEPs for electrons moving from vacuum to GaP with incident angle 50° and then moving from GaP to vacuum with escaping angle 0° . Solid circles are the results calculated using Eqs. (3.12) and (3.14). The solid and dashed curves are, respectively, a fit of the calculated results using Eq. (3.15) and the previous work (Kwei 1998). Open circles are the experimental data measured by Orosz *et al.* (Orosz 2003).

3.2 Memory Effect

Figure 3.5 illustrates the problem studied in the present work. A particle of charge q , velocity \vec{v}_0 and energy E_0 moves parallel to the interface of two media of dielectric functions $\varepsilon_1(\vec{k}, \omega)$ and $\varepsilon_2(\vec{k}, \omega)$. The interface is located at $z = 0$, with z -axis perpendicular to the interface plane and directed from $\varepsilon_1(\vec{k}, \omega)$ to $\varepsilon_2(\vec{k}, \omega)$. The particle is moving along y -direction at a distance D above the interface. At the moment $t = 0$, the particle experiences an inelastic interaction which changes particle velocity and energy to \vec{v} and E . Assuming the particle continues to move along the same direction, the induced potential at $t > 0$ is of special interest here.



3.2.1 Induced Potential

For $z > 0$, the scalar potential is produced by the particle and a fictitious charge at $z < 0$ near the interface. For $z < 0$, the potential is produced by a fictitious charge at particle position and by another fictitious charge at $z > 0$ near the interface. These fictitious charges should be established using boundary conditions that are satisfied at the interface. Thus the Poisson equations in Fourier space are

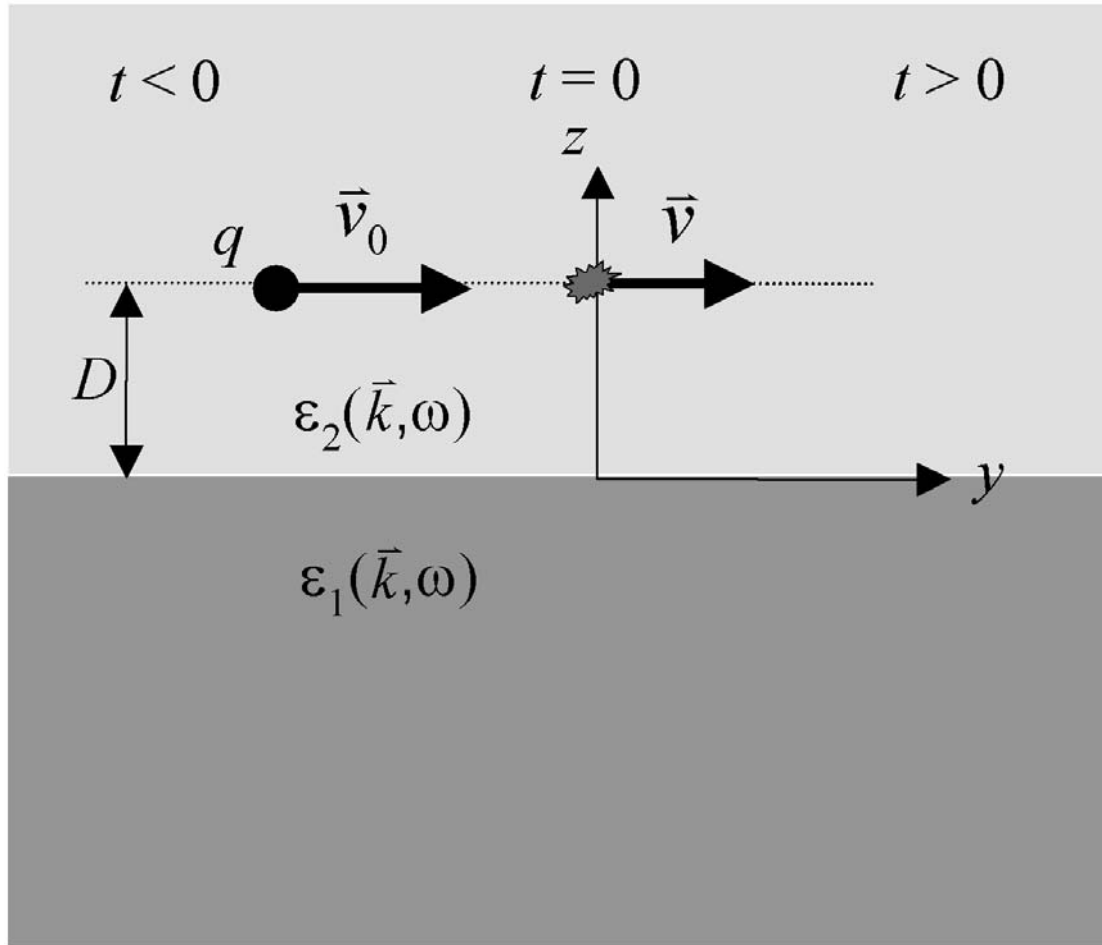


Fig. 3.5 A sketch of the problem studied in the present work. A particle of charge q , velocity \vec{v}_0 moves parallel to the interface of two media of dielectric functions $\epsilon_1(\vec{k}, \omega)$ and $\epsilon_2(\vec{k}, \omega)$. The interface is located at $z = 0$ and the particle is moving along y -direction at a distance D above the interface. At time $t = 0$, the particle experiences an inelastic interaction which changes particle velocity to \vec{v} . Special interest is on the induced potential and the stopping power at $t > 0$.

$$\Phi_1(\vec{k}, \omega) = \frac{4\pi}{k^2 \varepsilon_1(\vec{k}, \omega)} [\rho(\vec{k}, \omega) + \rho_f(\vec{Q}, \omega)] \quad (3.16)$$

for $z < 0$ and

$$\Phi_2(\vec{k}, \omega) = \frac{4\pi}{k^2 \varepsilon_2(\vec{k}, \omega)} [\rho(\vec{k}, \omega) - \rho_f(\vec{Q}, \omega)] \quad (3.17)$$

for $z > 0$, where $\vec{k} = (k_x, k_y, k_z) = (\vec{Q}, k_z)$ is the momentum transfer and ω is the

energy transfer. The Fourier transform of the charge density distribution of the

particle



$$\rho(\vec{r}, t) = q\delta(x)\delta(z - D)[\delta(y - v_0 t)\Theta(-t) + \delta(y - vt)\Theta(t)] \quad (3.18)$$

is given by

$$\rho(\vec{k}, \omega) = qe^{-ik_z D} \left[\int_{-\infty}^0 e^{i(\omega - k_y v_0)\tau} d\tau + \int_0^{\infty} e^{i(\omega - k_y v)\tau} d\tau \right], \quad (3.19)$$

where $\delta(\)$ and $\Theta(\)$ are the delta- and step-functions, respectively. To satisfy the

boundary conditions at the interface, the fictitious charge in Fourier space is given by

$$\rho_f(\vec{Q}, \omega) = \frac{\int_{-\infty}^{\infty} \frac{\rho(\vec{k}, \omega)}{k^2} \left[\frac{1}{\varepsilon_2(\vec{k}, \omega)} - \frac{1}{\varepsilon_1(\vec{k}, \omega)} \right] dk_z}{\int_{-\infty}^{\infty} \frac{1}{k^2} \left[\frac{1}{\varepsilon_2(\vec{k}, \omega)} + \frac{1}{\varepsilon_1(\vec{k}, \omega)} \right] dk_z} . \quad (3.20)$$

Combining Eqs. (3.19) and (3.20), one gets

$$\rho_f(\vec{Q}, \omega) = q \left[\int_{-\infty}^0 e^{i(\omega - k_y v_0)\tau} d\tau + \int_0^{\infty} e^{i(\omega - k_y v)\tau} d\tau \right] \left[\frac{\frac{1}{\bar{\varepsilon}_2(D, \vec{Q}, \omega)} - \frac{1}{\bar{\varepsilon}_1(D, \vec{Q}, \omega)}}{\frac{1}{\bar{\varepsilon}_2(\vec{Q}, \omega)} + \frac{1}{\bar{\varepsilon}_1(\vec{Q}, \omega)}} \right], \quad (3.21)$$

where the effective dielectric function is given by

$$\frac{1}{\bar{\varepsilon}_L(D, \vec{Q}, \omega)} = \frac{1}{2\pi} \int_{-\infty}^{\infty} \frac{e^{-ik_z D}}{k^2 \varepsilon_L(\vec{k}, \omega)} dk_z \quad (3.22)$$

for $L = 1$ and 2 and $\bar{\varepsilon}_L(\vec{Q}, \omega) = \bar{\varepsilon}_L(0, \vec{Q}, \omega)$.

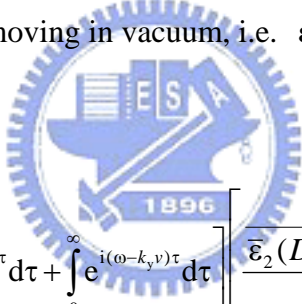
Substituting Eqs. (3.19) - (3.22) into Eqs. (3.16) and (3.17), one obtains the scalar potentials in Fourier space, i.e. $\Phi_1(\vec{k}, \omega)$ and $\Phi_2(\vec{k}, \omega)$. The induced potentials in Fourier space, $\Phi_{1,ind}(\vec{k}, \omega)$ and $\Phi_{2,ind}(\vec{k}, \omega)$, are then obtained by removing the vacuum potential of the particle from scalar potentials. One gets

$$\Phi_{1,ind}(\vec{k}, \omega) = \frac{4\pi}{k^2} \left(\frac{1}{\varepsilon_1(\vec{k}, \omega)} - 1 \right) \rho(\vec{k}, \omega) + \frac{4\pi}{k^2 \varepsilon_1(\vec{k}, \omega)} \rho_f(\vec{Q}, \omega) \quad (3.23)$$

for $z < 0$ and

$$\Phi_{2,ind}(\vec{k}, \omega) = \frac{4\pi}{k^2} \left(\frac{1}{\varepsilon_2(\vec{k}, \omega)} - 1 \right) \rho(\vec{k}, \omega) - \frac{4\pi}{k^2 \varepsilon_2(\vec{k}, \omega)} \rho_f(\vec{Q}, \omega) \quad (3.24)$$

for $z > 0$. If the particle is moving in vacuum, i.e. $\varepsilon_2 = 1$, one gets



$$\Phi_{2,ind}(\vec{k}, \omega) = -\frac{4\pi q}{k^2} \left[\int_{-\infty}^0 e^{i(\omega - k_y v_0)\tau} d\tau + \int_0^{\infty} e^{i(\omega - k_y v)\tau} d\tau \right] \left[\frac{\frac{1}{\bar{\varepsilon}_2(D, \vec{Q}, \omega)} - \frac{1}{\bar{\varepsilon}_1(D, \vec{Q}, \omega)}}{\frac{1}{\bar{\varepsilon}_2(\vec{Q}, \omega)} + \frac{1}{\bar{\varepsilon}_1(\vec{Q}, \omega)}} \right] \quad (3.25)$$

after substituting Eq. (3.21) into Eq. (3.24). Since ε is weakly dependent on k_z

than the rest of \vec{k} components, one may assume $\varepsilon(\vec{k}, \omega) = \varepsilon(\vec{Q}, \omega)$. This

assumption was previously adopted by Yubero *et al.* (Yubero 1992, 1996) in the

analyses of REELS spectra and by Kwei *et al.* (Kwei 1998, 1999) in the calculations

of electron elastic backscattering spectra. Using this assumption, Eq. (3.22) becomes

$$\frac{1}{\bar{\varepsilon}_L(D, \bar{Q}, \omega)} \approx \frac{e^{-|D|\varrho}}{2Q} \frac{1}{\varepsilon_L(\bar{Q}, \omega)} . \quad (3.26)$$

Applying the relation (Hoskins 1999) for the product of the step-function and the

delta-function, i.e. $\Theta(s)\delta(s) = \frac{1}{2}\delta(s)$, Eq. (3.25) may be written as

$$\Phi_{2,ind}(\bar{k}, \omega) = -\frac{4\pi^2 q}{k^2} \left[\delta(\omega - k_y v_0) + \delta(\omega - k_y v) \right] \left[e^{-|D|\varrho} \frac{\varepsilon_1(\bar{Q}, \omega) - 1}{\varepsilon_1(\bar{Q}, \omega) + 1} \right] \quad (3.27)$$

Applying $\varepsilon(\bar{Q}, \omega) = \varepsilon(Q, \omega)$ and $\varepsilon(Q, -\omega) = \varepsilon^*(Q, \omega)$, the induced potential in real

space is obtained by an inverse Fourier transform as

$$\begin{aligned} \Phi_{2,ind}(\bar{r}, t) = & \frac{-q}{\pi^2} \int_0^\infty d\omega \int_0^\infty dk \int_0^\pi \sin \theta d\theta \int_0^{2\pi} d\phi \delta(\omega - k_y v_0) e^{-|D|\varrho} \cos(k_z z) \operatorname{Re} \left[\frac{\varepsilon_1(Q, \omega) - 1}{\varepsilon_1(Q, \omega) + 1} e^{i(k_x x + k_y y - \omega t)} \right] \\ & + \frac{-q}{\pi^2} \int_0^\infty d\omega \int_0^\infty dk \int_0^\pi \sin \theta d\theta \int_0^{2\pi} d\phi \delta(\omega - k_y v) e^{-|D|\varrho} \cos(k_z z) \operatorname{Re} \left[\frac{\varepsilon_1(Q, \omega) - 1}{\varepsilon_1(Q, \omega) + 1} e^{i(k_x x + k_y y - \omega t)} \right] . \end{aligned} \quad (3.28)$$

Expanding the δ -function according to

$$\delta(\omega - kv \sin \theta \sin \phi) = \frac{1}{\sqrt{(kv \sin \theta)^2 - \omega^2}} \left\{ \delta\left(\phi - \sin^{-1} \frac{\omega}{kv \sin \theta}\right) + \delta\left[\phi - \left(\pi - \sin^{-1} \frac{\omega}{kv \sin \theta}\right)\right] \right\} , \quad (3.29)$$

and applying the conservation relations of energy and momentum, it gives

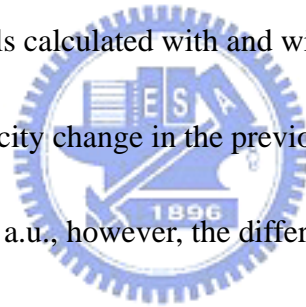
$$\begin{aligned}
\Phi_{2,ind}(\vec{r},t) = & \frac{-2q}{\pi^2} \int_0^E d\omega \int_{k_-}^{k_+} dk \int_{\frac{\omega}{v_0}}^k dQ \frac{Q}{k} \frac{\cos(z\sqrt{k^2-Q^2})}{\sqrt{k^2-Q^2} \sqrt{(Qv_0)^2-\omega^2}} e^{-D|Q|} \cos\left(\frac{x}{v_0} \sqrt{(Qv_0)^2-\omega^2}\right) \\
& \cdot \left\{ \text{Re} \left[\frac{\varepsilon_1(Q,\omega)-1}{\varepsilon_1(Q,\omega)+1} \right] \cos\left(\frac{\omega}{v_0}(y-v_0t)\right) - \text{Im} \left[\frac{\varepsilon_1(Q,\omega)-1}{\varepsilon_1(Q,\omega)+1} \right] \sin\left(\frac{\omega}{v_0}(y-v_0t)\right) \right\} \\
& + \frac{-2q}{\pi^2} \int_0^E d\omega \int_{k_-}^{k_+} dk \int_{\frac{\omega}{v}}^k dQ \frac{Q}{k} \frac{\cos(z\sqrt{k^2-Q^2})}{\sqrt{k^2-Q^2} \sqrt{(Qv)^2-\omega^2}} e^{-D|Q|} \cos\left(\frac{x}{v} \sqrt{(Qv)^2-\omega^2}\right) \\
& \cdot \left\{ \text{Re} \left[\frac{\varepsilon_1(Q,\omega)-1}{\varepsilon_1(Q,\omega)+1} \right] \cos\left(\frac{\omega}{v}(y-vt)\right) - \text{Im} \left[\frac{\varepsilon_1(Q,\omega)-1}{\varepsilon_1(Q,\omega)+1} \right] \sin\left(\frac{\omega}{v}(y-vt)\right) \right\}
\end{aligned} \quad (3.30)$$

where $Q = k \sin \theta$, $k_{\pm} = \sqrt{2ME} \pm \sqrt{2M(E-\omega)}$, M is the mass of the particle, and

$y_p = vt$ is the position of the particle at time t .

The induced potential for a proton moving parallel to the surface of Si was calculated using Eq. (3.30). Results at the position of proton for $y_p = 5$ a.u., $v_0 = 10$ a.u. and $D = 1$ a.u. are plotted in Fig. 3.6 (solid curve) as a function of proton velocity v . These results are compared with corresponding data without the memory effect (dotted curve), where the abscissa v here may also be interpreted as v_0 . It reveals that both curves show a dip around $v = 1.5$ a.u. The existence of a dip was also shown for a proton moving parallel to Al surface in the plasmon-pole dielectric function model (de Abajo 1993). As indicated in the figure, the magnitude of induced potential decreases with increasing velocity for velocities larger than the

dip velocity and increases with increasing velocity for velocities smaller than the dip velocity. Note that there is a significant difference between solid and dotted curves. At $v = 2$ a.u., for instance, solid and dotted curves correspond to $v_0 = 10$ a.u. (with memory effect) and $v_0 = 2$ a.u. (without memory effect), respectively. Since the velocity change, $v_0 - v$, in the solid curve is large so that the difference between solid and dotted curves is also large. At $v = 8$ a.u., on the other hand, solid and dotted curves correspond to $v_0 = 10$ a.u. and 8 a.u., respectively. In this case, the velocity change in the solid curve is small so that the difference is also small. Thus the difference in induced potentials calculated with and without the memory effect increases with increasing velocity change in the previous inelastic interaction when $v \geq 1.5$ a.u.. When $v < 1.5$ a.u., however, the difference decreases with increasing velocity change.



The induced potential shown in Fig. 3.6 is at proton position, i.e. $y = y_p$.

Figure 3.7 plots the induced potential at a position, along the trajectory of proton, with a distance $y - y_p$ from the proton for $y_p = 5$ a.u. and $D = 1$ a.u. The solid curve is results (with memory effect) of the induced potential for $v_0 = 5$ a.u. and $v = 3$ a.u. The dotted and dashed curves are corresponding results (without memory effect) for $v = v_0 = 3$ a.u. and 5 a.u., respectively. In all cases, the induced potential exhibits an oscillation behavior over the distance from the proton, a behavior which was also

observed by Arista (Arista 1994). Note that the induced potential for $v_0 = 5$ a.u. and $v = 3$ a.u. (with memory effect) lies between induced potentials for $v = v_0 = 3$ a.u. and 5 a.u. (without memory effect). This indicates that the induced potential carries a memory effect on proton previous velocity before its last inelastic interaction. A similar plot is made in Fig. 3.8 for a proton moving at distances $D = 1$ (solid curve), 2 (dotted curve) and 3 a.u. (dashed curve) from Si surface with $y_p = 5$ a.u., $v_0 = 5$ a.u. and $v = 3$ a.u. It is seen that as D increases the induced potential (absolute value) decreases. This reveals that the induced potential is greater for a proton moving closer to the solid surface.



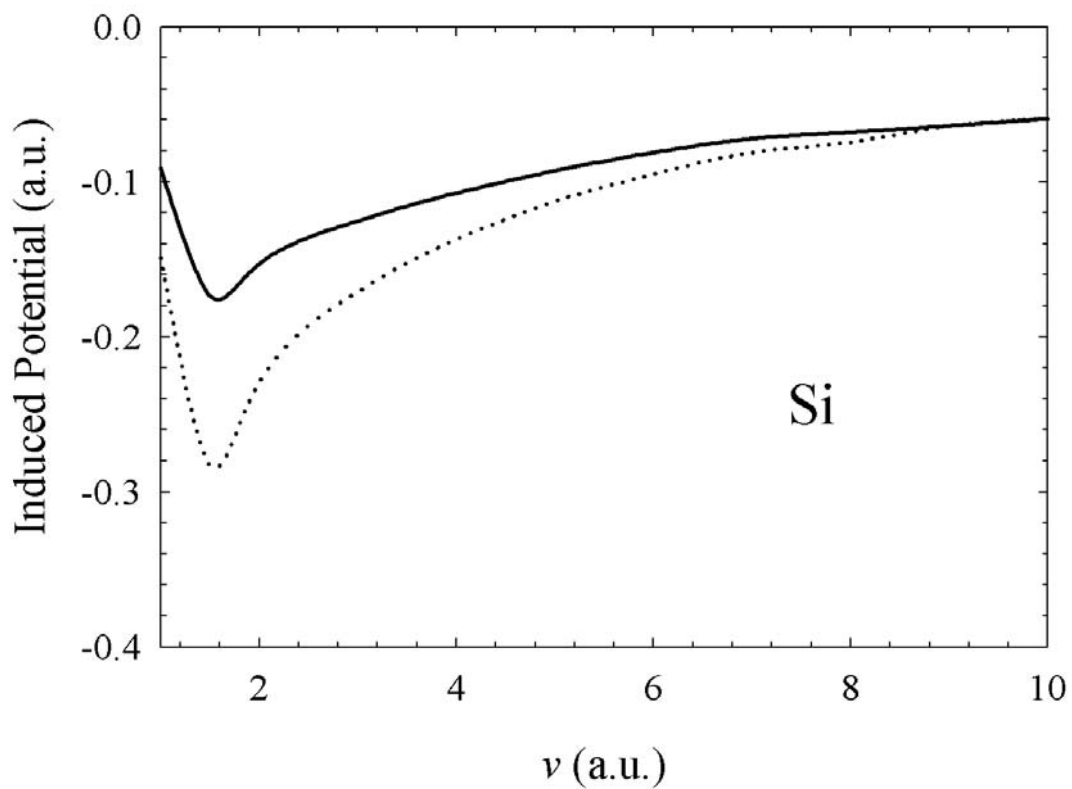


Fig. 3.6 The induced potential for a proton moving parallel to the surface of Si.

Results (solid curve) are plotted at proton position for $y_p = 5$ a.u., $v_0 = 10$ a.u. and

$D = 1$ a.u. as a function of proton velocity v . Corresponding results without the

memory effect are plotted (dotted curve) for a comparison.

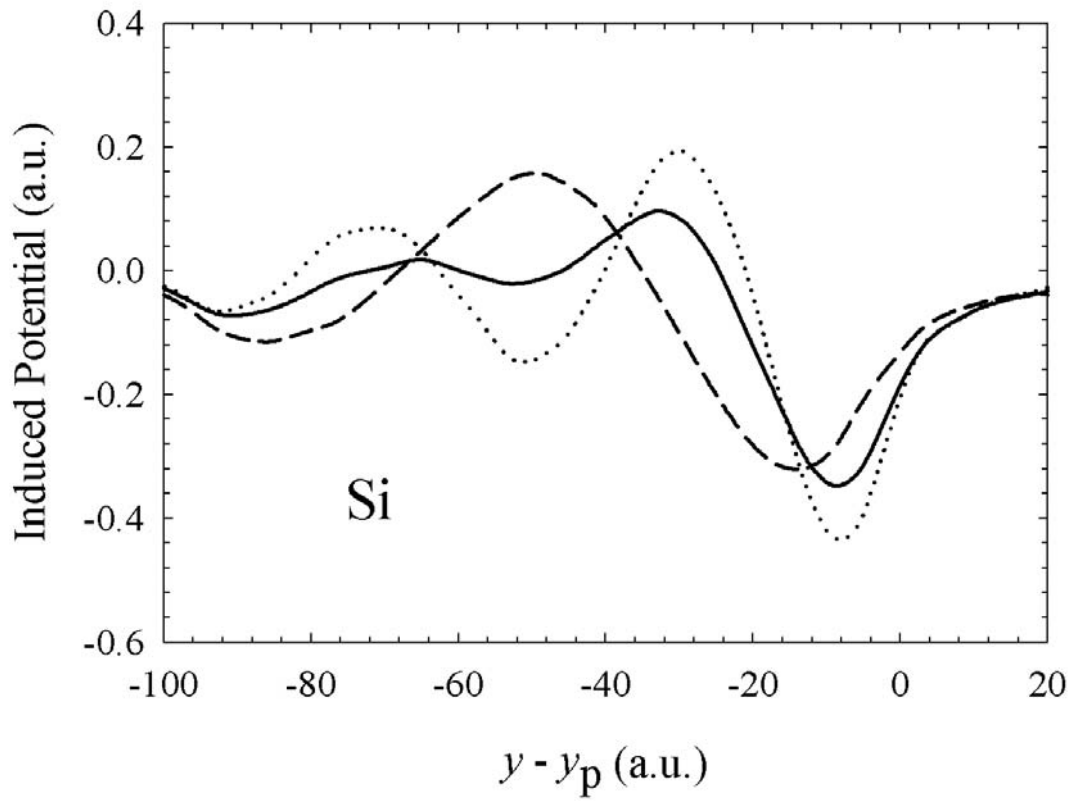


Fig. 3.7 The induced potential at a distance $y - y_p$ from the proton with $y_p = 5$ a.u. and $D = 1$ a.u. from Si surface. The solid curve is results with the memory effect for $\nu_0 = 5$ a.u. and $\nu = 3$ a.u. The dotted and dashed curves are results without the memory effect for $\nu = \nu_0 = 3$ a.u. and 5 a.u., respectively.

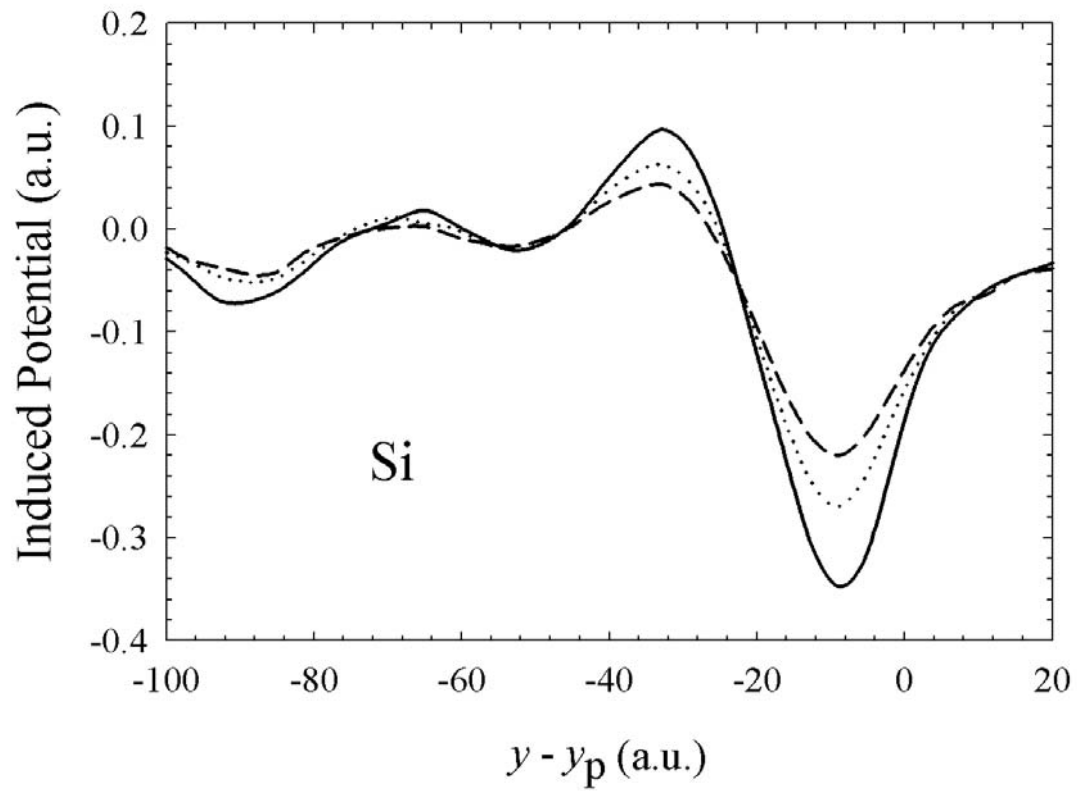


Fig. 3.8 The induced potential at a distance $y - y_p$ from the proton with $D = 1$ (solid curve), 2 (dotted curve) and 3 a.u. (dashed curve) from Si surface. Here $y_p = 5$ a.u., $v_0 = 5$ a.u. and $v = 3$ a.u.

3.2.2 Stopping Power

The stopping power is related to the derivative of $\Phi_{2,ind}(\vec{r}, t)$ at the position of particle, i.e. $\vec{r}_p = (x_p, y_p, z_p) = (0, vt, D)$, for $t > 0$. One finds

$$\begin{aligned}
 F(y_p) = & \frac{2q^2}{\pi^2 v_0} \int_0^E d\omega \int_{k_-}^{k_+} dk \int_{\frac{\omega}{v_0}}^k dQ \frac{Q}{k} \frac{\omega \cos\left(D\sqrt{k^2 - Q^2}\right)}{\sqrt{k^2 - Q^2} \sqrt{(Qv_0)^2 - \omega^2}} e^{-D|Q} \\
 & \cdot \left\{ \operatorname{Re} \left[\frac{\varepsilon_1(Q, \omega) - 1}{\varepsilon_1(Q, \omega) + 1} \right] \sin\left(\frac{\omega}{v_0 v} (v - v_0) y_p\right) + \operatorname{Im} \left[\frac{\varepsilon_1(Q, \omega) - 1}{\varepsilon_1(Q, \omega) + 1} \right] \cos\left(\frac{\omega}{v_0 v} (v - v_0) y_p\right) \right\} . \quad (3.31) \\
 & + \frac{2q^2}{\pi^2 v} \int_0^E d\omega \int_{k_-}^{k_+} dk \int_{\frac{\omega}{v}}^k dQ \frac{Q}{k} \frac{\omega \cos\left(D\sqrt{k^2 - Q^2}\right)}{\sqrt{k^2 - Q^2} \sqrt{(Qv)^2 - \omega^2}} e^{-D|Q} \operatorname{Im} \left[\frac{\varepsilon_1(Q, \omega) - 1}{\varepsilon_1(Q, \omega) + 1} \right]
 \end{aligned}$$

Letting $v = v_0$, Eqs. (3.30) and (3.31) reduce to the same formulas for the induced potential and the stopping power that were derived without memory effect by Kwei *et al* (Kwei 2003).

The stopping power is expressed in terms of the DIIMFP, μ , through

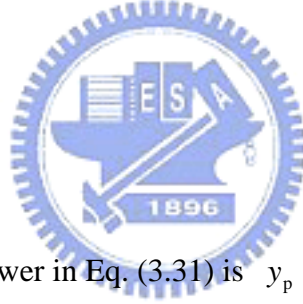
$$F(y_p) = \int_0^E \omega \mu(y_p, \omega) d\omega . \quad (3.32)$$

Therefore, one obtains the DIIMFP as

$$\begin{aligned}
\mu(y_p, \omega) = & \frac{2q^2}{\pi^2 v_0} \int_{k_-}^{k_+} dk \int_{\frac{\omega}{v_0}}^k dQ \frac{Q}{k} \frac{\cos(D\sqrt{k^2 - Q^2})}{\sqrt{k^2 - Q^2} \sqrt{(Qv_0)^2 - \omega^2}} e^{-D|Q|} \\
& \cdot \left\{ \operatorname{Re} \left[\frac{\varepsilon_1(Q, \omega) - 1}{\varepsilon_1(Q, \omega) + 1} \right] \sin \left(\frac{\omega}{v_0 v} (v - v_0) y_p \right) + \operatorname{Im} \left[\frac{\varepsilon_1(Q, \omega) - 1}{\varepsilon_1(Q, \omega) + 1} \right] \cos \left(\frac{\omega}{v_0 v} (v - v_0) y_p \right) \right\} \cdot \quad (3.33) \\
& + \frac{2q^2}{\pi^2 v} \int_0^E d\omega \int_{k_-}^{k_+} dk \int_{\frac{\omega}{v}}^k dQ \frac{Q}{k} \frac{\cos(D\sqrt{k^2 - Q^2})}{\sqrt{k^2 - Q^2} \sqrt{(Qv)^2 - \omega^2}} e^{-D|Q|} \operatorname{Im} \left[\frac{\varepsilon_1(Q, \omega) - 1}{\varepsilon_1(Q, \omega) + 1} \right]
\end{aligned}$$

And the IMFP, λ , is given by

$$\frac{1}{\lambda(y_p)} = \int_0^E \mu(y_p, \omega) d\omega. \quad (3.34)$$



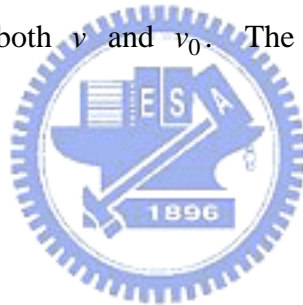
Note that the stopping power in Eq. (3.31) is y_p dependent. Thus the stopping power with memory effect may be obtained by an average over all particles paths

$$F = \frac{\int_0^\infty \frac{y_p}{\lambda(y_p)} e^{-y_p/\lambda(y_p)} (F(y_p)) dy_p}{\int_0^\infty \frac{y_p}{\lambda(y_p)} e^{-y_p/\lambda(y_p)} dy_p}, \quad (3.35)$$

where $\frac{y_p}{\lambda(y_p)} e^{-y_p/\lambda(y_p)}$ is the probability that the particle encounters an inelastic

interaction in the distance y_p (Yubero 1992; Raether 1980).

Figure 3.9 shows results of the stopping power for a proton moving parallel to and with at a distance $D = 2$ a.u. from the Si surface. Solid and dotted curves are for $v_0 = 10$ a.u. (with memory effect) and $v_0 = v$ (without memory effect), respectively. The existence of a maximum stopping power at a velocity around 1.5 a.u. was shown. The existence of a maximum was also found for some semi-infinite solids by Arista (Arista 1994). A notable difference between solid and dotted curves was shown in the figure. Without the memory effect, the stopping power is solely determined by v without reference to v_0 . With the memory effect, however, the stopping power is affected by both v and v_0 . The memory effect reduced the stopping power for the proton.



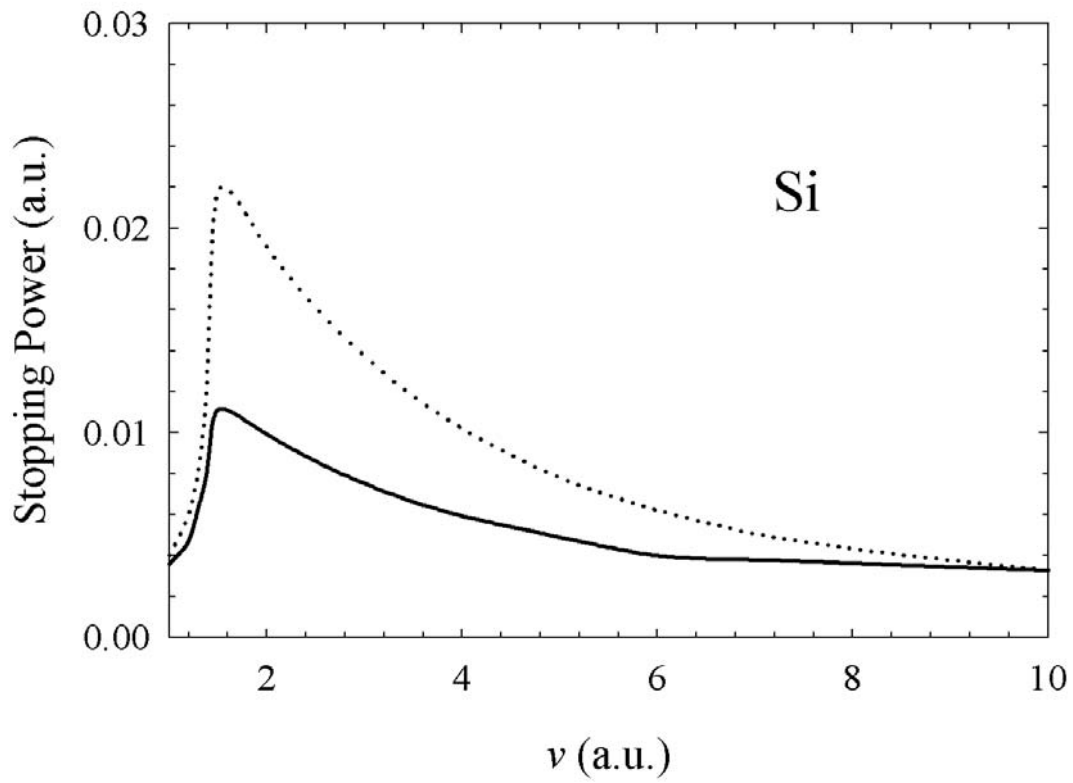


Fig. 3.9 Results of the stopping power for a proton moving parallel to with a distance $D = 2$ a.u. from the Si surface. Solid and dotted curves are for $v_0 = 10$ a.u. (with memory effect) and $v_0 = v$ (without memory effect), respectively.

3.2.3 Differential Inverse Inelastic Mean Free Path

Letting $q = M = 1$ in Eq. (3.33), one finds the position dependent DIIMFP for an electron

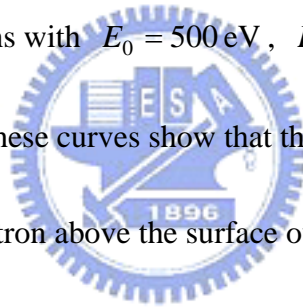
$$\begin{aligned} \mu(y_p, \omega) = & \frac{\sqrt{2}}{\pi^2 \sqrt{E_0}} \int_{k_-}^{k_+} dk \int_{\omega/\sqrt{2E_0}}^k dQ \frac{Q}{k} \frac{\cos(D\sqrt{k^2 - Q^2})}{\sqrt{k^2 - Q^2} \sqrt{2E_0 Q^2 - \omega^2}} e^{-D|Q|} \\ & \cdot \left\{ \operatorname{Re} \left[\frac{\varepsilon_1(Q, \omega) - 1}{\varepsilon_1(Q, \omega) + 1} \right] \sin \left(\frac{\sqrt{E} - \sqrt{E_0}}{\sqrt{2E_0 E}} \omega y_p \right) + \operatorname{Im} \left[\frac{\varepsilon_1(Q, \omega) - 1}{\varepsilon_1(Q, \omega) + 1} \right] \cos \left(\frac{\sqrt{E} - \sqrt{E_0}}{\sqrt{2E_0 E}} \omega y_p \right) \right\} . \quad (3.36) \\ & + \frac{\sqrt{2}}{\pi^2 \sqrt{E}} \int_0^E d\omega \int_{k_{\min}}^{k_{\max}} dk \int_{\omega/\sqrt{2E}}^k dQ \frac{Q}{k} \frac{\cos(D\sqrt{k^2 - Q^2})}{\sqrt{k^2 - Q^2} \sqrt{2E \cdot Q^2 - \omega^2}} e^{-D|Q|} \operatorname{Im} \left[\frac{\varepsilon_1(Q, \omega) - 1}{\varepsilon_1(Q, \omega) + 1} \right] \end{aligned}$$

The DIIMFP with the memory effect for an electron is then given by

$$\mu(\omega) = \frac{\int_0^\infty \frac{y_p}{\lambda(y_p)} e^{-y_p/\lambda(y_p)} (\mu(y_p, \omega)) dy_p}{\int_0^\infty \frac{y_p}{\lambda(y_p)} e^{-y_p/\lambda(y_p)} dy_p} . \quad (3.37)$$

DIIMFPs with the memory effect were calculated for electrons moving parallel to the Cu surface. Figure 3.10 shows a plot of the DIIMFP with the memory effect as a function of energy transfer for electrons with $D = 1$ a.u., $E_0 = 800$ eV and

$E = 500 \text{ eV}$. Corresponding DIIMFPs without the memory effect for $E_0 = E = 800 \text{ eV}$ and $E_0 = E = 500 \text{ eV}$ are plotted for comparison. It is seen that the DIIMFP with the memory effect exhibits a similar shape to that of the DIIMFP without the memory effect. The magnitude of the DIIMFP with the memory effect for preceding and succeeding electron energies E_0 and E lies between the DIIMFPs without the memory effect for constant electron energies E_0 and E . This result indicates that the moving electron keeps some memory of its previous energy E_0 in the next interaction. A plot of the DIIMFP with the memory effect is shown in Fig. 3.11 for electrons with $E_0 = 500 \text{ eV}$, $E = 300 \text{ eV}$ and $D = 1, 2$ and 3 a.u. above the Cu surface. These curves show that the DIIMFP decreases with increasing distance of the electron above the surface owing to the weaker response by the solid.



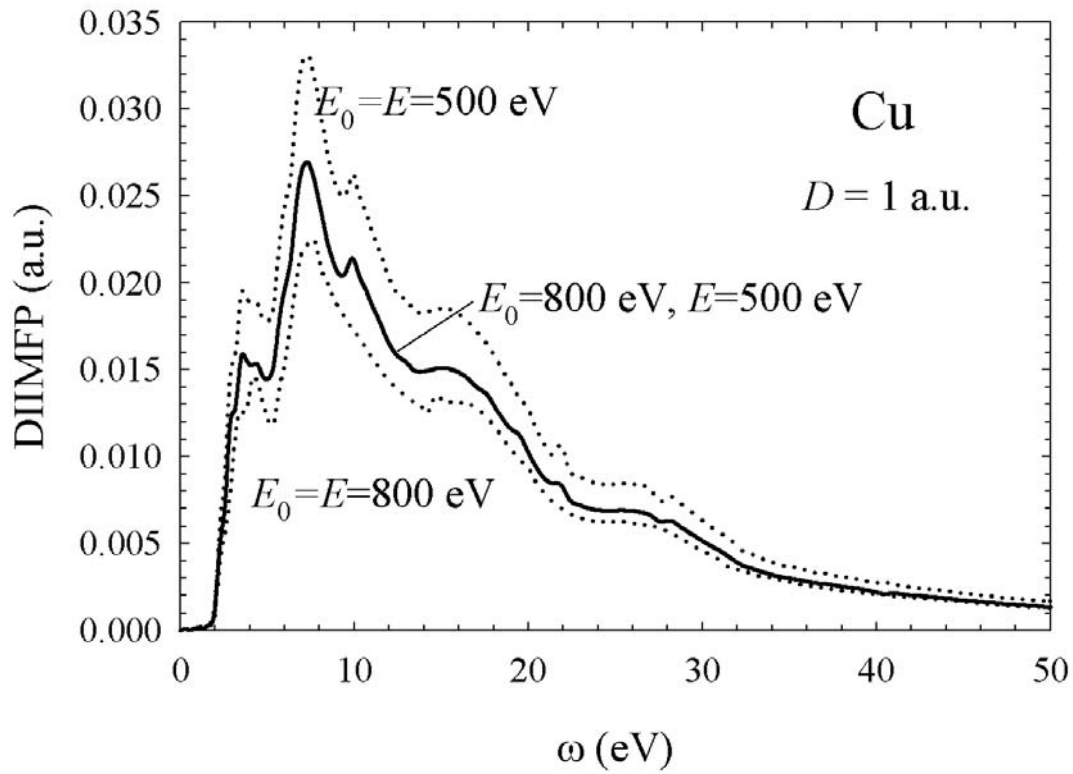


Fig. 3.10 A comparison of the DIIMFPs with (solid curve) and without (dotted curves) the memory effect for electrons moving parallel to the Cu surface at a distance $D = 1$ a.u. The DIIMFP with the memory effect is calculated for preceding and succeeding electron energies $E_0 = 800$ eV and $E = 500$ eV. The DIIMFPs without the memory effect are calculated for constant electron energies $E_0 = E = 500$ eV and $E_0 = E = 800$ eV.

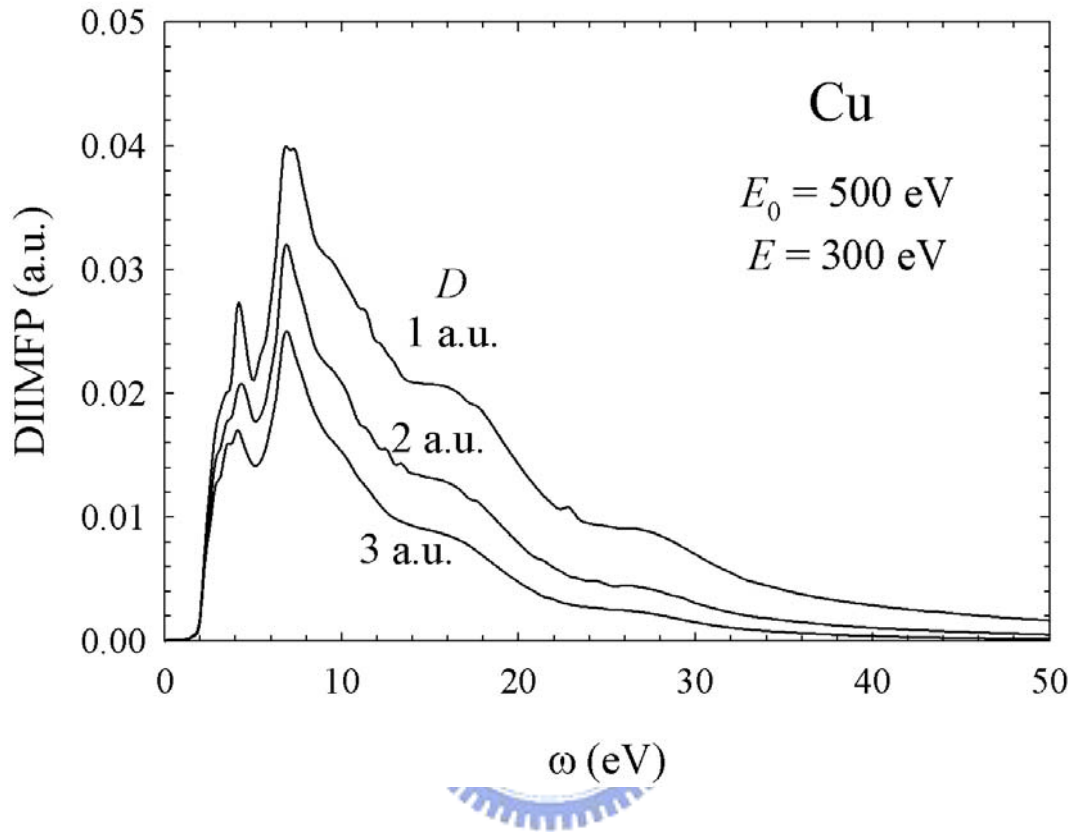


Fig. 3.11 A plot of the DIIMFPs with the memory effect for electrons of preceding and succeeding energies $E_0 = 500 \text{ eV}$ and $E = 300 \text{ eV}$. These electrons are moving at various distances D from the Cu surface.

3.2.4 Inelastic Mean Free Path

The IMFP with the memory effect for an electron may be calculated from

$$\lambda = \frac{1}{\int_0^E \mu(\omega) d\omega} . \quad (3.38)$$

A comparison of IMFPs with (solid curve) and without (dotted curve) the memory effect is shown in Fig. 3.12 for electrons moving parallel to the Cu surface at $D = 1$ a.u. The IMFP with the memory effect is calculated for preceding electron energy $E_0 = 800$ eV as a function of succeeding electron energy E . The IMFP without the memory effect is calculated for constant electron energy $E_0 = E$. At $E = 300$ eV, for instance, the solid and dotted curves correspond to $E_0 = 800$ eV (with memory effect) and $E_0 = 300$ eV (without memory effect), respectively. It should be noted that there is a significant difference between the solid and dotted curves. When the energy difference, $E_0 - E$, for the solid curve is large, the difference between solid and dotted curves is also large. At $E = 700$ eV, on the other hand, the solid and dotted curves correspond to $E_0 = 800$ eV and $E_0 = 700$ eV, respectively. In this case, the energy difference is small, and the difference between

the curves is also small. Thus the memory effect, proportional to the difference between solid and dotted curves, decreases with decreasing $E_0 - E$ and approaches zero at $E = E_0$. Moreover, the IMFP with the memory effect for given preceding energy E_0 and succeeding energy E is between the IMFPs without the memory effect for these given energies. The IMFP with the memory effect for $E_0 = 800$ eV and $E = 500$ eV (solid curve in Fig. 3.12), for instance, is between IMFPs without the memory effect for 500 eV and 800 eV (dotted curve). This result indicates that the previous electron energy has also an effect on the succeeding inelastic interaction.



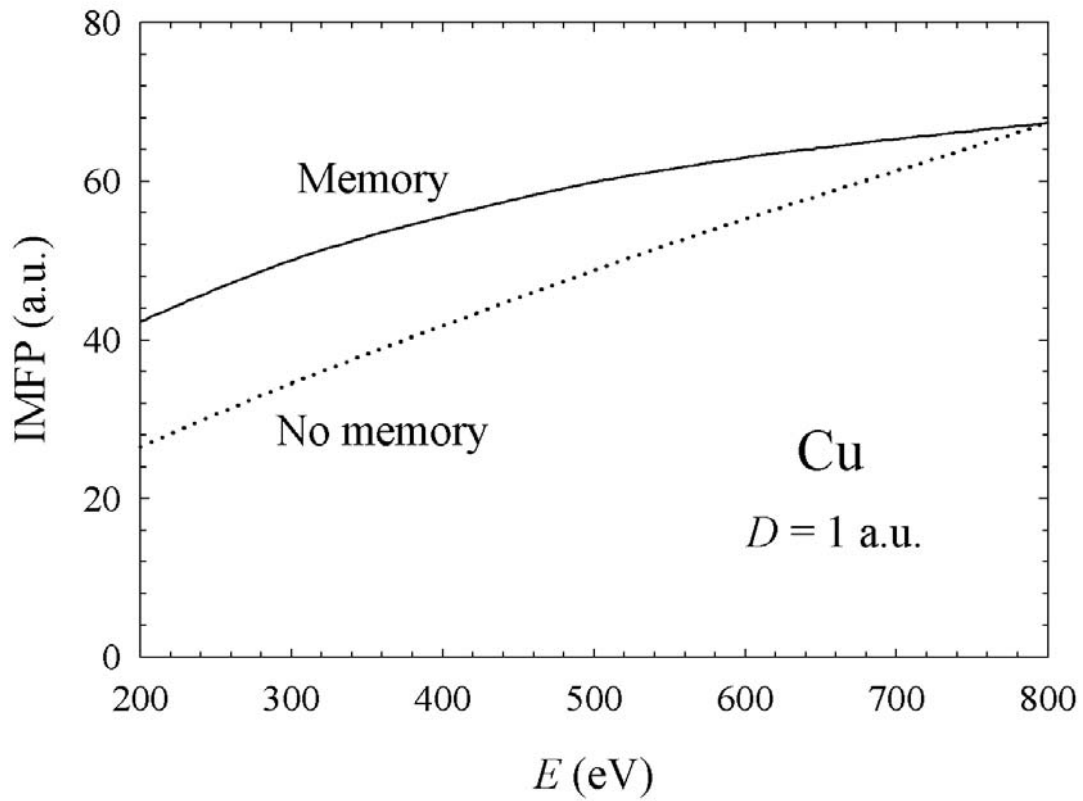


Fig. 3.12 A comparison of the IMFPs with (solid curve) and without (dotted curve) the memory effect for electrons moving parallel to the Cu surface at a distance $D = 1$ a.u. The IMFP with the memory effect is calculated for a preceding electron energy $E_0 = 800$ eV as a function of succeeding electron energy E . The IMFP without the memory effect is calculated for constant electron energy $E_0 = E$.

CHAPTER 4

ELECTRONIC EXCITATIONS IN CYLINDRICAL SYSTEMS

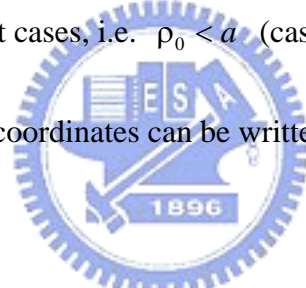
In the past few years, new developments in fabrications have allowed the production of miniaturized devices with typical sizes ranging in the nanometer scale. The study of these devices in surface-sensitive electron spectroscopies has become an active field of research. Quantitative information on the electron inelastic interaction cross sections plays a crucial role in such surface spectroscopies (Tougaard 1987; Tanuma 1991; Jablonski 2005; Werner 2005). Recently, several theoretical approaches have been developed to evaluate these cross-sections in cylindrical systems (Chu 1984; Walsh 1989; Zabala 1989, 2001; Rivacoba 1995; Tökési 1999, 2000; Arista 2001; Gervasoni 2003). In this chapter, a theoretical model of inelastic scattering for electrons moving parallel to the axis of a cylindrical wire or cavity will be constructed. After that, a more general model inelastic scattering for electrons moving parallel to the axis of a clad cylindrical system will be derived.

4.1 Inelastic Interactions of Electrons with Cylindrical Systems

Figure 4.1 illustrates the configuration in which an electron with velocity \bar{v} and energy $E = v^2/2$ moves parallel to the axis of a cylinder of radius a and dielectric function $\epsilon_1(k, \omega)$. This cylinder is embedded in a surrounding medium of dielectric function $\epsilon_2(k, \omega)$. At time t , the electron is at a position $\bar{x}_0 = (\rho_0, 0, vt)$ in cylindrical coordinates.

4.1.1 Induced Potential

Considering two different cases, i.e. $\rho_0 < a$ (case I) and $\rho_0 > a$ (case II), the scalar potential in cylindrical coordinates can be written as (Jackson 1975)



$$\Phi_1^{(p)}(\rho, \phi, z, t) = \frac{-1}{\pi\epsilon_1} \sum_{m=-\infty}^{\infty} \int_{-\infty}^{\infty} dk A_m^{(p)} I_m(k\rho) e^{ik(z-vt)+im\phi} + \delta_{p,I} \frac{1}{\epsilon_1} \Phi_0(\rho, \phi, z, t) \quad (4.1a)$$

for $\rho < a$ and

$$\Phi_2^{(p)}(\rho, \phi, z, t) = \frac{-1}{\pi\epsilon_2} \sum_{m=-\infty}^{\infty} \int_{-\infty}^{\infty} dk B_m^{(p)} K_m(k\rho) e^{ik(z-vt)+im\phi} + \delta_{p,II} \frac{1}{\epsilon_2} \Phi_0(\rho, \phi, z, t) \quad (4.1b)$$

for $\rho > a$. Here $A_m^{(p)}$ and $B_m^{(p)}$ are coefficients to be determined, $p = I$ and II are for cases I and II respectively, I_m and K_m are modified Bessel functions, δ is

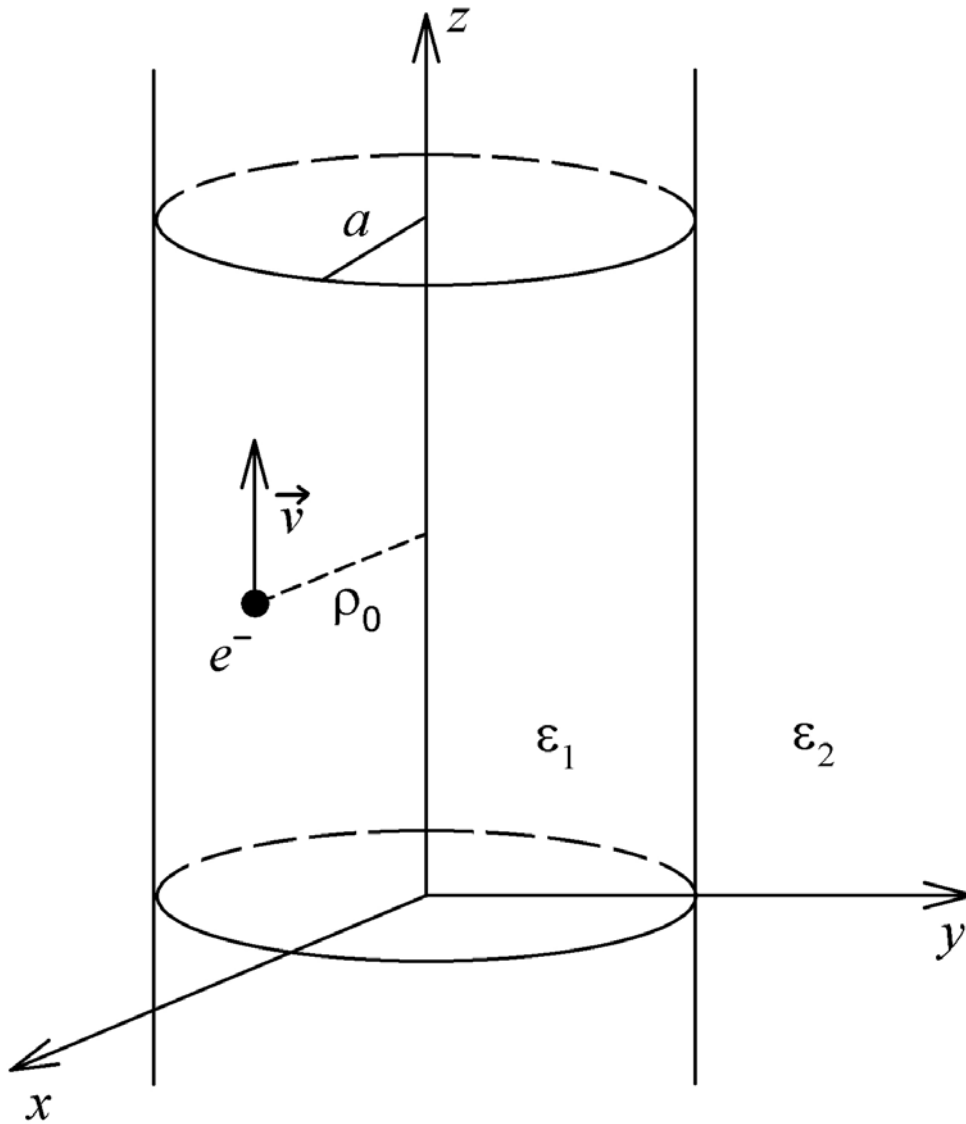


Fig. 4.1 A sketch of the configuration studied in the present work. An electron of velocity \vec{v} moves parallel to and at a distance ρ_0 from the axis of an infinitely long cylinder of radius a . The media inside and outside the cylinder have dielectric functions $\varepsilon_1(k, \omega)$ and $\varepsilon_2(k, \omega)$, respectively.

the delta function,

$$\Phi_0(\rho, \phi, z, t) = \frac{-1}{\pi} \sum_{m=-\infty}^{\infty} \int_{-\infty}^{\infty} dk I_m(k\rho_<) K_m(k\rho_>) e^{ik(z-vt)+im\phi} \quad (4.2)$$

is the potential of the electron in vacuum with $\rho_> = \max(\rho, \rho_0)$ and

$\rho_< = \min(\rho, \rho_0)$. The Fourier transforms of these potentials are

$$\Phi_1^{(p)}(\rho, \phi, k, \omega) = \frac{-4\pi}{\epsilon_1(k, \omega)} \sum_{m=-\infty}^{\infty} A_m^{(p)}(k, \omega) I_m(k\rho) e^{im\phi} \delta(\omega - kv) + \delta_{p,1} \frac{1}{\epsilon_1(k, \omega)} \Phi_0(\rho, \phi, k, \omega) \quad (4.3a)$$



for $\rho < a$, and

$$\Phi_2^{(p)}(\rho, \phi, k, \omega) = \frac{-4\pi}{\epsilon_2(k, \omega)} \sum_{m=-\infty}^{\infty} B_m^{(p)}(k, \omega) K_m(k\rho) e^{im\phi} \delta(\omega - kv) + \delta_{p,II} \frac{1}{\epsilon_2(k, \omega)} \Phi_0(\rho, \phi, k, \omega) \quad (4.3b)$$

for $\rho > a$, where

$$\Phi_0(\rho, \phi, k, \omega) = -4\pi \sum_{m=-\infty}^{\infty} I_m(k\rho_<) K_m(k\rho_>) e^{im\phi} \delta(\omega - kv) \quad (4.4)$$

4.1.1.1 Case I. Electrons Moving in Medium 1 (i.e. $\rho_0 < a$)

Applying boundary conditions, i.e. continuity of the potential and the normal

component of electric displacement at the interface $\rho = a$, one finds

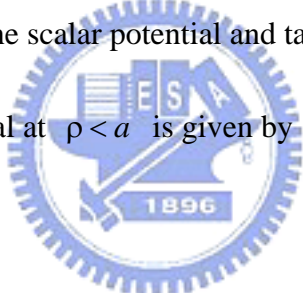
$$A_m^{(1)}(k, \omega) = \frac{[\varepsilon_2(k, \omega) - \varepsilon_1(k, \omega)]K_m(ka)K_m'(ka)I_m(k\rho_0)}{\varepsilon_1(k, \omega)K_m(ka)I_m'(ka) - \varepsilon_2(k, \omega)I_m(ka)K_m'(ka)} \quad (4.5a)$$

$$B_m^{(1)}(k, \omega) = \frac{\varepsilon_2(k, \omega)[K_m(ka)I_m'(ka) - I_m(ka)K_m'(ka)]I_m(k\rho_0)}{\varepsilon_1(k, \omega)K_m(ka)I_m'(ka) - \varepsilon_2(k, \omega)I_m(ka)K_m'(ka)}, \quad (4.5b)$$

where $I_m'(x) = dI_m(x)/dx$ and $K_m'(x) = dK_m(x)/dx$. Removing the vacuum

potential of an electron from the scalar potential and taking the inverse Fourier

transform, the induced potential at $\rho < a$ is given by



$$\Phi_{1,ind}^{(1)}(\rho, \phi, z, t) = \frac{-2}{\pi v} \sum_{m=-\infty}^{\infty} e^{im\phi} \int_0^E d\omega \left[\begin{aligned} & I_m\left(\frac{\omega}{v}\rho\right) \left\{ \operatorname{Re} \left[\frac{A_m^{(1)}\left(\frac{\omega}{v}, \omega\right)}{\varepsilon_1\left(\frac{\omega}{v}, \omega\right)} \cos\left(\omega\left(\frac{z}{v} - t\right)\right) - \operatorname{Im} \left[\frac{A_m^{(1)}\left(\frac{\omega}{v}, \omega\right)}{\varepsilon_1\left(\frac{\omega}{v}, \omega\right)} \sin\left(\omega\left(\frac{z}{v} - t\right)\right) \right] \right\} \\ & + I_m\left(\frac{\omega}{v}\rho_{<}\right) K_m\left(\frac{\omega}{v}\rho_{>}\right) \left\{ \operatorname{Re} \left[\frac{1}{\varepsilon_1\left(\frac{\omega}{v}, \omega\right)} - 1 \right] \cos\left(\omega\left(\frac{z}{v} - t\right)\right) - \operatorname{Im} \left[\frac{1}{\varepsilon_1\left(\frac{\omega}{v}, \omega\right)} \right] \sin\left(\omega\left(\frac{z}{v} - t\right)\right) \right\} \end{aligned} \right]. \quad (4.6)$$

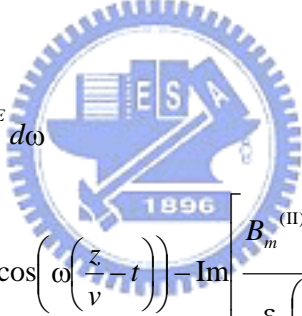
4.1.1.2 Case II. Electrons Moving in Medium 2 (i.e. $\rho_0 > a$)

Similarly, applying boundary conditions, one finds

$$A_m^{(II)}(k, \omega) = \frac{\varepsilon_1(k, \omega)[K_m(ka)I_m'(ka) - I_m(ka)K_m'(ka)]K_m(k\rho_0)}{\varepsilon_1(k, \omega)K_m(ka)I_m'(ka) - \varepsilon_2(k, \omega)I_m(ka)K_m'(ka)}, \quad (4.7a)$$

$$B_m^{(II)}(k, \omega) = \frac{[\varepsilon_2(k, \omega) - \varepsilon_1(k, \omega)]I_m(ka)I_m'(ka)K_m(k\rho_0)}{\varepsilon_1(k, \omega)K_m(ka)I_m'(ka) - \varepsilon_2(k, \omega)I_m(ka)K_m'(ka)}. \quad (4.7b)$$

Removing the vacuum potential of an electron from the scalar potential and taking the inverse Fourier transform, the induced potential at $\rho > a$ is given by



$$\Phi_{2,ind}^{(II)}(\rho, \phi, z, t) = \frac{-2}{\pi v} \sum_{m=-\infty}^{\infty} e^{im\phi} \int_0^E d\omega \left[K_m\left(\frac{\omega}{v}\rho\right) \left\{ \operatorname{Re} \left[\frac{B_m^{(II)}\left(\frac{\omega}{v}, \omega\right)}{\varepsilon_2\left(\frac{\omega}{v}, \omega\right)} \cos\left(\omega\left(\frac{z}{v} - t\right)\right) - \operatorname{Im} \left[\frac{B_m^{(II)}\left(\frac{\omega}{v}, \omega\right)}{\varepsilon_2\left(\frac{\omega}{v}, \omega\right)} \sin\left(\omega\left(\frac{z}{v} - t\right)\right) \right] \right\} \right. \\ \left. + I_m\left(\frac{\omega}{v}\rho_{<}\right) K_m\left(\frac{\omega}{v}\rho_{>}\right) \left\{ \operatorname{Re} \left[\frac{1}{\varepsilon_2\left(\frac{\omega}{v}, \omega\right)} - 1 \right] \cos\left(\omega\left(\frac{z}{v} - t\right)\right) - \operatorname{Im} \left[\frac{1}{\varepsilon_2\left(\frac{\omega}{v}, \omega\right)} \right] \sin\left(\omega\left(\frac{z}{v} - t\right)\right) \right\} \right]. \quad (4.8)$$

4.1.2 Stopping Power

4.1.2.1 Case I. Electrons Moving in Medium 1 (i.e. $\rho_0 < a$)

Since the stopping power, $F^{(I)}$, is related to the derivative of $\Phi_{1,ind}^{(I)}(\rho, \phi, z, t)$

at the position of electrons. One obtains

$$F^{(I)} = \frac{-2}{\pi v^2} \sum_{m=-\infty}^{\infty} \int_0^E d\omega \omega I_m \left(\frac{\omega}{v} \rho_0 \right) \left\{ \text{Im} \left[\frac{A_m^{(I)} \left(\frac{\omega}{v}, \omega \right)}{\varepsilon_1 \left(\frac{\omega}{v}, \omega \right)} \right] + K_m \left(\frac{\omega}{v} \rho_0 \right) \text{Im} \left[\frac{1}{\varepsilon_1 \left(\frac{\omega}{v}, \omega \right)} \right] \right\}. \quad (4.9)$$

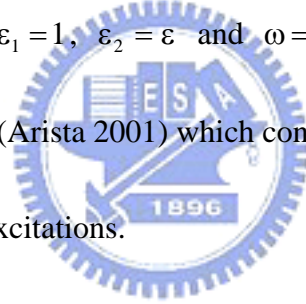
Note that this equation contains contributions from all relevant excitations including

volume, surface and interface excitations. For an electron moving inside a

cylindrical cavity, i.e. taking $\varepsilon_1 = 1$, $\varepsilon_2 = \varepsilon$ and $\omega = kv$ in Eq. (4.9), one obtains

the formula derived by Arista (Arista 2001) which contains only surface excitations

but no volume and interface excitations.



4.1.2.2 Case II. Electrons Moving in Medium 2 (i.e. $\rho_0 > a$)

Since the stopping power, $F^{(II)}$, is related to the derivative of $\Phi_{2,ind}^{(II)}(\rho, \phi, z, t)$

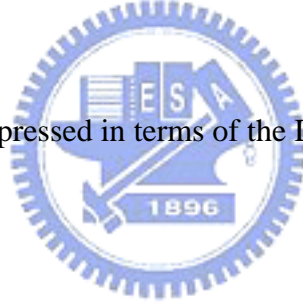
at the position of electrons. One obtains

$$F^{(II)} = \frac{-2}{\pi v^2} \sum_{m=-\infty}^{\infty} \int_0^E d\omega \omega K_m \left(\frac{\omega}{v} \rho_0 \right) \left\{ \text{Im} \left[\frac{B_m^{(II)} \left(\frac{\omega}{v}, \omega \right)}{\varepsilon_2 \left(\frac{\omega}{v}, \omega \right)} \right] + I_m \left(\frac{\omega}{v} \rho_0 \right) \text{Im} \left[\frac{1}{\varepsilon_2 \left(\frac{\omega}{v}, \omega \right)} \right] \right\}. \quad (4.10)$$

Similarly, this equation contains contributions from all relevant excitations including volume, surface and interface excitations. For an electron moving outside a cylindrical wire, i.e. taking $\epsilon_1 = \epsilon$, $\epsilon_2 = 1$ and $\omega = kv$ in Eq. (4.10), one obtains the formula derived by Gervasoni (Gervasoni 2003) which contains only surface excitations but no volume and interface excitations.

4.1.3 Differential Inverse Inelastic Mean Free Path

The stopping power is expressed in terms of the DIIMFP, $\mu^{(p)}$, through



$$F^{(p)} = \int_0^E \omega \mu^{(p)}(E, \omega) d\omega \quad , \quad (4.11)$$

where $p = I$ and II are for cases I and II respectively. Therefore, one obtains the

DIIMFP for an electron moving inside the cylinder, i.e. $\rho_0 < a$, as

$$\mu^{(I)}(E, \omega) = \frac{-2}{\pi v^2} \sum_{m=-\infty}^{\infty} I_m \left(\frac{\omega}{v} \rho_0 \right) \left\{ \text{Im} \left[\frac{A_m^{(I)} \left(\frac{\omega}{v}, \omega \right)}{\epsilon_1 \left(\frac{\omega}{v}, \omega \right)} \right] + K_m \left(\frac{\omega}{v} \rho_0 \right) \text{Im} \left[\frac{1}{\epsilon_1 \left(\frac{\omega}{v}, \omega \right)} \right] \right\} . \quad (4.12)$$

A similar approach can be made for an electron moving outside the cylinder, i.e.

$\rho_0 > a$. The DIIMFP is given by

$$\mu^{(II)}(E, \omega) = \frac{-2}{\pi v^2} \sum_{m=-\infty}^{\infty} K_m\left(\frac{\omega}{v} \rho_0\right) \left\{ \text{Im} \left[\frac{B_m^{(II)}\left(\frac{\omega}{v}, \omega\right)}{\varepsilon_2\left(\frac{\omega}{v}, \omega\right)} \right] + I_m\left(\frac{\omega}{v} \rho_0\right) \text{Im} \left[\frac{1}{\varepsilon_2\left(\frac{\omega}{v}, \omega\right)} \right] \right\}, \quad (4.13)$$

Taking $a \rightarrow \infty$ and $\varepsilon_1 = \varepsilon_2 = \varepsilon$ in Eq. (4.12) or $a = 0$ and $\varepsilon_1 = \varepsilon_2 = \varepsilon$ in Eq.

(4.13), the DIIMFP in an infinite medium is obtained as

$$\mu(E, \omega) = \frac{-2}{\pi v^2} \sum_{m=-\infty}^{\infty} I_m\left(\frac{\omega}{v} \rho_0\right) K_m\left(\frac{\omega}{v} \rho_0\right) \text{Im} \left[\frac{1}{\varepsilon\left(\frac{\omega}{v}, \omega\right)} \right]. \quad (4.14)$$

Using Eqs. (4.12) and (4.13), the DIIMFP was calculated for an electron moving parallel to the axis of a cylindrical structure. In these calculations, a sum-rule-constrained extended Drude dielectric function with dispersion (Kwei 2003) was applied. Figure 4.2 shows the results of this DIIMFP as a function of energy loss ω for a 500 eV electron at several distances ρ_0 from the center of a Si cylinder of radius $a = 20$ a.u. For an electron moving inside the solid, i.e. $\rho_0 < a$, the DIIMFP (upper diagram) contains two peaks corresponding to surface and volume

excitations. As the electron moves closer to the cylinder surface, i.e. $\rho_0 \rightarrow a$, the volume excitation peak (~ 17 eV) decreases in intensity, whereas the surface excitation peak (~ 12 eV) increases in intensity. For an electron moving in vacuum, i.e. $\rho_0 > a$, the DIIMFP (lower diagram) is due entirely to contributions from surface excitations. The DIIMFP becomes smaller for larger electron distance from the surface.

Similar results for the DIIMFP of a 500 eV electron moving parallel to the axis of a cylindrical cavity in Si are plotted in Fig. 4.3. Again, surface excitations (~ 12 eV) occur for an electron moving either in the cavity (upper diagram) or in Si (lower diagram), whereas volume excitations (~ 17 eV) occur only for an electron in Si. For an electron outside the cavity (lower diagram), the contributions from surface and volume excitations become smaller and larger, respectively, for increasing ρ_0 . At $\rho_0 \sim 30$ a.u., the DIIMFP is due entirely to volume excitations.

Figure 4.4 is a plot of the DIIMFP for an electron moving outside the Si cylinder ($a = 20$ a.u.) at $\rho_0 = 21$ a.u. for several electron energies. It is seen that the DIIMFP, contributed only from surface excitations, decreases with increasing electron energy. The peak surface plasmon energy, however, remains unchanged.

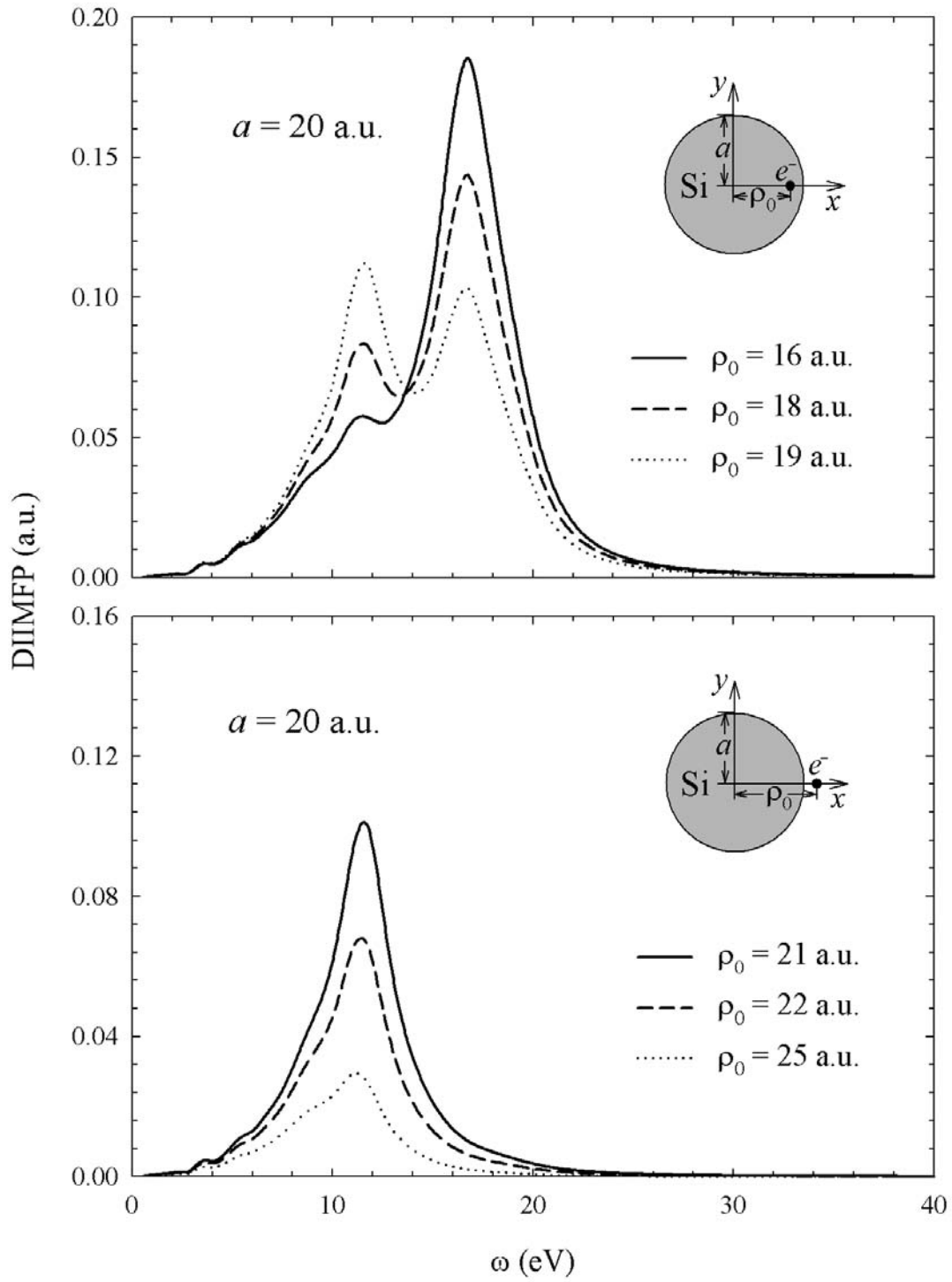


Fig. 4.2 Calculated DIIMFPs for a 500 eV electron moving parallel to the axis of a Si cylinder (radius $a = 20$ a.u.) in vacuum for several electron distances ρ_0 from the axis.

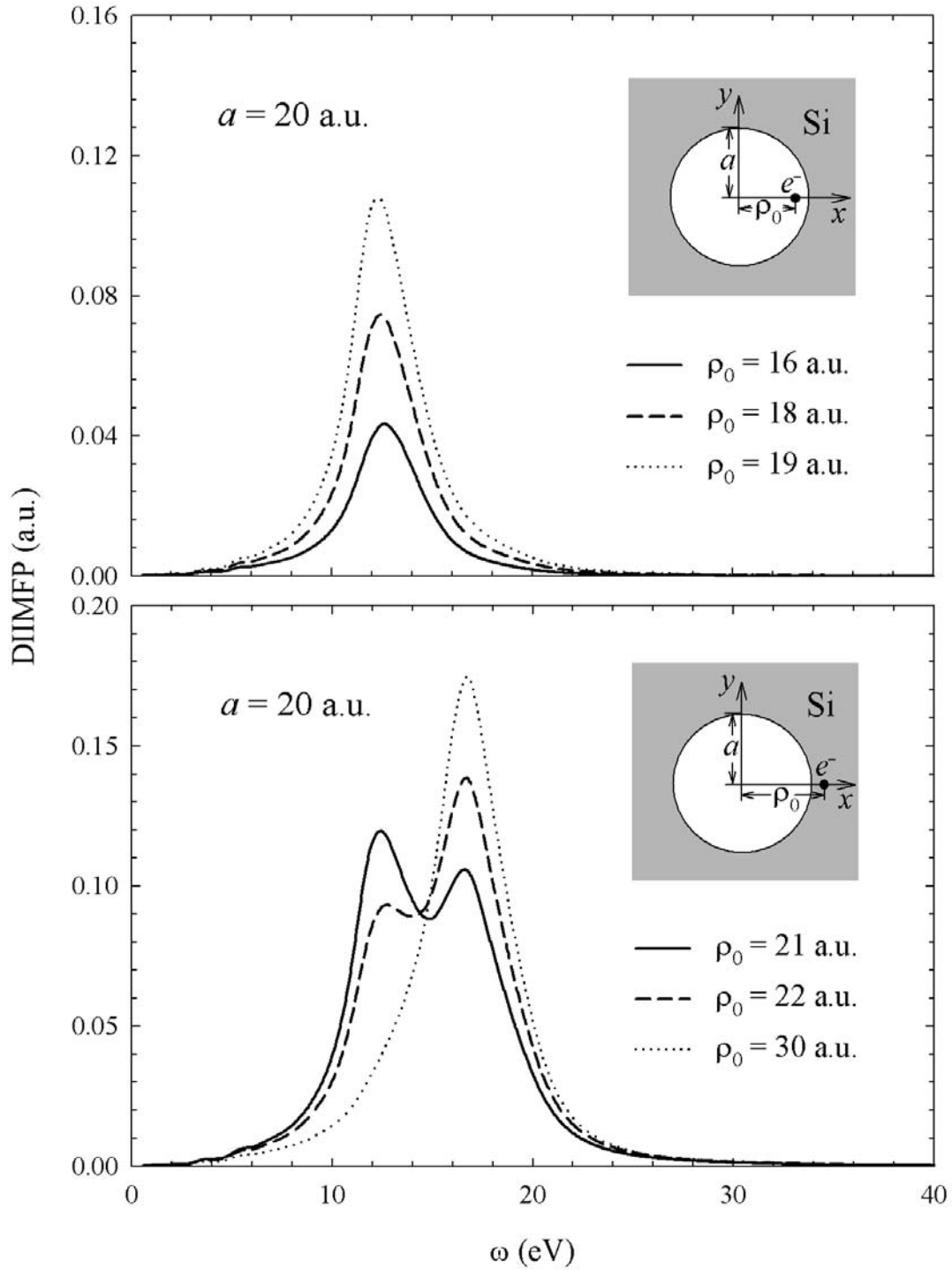


Fig. 4.3 Calculated DIIMFPs for a 500 eV electron moving parallel to the axis of a cylindrical cavity (radius $a = 20$ a.u.) in Si for several electron distances ρ_0 from the axis.

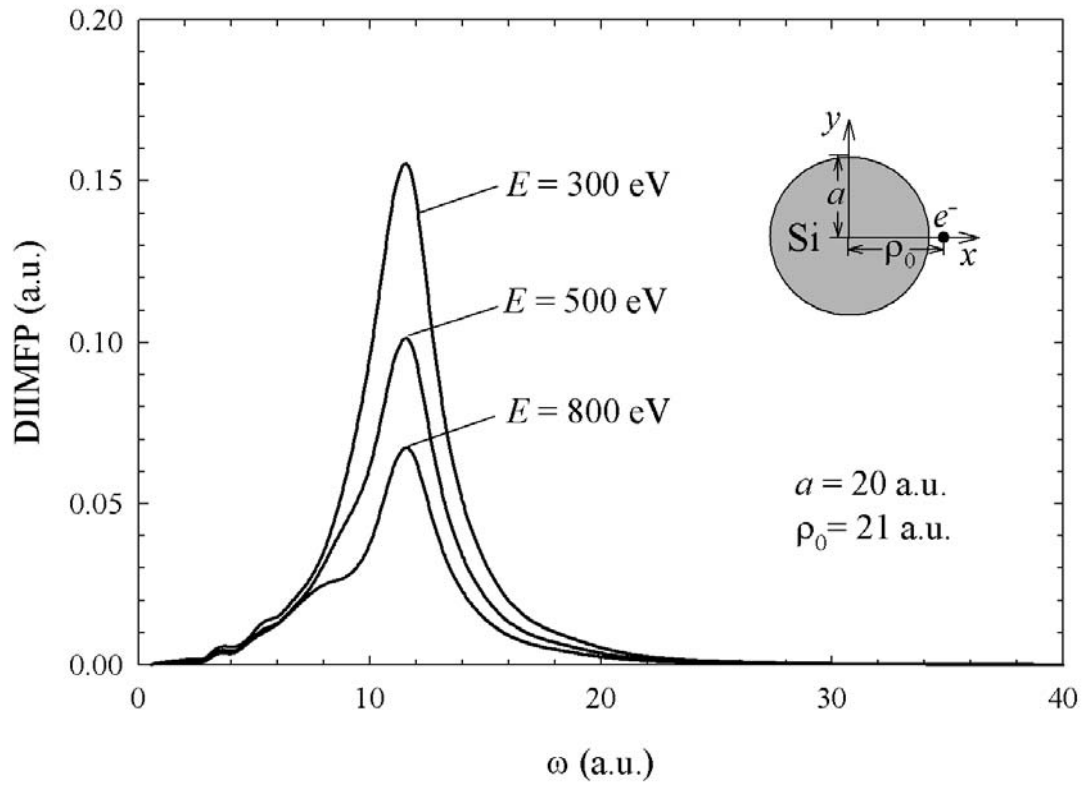


Fig. 4.4 Calculated results of the DIIMFP for an electron moving parallel to and at a distance $\rho_0 = 21$ a.u. from the axis of a Si cylinder (radius $a = 20$ a.u.) in vacuum for several electron energies.

4.1.4 Inverse Inelastic Mean Free Path

The IIMFP may be calculated by the integration of differential inelastic mean free path according to

$$\mu^{(p)}(E) = \int_0^E \mu^{(p)}(E, \omega) d\omega, \quad (4.15)$$

where $p = I$ and II for the case of an electron moving inside and outside the cylinder, respectively.

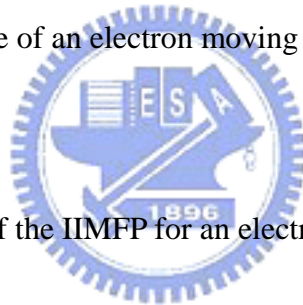


Figure 4.5 shows a plot of the IIMFP for an electron moving inside ($\rho_0 < a$) or outside ($\rho_0 > a$) the cylindrical cavity in Si as a function of electron distance from the cavity center ρ_0 for several electron energies. It is seen that the IIMFP decreases with increasing electron energy. In the region $\rho_0 \geq a$, the IIMFP is both contributed from volume and surface excitations. The contribution from surface excitations confines near the cavity boundary and increases as $\rho_0 \rightarrow a$. On the other hand, the contribution from volume excitations simultaneously decreases near the boundary. The decrease in volume excitations is, to a good approximation, compensated by the increase in surface excitations (Kwei 1998). This makes the IIMFP spatially

non-varying and approaching the value of an infinite Si until electron is closer within ~ 2 a.u. from the cavity boundary. There, the contribution from volume excitations becomes negligibly small so that the IIMFP drops abruptly. For $\rho_0 < a$, i.e. electron inside the cavity, the IIMFP is non-zero due to surface excitations. The IIMFP decreases with increasing electron distance from the cavity boundary.



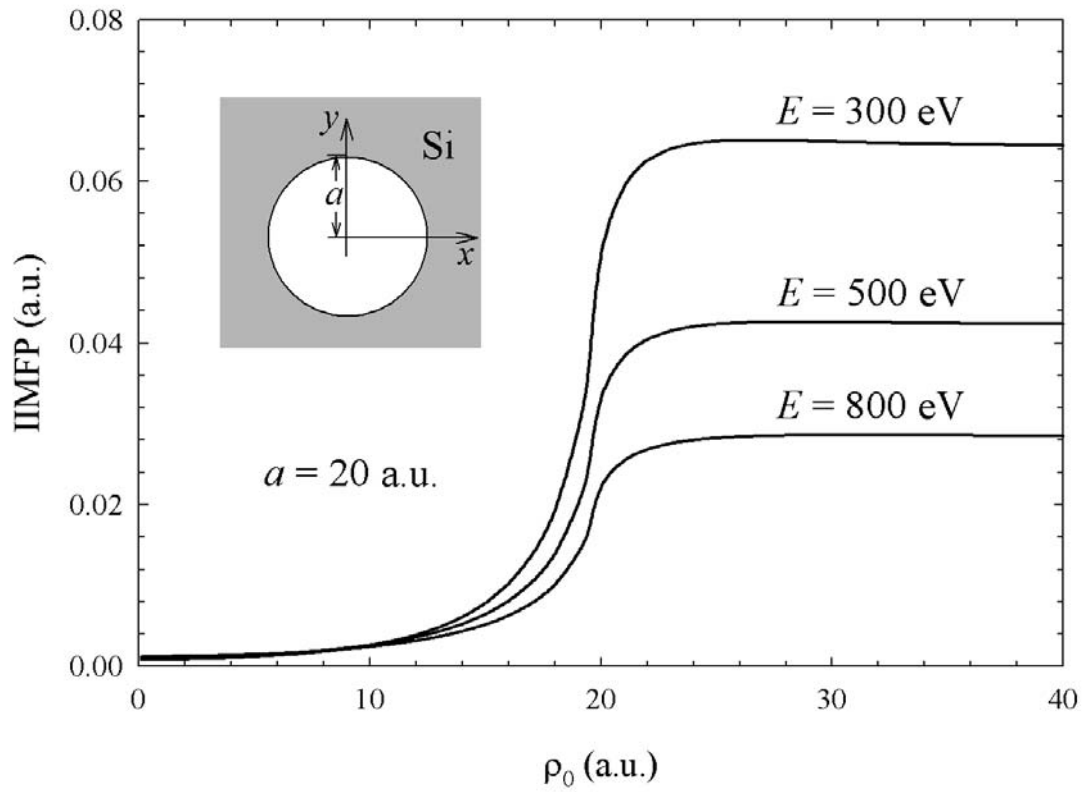


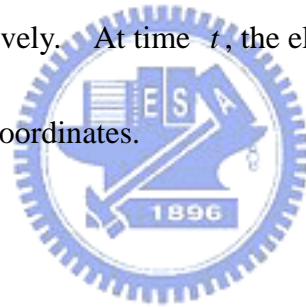
Fig. 4.5 Calculated results of the IIMFP for an electron moving parallel to the axis of a cylindrical cavity (radius $a = 20$ a.u.) in Si for several electron energies.

4.2 Inelastic Interactions of Electrons with Clad Cylindrical Systems

Figure 4.6 illustrates the studied problem. An electron with velocity \vec{v} and energy $E = v^2/2$ moves parallel to the axis of two infinitely long, coaxial cylindrical interfaces of inner radius a and outer radius b . The cylinder has dielectric functions $\epsilon_1(k, \omega)$, $\epsilon_2(k, \omega)$ and $\epsilon_3(k, \omega)$ in different radii ρ for $\rho < a$,

$a < \rho < b$ and $\rho > b$, respectively. At time t , the electron is at a position

$\vec{x}_0 = (\rho_0, 0, vt)$ in cylindrical coordinates.



4.2.1 Induced Potential

Considering three different cases, i.e. $\rho_0 < a$ (case I), $a < \rho_0 < b$ (case II) and $\rho_0 > b$ (case III), the potential in cylindrical coordinates can be expressed as

(Jackson 1975)

$$\Phi_1^{(p)}(\rho, \phi, z, t) = \frac{-1}{\pi \epsilon_1} \sum_{m=-\infty}^{\infty} \int_{-\infty}^{\infty} dk A_m^{(p)} I_m(k\rho) e^{ik(z-vt)+im\phi} + \delta_{p,I} \frac{1}{\epsilon_1} \Phi_0(\rho, \phi, z, t) \quad (4.16a)$$

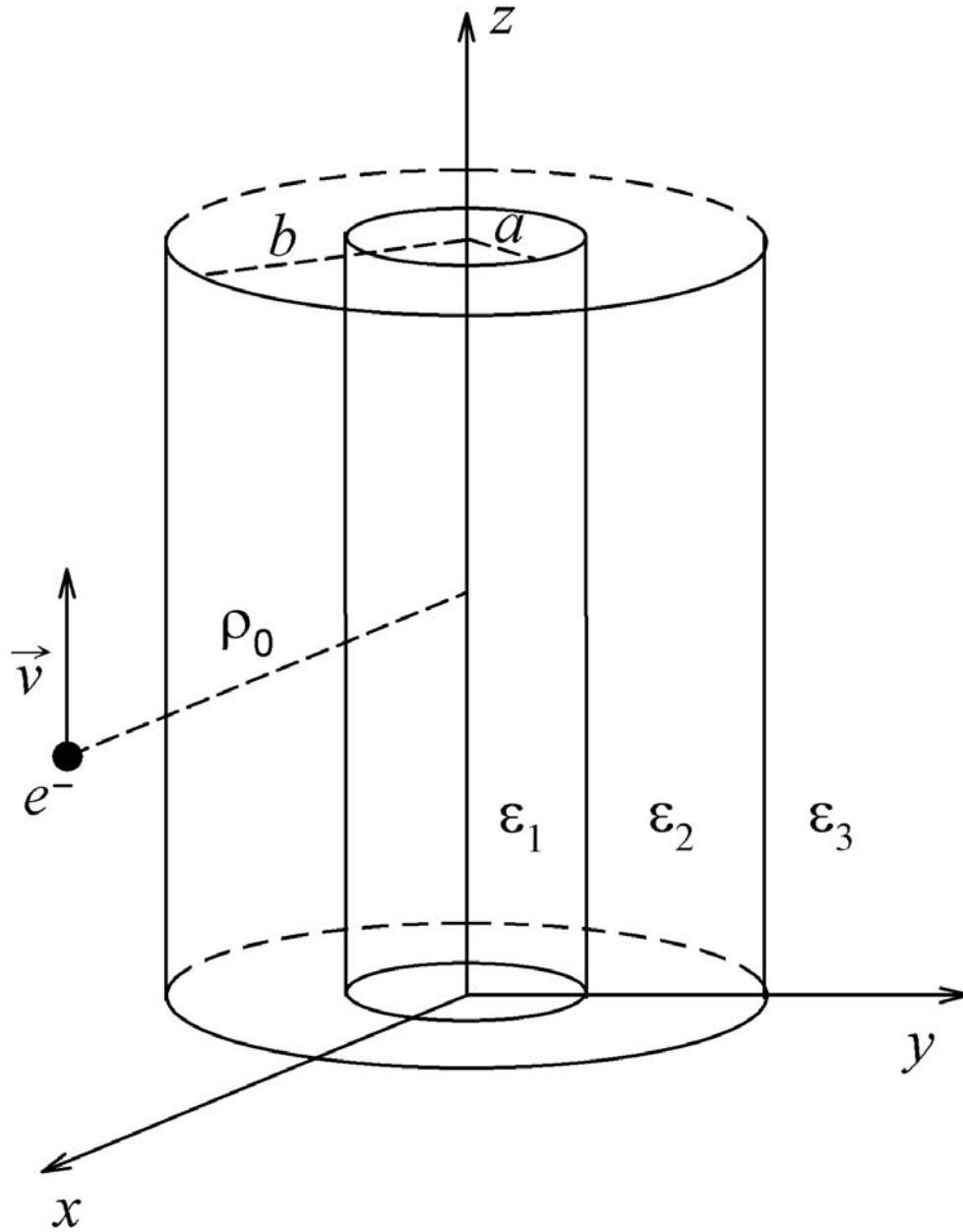


Fig. 4.6 A sketch of the problem studied in the present work. An electron of velocity \vec{v} moves parallel to and at a distance ρ_0 from the axis of an infinitely long clad cylindrical system with inner radius a and outer radius b . The media in the regions $\rho < a$, $a < \rho < b$ and $\rho > b$ have dielectric functions $\epsilon_1(k, \omega)$, $\epsilon_2(k, \omega)$ and $\epsilon_3(k, \omega)$, respectively.

for $\rho < a$,

$$\Phi_2^{(p)}(\rho, \phi, z, t) = \frac{-1}{\pi \varepsilon_2} \sum_{m=-\infty}^{\infty} \int_{-\infty}^{\infty} dk [B_m^{(p)} I_m(k\rho) + C_m^{(p)} K_m(k\rho)] e^{ik(z-vt)+im\phi} + \delta_{p,II} \frac{1}{\varepsilon_2} \Phi_0(\rho, \phi, z, t) \quad (4.16b)$$

for $a < \rho < b$, and

$$\Phi_3^{(p)}(\rho, \phi, z, t) = \frac{-1}{\pi \varepsilon_3} \sum_{m=-\infty}^{\infty} \int_{-\infty}^{\infty} dk D_m^{(p)} K_m(k\rho) e^{ik(z-vt)+im\phi} + \delta_{p,III} \frac{1}{\varepsilon_3} \Phi_0(\rho, \phi, z, t) \quad (4.16c)$$

for $\rho > b$. Here $A_m^{(p)}$, $B_m^{(p)}$, $C_m^{(p)}$ and $D_m^{(p)}$ are coefficients to be determined, $p = I, II$ and III are for cases I, II and III respectively, I_m and K_m are modified Bessel functions, δ is the delta function,

$$\Phi_0(\rho, \phi, z, t) = \frac{-1}{\pi} \sum_{m=-\infty}^{\infty} \int_{-\infty}^{\infty} dk I_m(k\rho_<) K_m(k\rho_>) e^{ik(z-vt)+im\phi} \quad (4.17)$$

is the potential of the electron in vacuum with $\rho_> = \max(\rho, \rho_0)$ and

$\rho_< = \min(\rho, \rho_0)$.

The Fourier transforms of the potentials are

$$\Phi_1^{(p)}(\rho, \phi, k, \omega) = \frac{-4\pi}{\varepsilon_1(k, \omega)} \sum_{m=-\infty}^{\infty} A_m^{(p)}(k, \omega) I_m(k\rho) e^{im\phi} \delta(\omega - kv) + \delta_{p,I} \frac{1}{\varepsilon_1(k, \omega)} \Phi_0(\rho, \phi, k, \omega) \quad (4.18a)$$

for $\rho < a$,

$$\begin{aligned} \Phi_2^{(p)}(\rho, \phi, k, \omega) = & \frac{-4\pi}{\varepsilon_2(k, \omega)} \sum_{m=-\infty}^{\infty} [B_m^{(p)}(k, \omega) I_m(k\rho) + C_m^{(p)}(k, \omega) K_m(k\rho)] e^{im\phi} \delta(\omega - kv) \\ & + \delta_{p,II} \frac{1}{\varepsilon_2(k, \omega)} \Phi_0(\rho, \phi, k, \omega) \end{aligned} \quad (4.18b)$$

for $a < \rho < b$, and



$$\Phi_3^{(p)}(\rho, \phi, k, \omega) = \frac{-4\pi}{\varepsilon_3(k, \omega)} \sum_{m=-\infty}^{\infty} D_m^{(p)}(k, \omega) K_m(k\rho) e^{im\phi} \delta(\omega - kv) + \delta_{p,III} \frac{1}{\varepsilon_3(k, \omega)} \Phi_0(\rho, \phi, k, \omega) \quad (4.18c)$$

for $\rho > b$, where

$$\Phi_0(\rho, \phi, k, \omega) = -4\pi \sum_{m=-\infty}^{\infty} I_m(k\rho_<) K_m(k\rho_>) e^{im\phi} \delta(\omega - kv) . \quad (4.19)$$

4.2.1.1 Case I. Electrons Moving in Medium 1 (i.e. $\rho_0 < a$)

By matching the boundary conditions, i.e. continuities of the potential and the normal component of electric displacement at the interfaces $\rho = a$ and $\rho = b$, one finds

$$A_m^{(1)}(k, \omega) = B_m^{(1)}(k, \omega) + \left[C_m^{(1)}(k, \omega) - I_m(k\rho_0) \right] \frac{K_m'(ka)}{I_m'(ka)}, \quad (4.20a)$$

$$B_m^{(1)}(k, \omega) = \frac{[\varepsilon_3(k, \omega) - \varepsilon_2(k, \omega)] C_m^{(1)}(k, \omega)}{\varepsilon_2(k, \omega) \frac{I_m'(kb)}{K_m'(kb)} - \varepsilon_3(k, \omega) \frac{I_m(kb)}{K_m(kb)}}, \quad (4.20b)$$

$$C_m^{(1)}(k, \omega) = \frac{\varepsilon_2(k, \omega) \left[\frac{K_m'(ka)}{I_m'(ka)} - \frac{K_m(ka)}{I_m(ka)} \right] I_m(k\rho_0)}{\frac{[\varepsilon_3(k, \omega) - \varepsilon_2(k, \omega)] [\varepsilon_2(k, \omega) - \varepsilon_1(k, \omega)]}{\varepsilon_2(k, \omega) \frac{I_m'(kb)}{K_m'(kb)} - \varepsilon_3(k, \omega) \frac{I_m(kb)}{K_m(kb)}} + \varepsilon_2(k, \omega) \frac{K_m'(ka)}{I_m'(ka)} - \varepsilon_1(k, \omega) \frac{K_m(ka)}{I_m(ka)}}, \quad (4.20c)$$

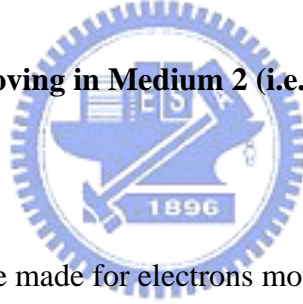
$$D_m^{(1)}(k, \omega) = \frac{I_m'(kb)}{K_m'(kb)} B_m^{(1)}(k, \omega) + C_m^{(1)}(k, \omega), \quad (4.20d)$$

where $I_m'(x) = dI_m(x)/dx$ and $K_m'(x) = dK_m(x)/dx$. Removing the vacuum potential and taking the inverse Fourier transform, one obtains the induced potential in

the spatial space as

$$\Phi_{1,ind}^{(1)}(\rho, \phi, z, t) = \frac{-2}{\pi v} \sum_{m=-\infty}^{\infty} e^{im\phi} \int_0^E d\omega \left[\begin{aligned} & I_m\left(\frac{\omega}{v}\rho\right) \left\{ \operatorname{Re} \left[\frac{A_m^{(1)}\left(\frac{\omega}{v}, \omega\right)}{\varepsilon_1\left(\frac{\omega}{v}, \omega\right)} \cos\left(\omega\left(\frac{z}{v}-t\right)\right) - \operatorname{Im} \left[\frac{A_m^{(1)}\left(\frac{\omega}{v}, \omega\right)}{\varepsilon_1\left(\frac{\omega}{v}, \omega\right)} \sin\left(\omega\left(\frac{z}{v}-t\right)\right) \right] \right\} \\ & + I_m\left(\frac{\omega}{v}\rho_{<}\right) K_m\left(\frac{\omega}{v}\rho_{>}\right) \left\{ \operatorname{Re} \left[\frac{1}{\varepsilon_1\left(\frac{\omega}{v}, \omega\right)} - 1 \right] \cos\left(\omega\left(\frac{z}{v}-t\right)\right) - \operatorname{Im} \left[\frac{1}{\varepsilon_1\left(\frac{\omega}{v}, \omega\right)} \right] \sin\left(\omega\left(\frac{z}{v}-t\right)\right) \right\} \end{aligned} \right]. \quad (4.21)$$

4.2.1.2 Case II. Electrons Moving in Medium 2 (i.e. $a < \rho_0 < b$)



A similar approach can be made for electrons moving in medium 2. After some mathematical manipulations, one finds

$$A_m^{(II)}(k, \omega) = B_m^{(II)}(k, \omega) + \frac{K_m'(ka)}{I_m'(ka)} C_m^{(II)}(k, \omega) + K_m(k\rho_0), \quad (4.22a)$$

$$B_m^{(II)}(k, \omega) = \frac{[\varepsilon_3(k, \omega) - \varepsilon_2(k, \omega)] \{ X_m(k, \omega) I_m(k\rho_0) - [\varepsilon_2(k, \omega) - \varepsilon_1(k, \omega)] K_m(k\rho_0) \}}{X_m(k, \omega) Y_m(k, \omega) - [\varepsilon_2(k, \omega) - \varepsilon_3(k, \omega)] [\varepsilon_2(k, \omega) - \varepsilon_1(k, \omega)]}, \quad (4.22b)$$

$$C_m^{(II)}(k, \omega) = \frac{[\varepsilon_1(k, \omega) - \varepsilon_2(k, \omega)]\{Y_m(k, \omega)K_m(k\rho_0) - [\varepsilon_2(k, \omega) - \varepsilon_3(k, \omega)]I_m(k\rho_0)\}}{X_m(k, \omega)Y_m(k, \omega) - [\varepsilon_2(k, \omega) - \varepsilon_1(k, \omega)][\varepsilon_2(k, \omega) - \varepsilon_3(k, \omega)]}, \quad (4.22c)$$

$$D_m^{(II)}(k, \omega) = \frac{I_m'(kb)}{K_m'(kb)} B_m^{(II)}(k, \omega) + C_m^{(II)}(k, \omega) + I_m(k\rho_0), \quad (4.22d)$$

where

$$X_m(k, \omega) = \varepsilon_2(k, \omega) \frac{K_m'(ka)}{I_m'(ka)} - \varepsilon_1(k, \omega) \frac{K_m(ka)}{I_m(ka)} \quad (4.23a)$$

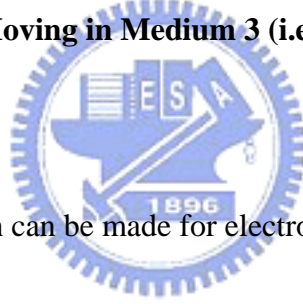
and

$$Y_m(k, \omega) = \varepsilon_2(k, \omega) \frac{I_m'(kb)}{K_m'(kb)} - \varepsilon_3(k, \omega) \frac{I_m(kb)}{K_m(kb)}. \quad (4.23b)$$

Therefore, the induced potential in the spatial space is then obtained as

$$\Phi_{2,ind}^{(II)}(\rho, \phi, z, t) = \frac{-2}{\pi v} \sum_{m=-\infty}^{\infty} e^{im\phi} \int_0^E d\omega \left[\begin{aligned} & I_m \left(\frac{\omega}{v} \rho \right) \left\{ \operatorname{Re} \left[\frac{B_m^{(II)} \left(\frac{\omega}{v}, \omega \right)}{\varepsilon_2 \left(\frac{\omega}{v}, \omega \right)} \cos \left(\omega \left(\frac{z}{v} - t \right) \right) - \operatorname{Im} \left[\frac{B_m^{(II)} \left(\frac{\omega}{v}, \omega \right)}{\varepsilon_2 \left(\frac{\omega}{v}, \omega \right)} \sin \left(\omega \left(\frac{z}{v} - t \right) \right) \right] \right\} \\ & + K_m \left(\frac{\omega}{v} \rho \right) \left\{ \operatorname{Re} \left[\frac{C_m^{(II)} \left(\frac{\omega}{v}, \omega \right)}{\varepsilon_2 \left(\frac{\omega}{v}, \omega \right)} \cos \left(\omega \left(\frac{z}{v} - t \right) \right) - \operatorname{Im} \left[\frac{C_m^{(II)} \left(\frac{\omega}{v}, \omega \right)}{\varepsilon_2 \left(\frac{\omega}{v}, \omega \right)} \sin \left(\omega \left(\frac{z}{v} - t \right) \right) \right] \right\} \\ & + I_m \left(\frac{\omega}{v} \rho_{<} \right) K_m \left(\frac{\omega}{v} \rho_{>} \right) \left\{ \operatorname{Re} \left[\frac{1}{\varepsilon_2 \left(\frac{\omega}{v}, \omega \right)} - 1 \right] \cos \left(\omega \left(\frac{z}{v} - t \right) \right) - \operatorname{Im} \left[\frac{1}{\varepsilon_2 \left(\frac{\omega}{v}, \omega \right)} \right] \sin \left(\omega \left(\frac{z}{v} - t \right) \right) \right\} \end{aligned} \right]. \quad (4.24)$$

4.2.1.3 Case III. Electrons Moving in Medium 3 (i.e. $\rho_0 > b$)



Again, a similar approach can be made for electrons moving in medium 3.

After mathematical manipulations, the coefficients can be found as

$$A_m^{(III)}(k, \omega) = B_m^{(III)}(k, \omega) + \frac{K_m'(ka)}{I_m'(ka)} C_m^{(III)}(k, \omega), \quad (4.25a)$$

$$B_m^{(III)}(k, \omega) = \frac{\varepsilon_2(k, \omega) \left[\frac{I_m'(kb)}{K_m'(kb)} - \frac{I_m(kb)}{K_m(kb)} \right] K_m(k\rho_0)}{\frac{[\varepsilon_1(k, \omega) - \varepsilon_2(k, \omega)][\varepsilon_2(k, \omega) - \varepsilon_3(k, \omega)]}{\varepsilon_2(k, \omega) \frac{K_m'(ka)}{I_m'(ka)} - \varepsilon_1(k, \omega) \frac{K_m(ka)}{I_m(ka)}} + \varepsilon_2(k, \omega) \frac{I_m'(kb)}{K_m'(kb)} - \varepsilon_3(k, \omega) \frac{I_m(kb)}{K_m(kb)}}, \quad (4.25b)$$

$$C_m^{(III)}(k, \omega) = \frac{[\varepsilon_1(k, \omega) - \varepsilon_2(k, \omega)]B_m^{(III)}(k, \omega)}{\varepsilon_2(k, \omega) \frac{K_m'(ka)}{I_m'(ka)} - \varepsilon_1(k, \omega) \frac{K_m(ka)}{I_m(ka)}} , \quad (4.25c)$$

$$D_m^{(III)}(k, \omega) = \left[B_m^{(III)}(k, \omega) - K_m(k\rho_0) \right] \frac{I_m'(kb)}{K_m'(kb)} + C_m^{(III)}(k, \omega) . \quad (4.25d)$$

Therefore, the induced potential in the spatial space is then obtained as

$$\Phi_{3,ind}^{(III)}(\rho, \phi, z, t) = \frac{-2}{\pi v} \sum_{m=-\infty}^{\infty} e^{im\phi} \int_0^E d\omega \left[\begin{aligned} & K_m\left(\frac{\omega}{v}\rho\right) \left\{ \operatorname{Re} \left[\frac{D_m^{(III)}\left(\frac{\omega}{v}, \omega\right)}{\varepsilon_3\left(\frac{\omega}{v}, \omega\right)} \cos\left(\omega\left(\frac{z}{v}-t\right)\right) - \operatorname{Im} \left[\frac{D_m^{(III)}\left(\frac{\omega}{v}, \omega\right)}{\varepsilon_3\left(\frac{\omega}{v}, \omega\right)} \sin\left(\omega\left(\frac{z}{v}-t\right)\right) \right] \right\} \right. \\ & \left. + I_m\left(\frac{\omega}{v}\rho_{<}\right) K_m\left(\frac{\omega}{v}\rho_{>}\right) \left\{ \operatorname{Re} \left[\frac{1}{\varepsilon_3\left(\frac{\omega}{v}, \omega\right)} - 1 \right] \cos\left(\omega\left(\frac{z}{v}-t\right)\right) - \operatorname{Im} \left[\frac{1}{\varepsilon_3\left(\frac{\omega}{v}, \omega\right)} \right] \sin\left(\omega\left(\frac{z}{v}-t\right)\right) \right\} \right] . \quad (4.26) \end{aligned}$$

4.2.2 Stopping Power

4.2.2.1 Case I. Electrons Moving in Medium 1 (i.e. $\rho_0 < a$)

The stopping power, $F^{(1)}$, is related to the derivative of $\Phi_{1,ind}^{(1)}(\rho, \phi, z, t)$ at the position of electrons. One gets

$$F^{(I)} = \frac{-2}{\pi v^2} \sum_{m=-\infty}^{\infty} \int_0^E d\omega \omega I_m \left(\frac{\omega}{v} \rho_0 \right) \left\{ \text{Im} \left[\frac{A_m^{(I)} \left(\frac{\omega}{v}, \omega \right)}{\varepsilon_1 \left(\frac{\omega}{v}, \omega \right)} \right] + K_m \left(\frac{\omega}{v} \rho_0 \right) \text{Im} \left[\frac{1}{\varepsilon_1 \left(\frac{\omega}{v}, \omega \right)} \right] \right\}. \quad (4.27)$$

4.2.2.2 Case II. Electrons Moving in Medium 2 (i.e. $a < \rho_0 < b$)

The stopping power, $F^{(II)}$, is related to the derivative of $\Phi_{2,ind}^{(II)}(\rho, \phi, z, t)$ at the position of electrons. One gets

$$F^{(II)} = \frac{-2}{\pi v^2} \sum_{m=-\infty}^{\infty} \int_0^E d\omega \omega \left\{ \begin{aligned} & I_m \left(\frac{\omega}{v} \rho_0 \right) \text{Im} \left[\frac{B_m^{(II)} \left(\frac{\omega}{v}, \omega \right)}{\varepsilon_2 \left(\frac{\omega}{v}, \omega \right)} \right] + K_m \left(\frac{\omega}{v} \rho_0 \right) \text{Im} \left[\frac{C_m^{(II)} \left(\frac{\omega}{v}, \omega \right)}{\varepsilon_2 \left(\frac{\omega}{v}, \omega \right)} \right] \\ & + I_m \left(\frac{\omega}{v} \rho_0 \right) K_m \left(\frac{\omega}{v} \rho_0 \right) \text{Im} \left[\frac{1}{\varepsilon_2 \left(\frac{\omega}{v}, \omega \right)} \right] \end{aligned} \right\}. \quad (4.28)$$

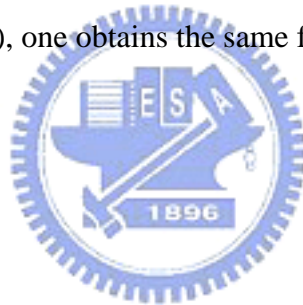
4.2.2.3 Case III. Electrons Moving in Medium 3 (i.e. $\rho_0 > b$)

The stopping power, $F^{(III)}$, is related to the derivative of $\Phi_{3,ind}^{(III)}(\rho, \phi, z, t)$ at the position of electrons. One gets

$$F^{(III)} = \frac{-2}{\pi v^2} \sum_{m=-\infty}^{\infty} \int_0^E d\omega \omega K_m \left(\frac{\omega}{v} \rho_0 \right) \left\{ \text{Im} \left[\frac{D_m^{(III)} \left(\frac{\omega}{v}, \omega \right)}{\varepsilon_3 \left(\frac{\omega}{v}, \omega \right)} \right] + I_m \left(\frac{\omega}{v} \rho_0 \right) \text{Im} \left[\frac{1}{\varepsilon_3 \left(\frac{\omega}{v}, \omega \right)} \right] \right\} . \quad (4.29)$$

4.2.2.4 Limiting Cases

Taking $\varepsilon_2 = \varepsilon_3$ in Eq (4.27) or $\varepsilon_1 = \varepsilon_2$ in Eq (4.29), one obtains the same formulas of the stopping power as that derived in Eq. (4.9). Taking $\varepsilon_1 = \varepsilon_2$ in Eq (4.29) or $\varepsilon_2 = \varepsilon_3$ in Eq (4.27), one obtains the same formulas of the stopping power as that derived in Eq. (4.10).



4.2.3 Differential Inverse Inelastic Mean Free Path

The stopping power is expressed in terms of the DIIMFP, $\mu^{(p)}$, through

$$F^{(p)} = \int_0^E \omega \mu^{(p)}(E, \omega) d\omega , \quad (4.30)$$

where $p = I, II$ and III are for cases I, II and III respectively. Therefore, one obtains the DIIMFPs as

$$\mu^{(I)}(E, \omega) = \frac{-2}{\pi v^2} \sum_{m=-\infty}^{\infty} I_m \left(\frac{\omega}{v} \rho_0 \right) \left\{ \text{Im} \left[\frac{A_m^{(I)} \left(\frac{\omega}{v}, \omega \right)}{\varepsilon_1 \left(\frac{\omega}{v}, \omega \right)} \right] + K_m \left(\frac{\omega}{v} \rho_0 \right) \text{Im} \left[\frac{1}{\varepsilon_1 \left(\frac{\omega}{v}, \omega \right)} \right] \right\} . \quad (4.31)$$

for an electron moving in medium 1,

$$\mu^{(II)}(E, \omega) = \frac{-2}{\pi v^2} \sum_{m=-\infty}^{\infty} \left\{ \begin{aligned} & I_m \left(\frac{\omega}{v} \rho_0 \right) \text{Im} \left[\frac{B_m^{(II)} \left(\frac{\omega}{v}, \omega \right)}{\varepsilon_2 \left(\frac{\omega}{v}, \omega \right)} \right] + K_m \left(\frac{\omega}{v} \rho_0 \right) \text{Im} \left[\frac{C_m^{(II)} \left(\frac{\omega}{v}, \omega \right)}{\varepsilon_2 \left(\frac{\omega}{v}, \omega \right)} \right] \\ & + I_m \left(\frac{\omega}{v} \rho_0 \right) K_m \left(\frac{\omega}{v} \rho_0 \right) \text{Im} \left[\frac{1}{\varepsilon_2 \left(\frac{\omega}{v}, \omega \right)} \right] \end{aligned} \right\} . \quad (4.32)$$

for an electron moving in medium 2, and

$$\mu^{(III)}(E, \omega) = \frac{-2}{\pi v^2} \sum_{m=-\infty}^{\infty} K_m \left(\frac{\omega}{v} \rho_0 \right) \left\{ \text{Im} \left[\frac{D_m^{(III)} \left(\frac{\omega}{v}, \omega \right)}{\varepsilon_3 \left(\frac{\omega}{v}, \omega \right)} \right] + I_m \left(\frac{\omega}{v} \rho_0 \right) \text{Im} \left[\frac{1}{\varepsilon_3 \left(\frac{\omega}{v}, \omega \right)} \right] \right\} . \quad (4.33)$$

for an electron moving in medium 3.

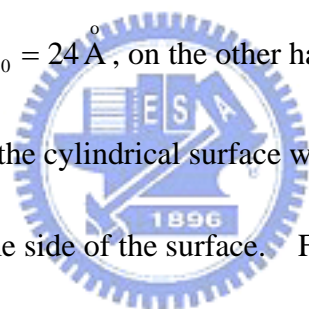
Taking $\varepsilon_2 = \varepsilon_3$ in Eq (4.31) or $\varepsilon_1 = \varepsilon_2$ in Eq (4.32), one obtains the same formulas of the DIIMFP as that derived in Eq. (4.12). Taking $\varepsilon_2 = \varepsilon_3$ in Eq (4.32) or $\varepsilon_1 = \varepsilon_2$ in Eq (4.33), one obtains the same formulas of the DIIMFP as that derived in Eq. (4.13). Taking $\varepsilon_1 = \varepsilon_2 = \varepsilon_3 = \varepsilon$ in Eqs. (4.31), (4.32) or (4.33), one obtains the DIIMFP for an infinite solid as Eq. (4.14). Equation (4.14) may also be found by taking $a \rightarrow \infty$ in Eq. (4.31), $a = 0$ and $b \rightarrow \infty$ in Eq. (4.32), or $a = b = 0$ in Eq. (4.33).

Using Eqs. (4.31), (4.32) and (4.33), the DIIMFP for an electron moving parallel to the axis of a Si cylindrical tube of inner radius $a = 15 \text{ \AA}$ and outer radius $b = 25 \text{ \AA}$ is calculated. In these calculations, a sum-rule-constrained extended Drude dielectric function with dispersion (Kwei 2003) was applied. Figure 4.7 shows the results for the DIIMFP of a 500 eV electron traveling inside the Si tube, i.e. $\rho_0 < a$, at several distances ρ_0 as a function of energy transfer. It is seen that the DIIMFP is entirely contributed from surface excitations. The surface excitation peak ($\sim 12 \text{ eV}$) decreases in magnitude for decreasing ρ_0 due to the weaker response by the solid surface.

The DIIMFP of a 500 eV electron traveling inside the cylindrical shell of the Si tube, i.e. $a < \rho_0 < b$, is plotted in Fig. 4.8 as a function of energy transfer for several values of ρ_0 . Since now the electron travels inside the solid, the DIIMFP exhibits

overlapping peaks due to the contributions from surface and volume excitations.

The relative contributions from surface and volume excitations depend on the location of the electron. As the electron moves along the midline between inner and outer surfaces (solid curve), volume excitations (the peak at ~17 eV) dominate. When the electron moves near the inner surface (dashed curve) or the outer surface (dotted curve), surface excitations (the peak at ~12 eV) become more prominent. In the case of $\rho_0 = 16 \text{ \AA}$, for instance, the electron moves at 1 \AA away from and parallel to the cylindrical surface where the electron and the cylindrical axis are on opposite sides of the surface. In the case of $\rho_0 = 24 \text{ \AA}$, on the other hand, the electron moves also at 1 \AA away from and parallel to the cylindrical surface where the electron and the cylindrical axis are on the same side of the surface. For $\rho_0 = 16 \text{ \AA}$, the electron moves along the cylindrical surface bending away from it, leading to reduced surface excitations and increased volume excitations. For $\rho_0 = 24 \text{ \AA}$, the electron moves along the cylindrical surface bending towards it, leading to enhanced surface excitations and decreased volume excitations.



Similar results on the DIIMFP of a 500 eV electron moving outside the Si tube, i.e. $\rho_0 > b$, for several ρ_0 are plotted in Fig. 4.9 as a function of energy transfer. It is seen that in this case the DIIMFP is totally contributed from surface excitations, with its value decreasing for increasing electron distance from the surface. Figure

4.10 shows the DIIMFP for electrons with various energies moving outside the Si tube at $\rho_0 = 26 \text{ \AA}$. It is seen that the DIIMFP decreases with increasing electron energy. This indicates that the contribution from surface excitations also decreases as electron velocity increases.

Figure 4.11 shows the DIIMFP for a 500 eV electron moving at $\rho_0 = 26 \text{ \AA}$ outside a Si cylinder clad in a SiO_2 film with outer radius $b = 25 \text{ \AA}$ and inner radius $a = 15 \text{ \AA}$, 22 \AA or 24 \AA . For comparisons, corresponding results of a SiO_2 cylindrical wire ($a = 0 \text{ \AA}$) and a Si cylindrical wire ($a = 25 \text{ \AA}$) are included. In the case of $a = 0 \text{ \AA}$, the DIIMFP exhibits a broad distribution contributed from surface excitations of SiO_2 . For $a = 25 \text{ \AA}$, on the other hand, the DIIMFP is purely contributed from surface excitations of Si. For the Si cylinder clad in a SiO_2 film of thickness 1 \AA ($a = 24 \text{ \AA}$) or 3 \AA ($a = 22 \text{ \AA}$), the DIIMFP reveals the contributions from surface (SiO_2 -vacuum) excitations and interface (Si- SiO_2) excitations. For the case of a Si cylinder clad in a 10 \AA ($a = 15 \text{ \AA}$) SiO_2 film, the DIIMFP approaches to that of the SiO_2 cylinder wire. Another words, as the film thickness increases the DIIMFP gradually changes from a value of the Si cylindrical wire to that of the SiO_2 wire. When the film thickness is greater than 10 \AA , nearly no contribution from interface excitations is found.

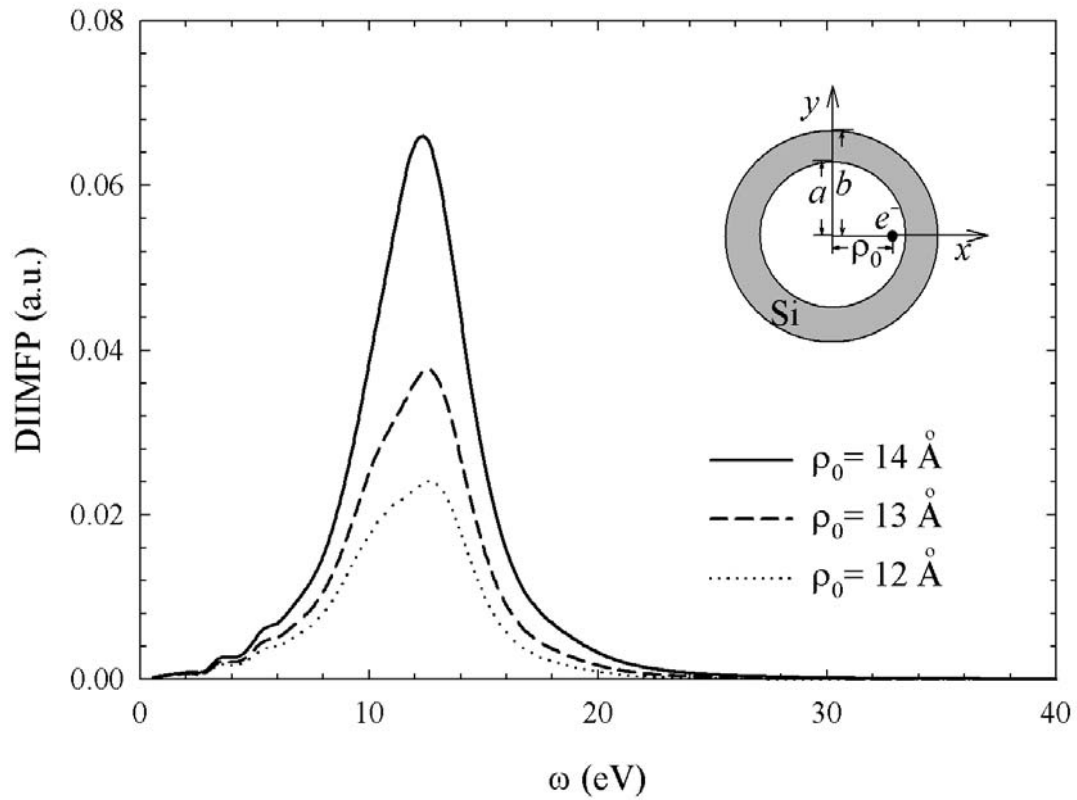


Fig. 4.7 Calculated DIIMFP for a 500 eV electron moving parallel to and at a distance $\rho_0 < 15 \text{ \AA}$ from the axis of a Si tube of inner radius $a = 15 \text{ \AA}$ and outer radius $b = 25 \text{ \AA}$.

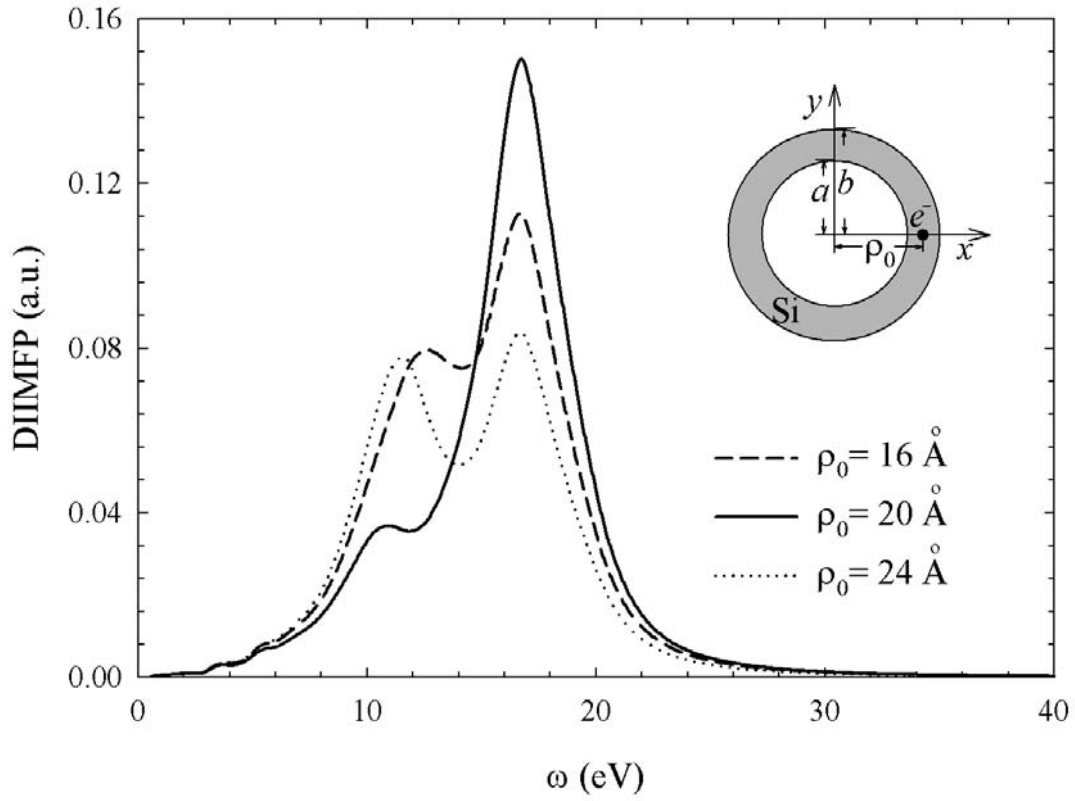


Fig. 4.8 Calculated DIIMFP for a 500 eV electron moving parallel to and at a distance $15 \text{ \AA} < \rho_0 < 25 \text{ \AA}$ from the axis of a Si tube of inner radius $a = 15 \text{ \AA}$ and outer radius $b = 25 \text{ \AA}$.

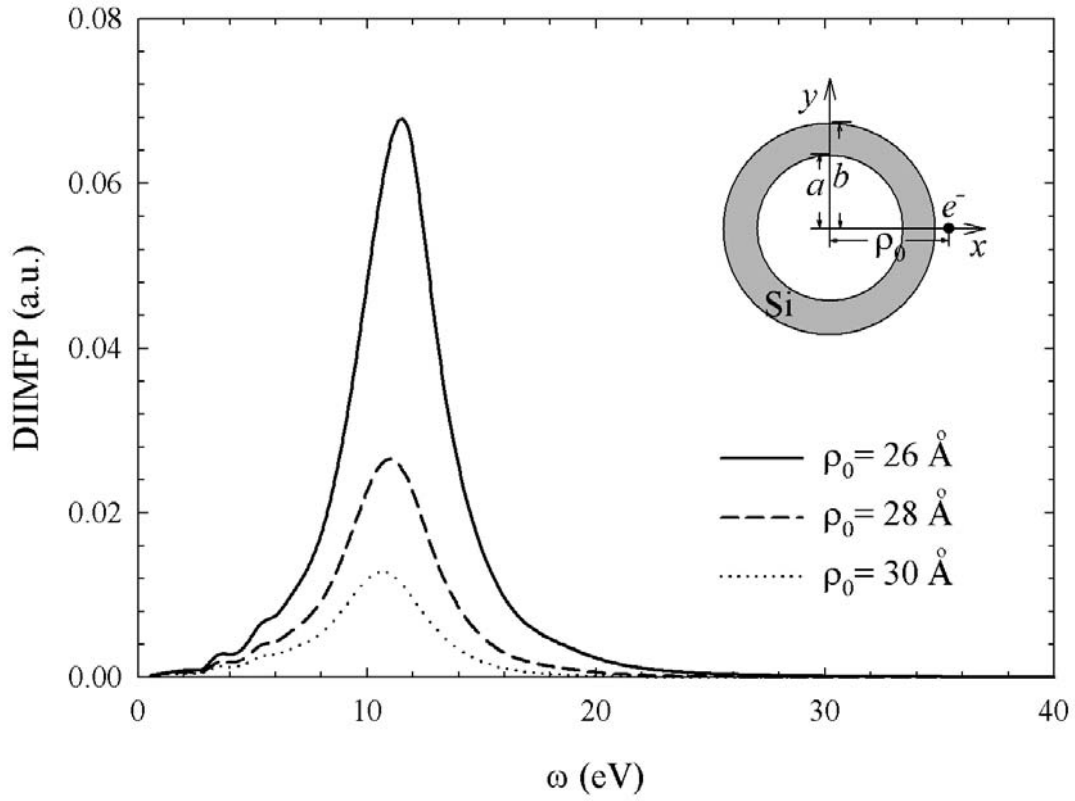


Fig. 4.9 Calculated DIIMFP for a 500 eV electron moving parallel to and at a distance $\rho_0 > 25 \text{ \AA}$ from the axis of a Si tube of inner radius $a = 15 \text{ \AA}$ and outer radius $b = 25 \text{ \AA}$.

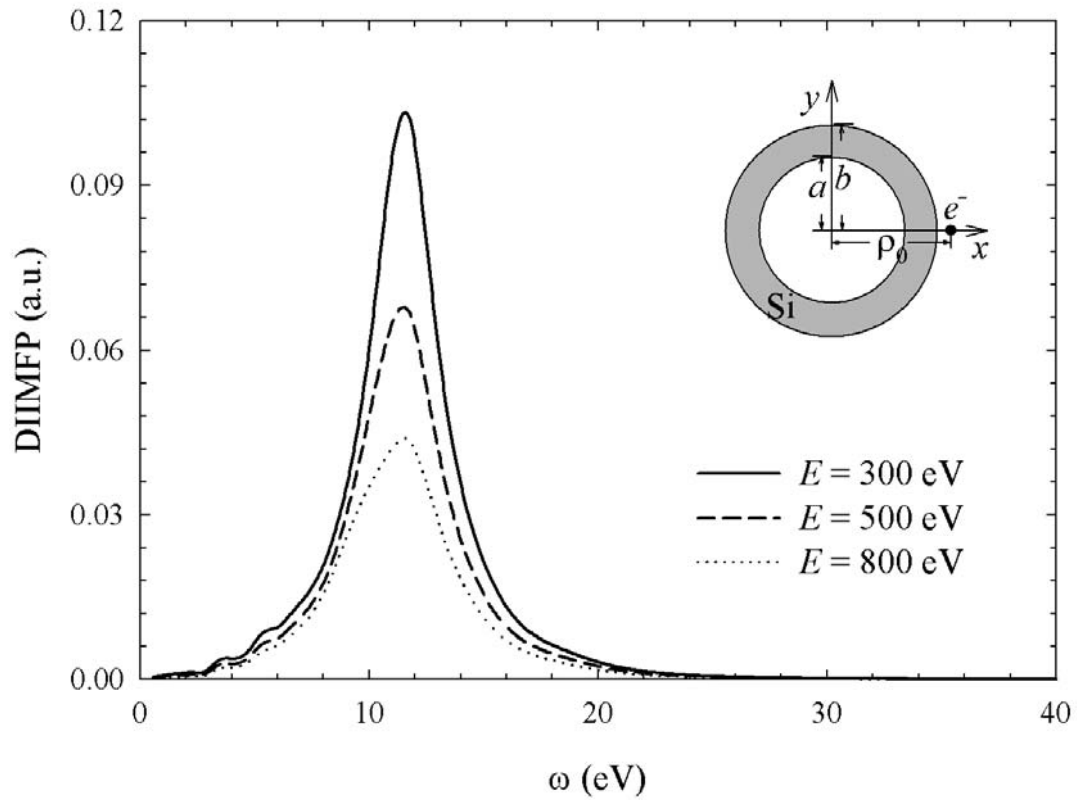


Fig. 4.10 Calculated DIIMFP for an electron moving parallel to and at a distance

$\rho_0 = 26 \text{ \AA}$ from the axis of a Si tube of inner radius $a = 15 \text{ \AA}$ and outer radius

$b = 25 \text{ \AA}$ for several electron energies.

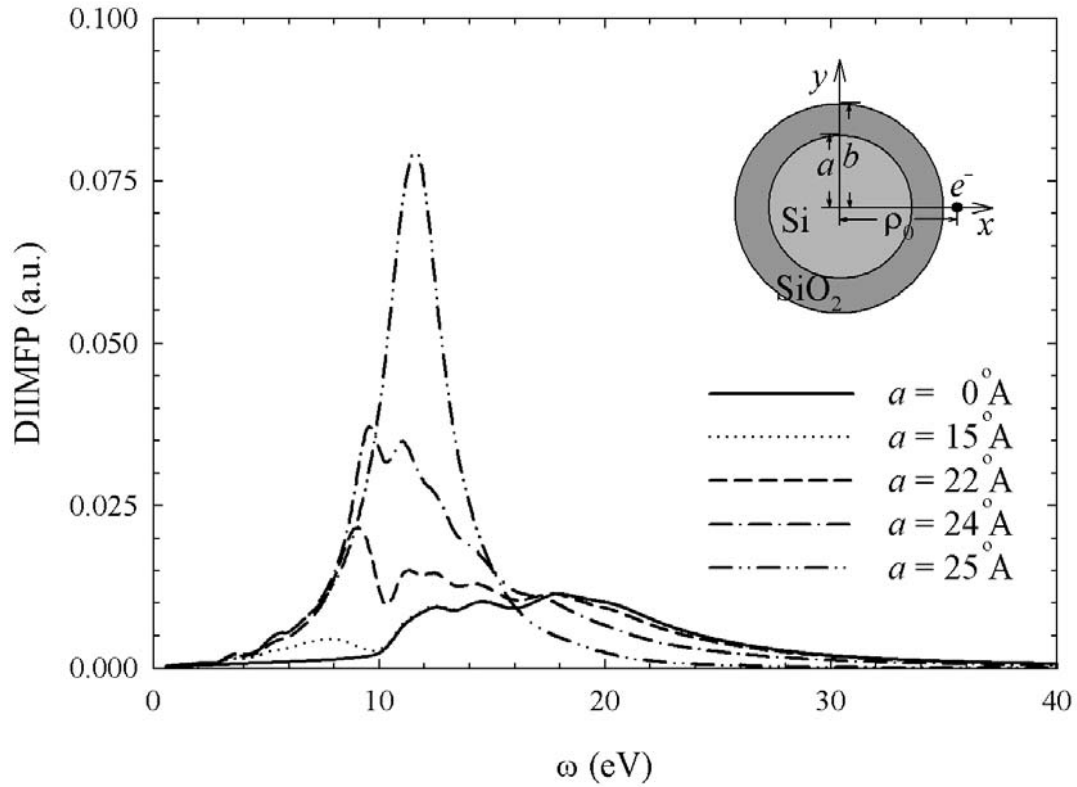


Fig. 4.11 Calculated DIIMFP for a 500 eV electron moving parallel to and at a distance $\rho_0 = 26 \text{ \AA}$ from the axis of a Si cylinder clad in a SiO_2 film, having outer radius $b = 25 \text{ \AA}$ and inner radius $a = 0, 15, 22, 24$ or 25 \AA . Results of $a = 0$ and 25 \AA correspond to the SiO_2 and the Si cylindrical wires.

CHAPTER 5

SUMMARY

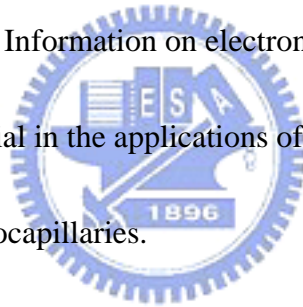
In this dissertation, electronic excitations produced by the inelastic interaction between charged particles and solids were studied theoretically.

Electronic excitations are the important mechanism responsible for the energy loss of electrons in electron spectroscopies. The description of electronic excitations was based on the extended Drude model which characterized the dielectric response functions. Experimental data taken from the optical ellipsometry for small energy transfers and the electron energy-loss spectra for large energy transfers were used to obtain parameters in the model dielectric functions for semiconducting III-V compounds. To assure the accuracy of the dielectric functions, sum-rules and critical-point energies are checked.

In the research on electronic excitations in planar systems, the inelastic response to a probe electron moving across the solid surface was determined. The angular and energy dependences of the SEP for electrons moving in vacuum and across the surface were analyzed. The SEP was fitted to a simple formula for the applications in electron surface-sensitive spectroscopies. Moreover, a theoretical treatment was developed to account for the memory effect on the induced potential, stopping power,

DIIMFP, IMFP for a charged particle moving close and parallel to the surface of a solid. It was found that the consideration of memory effect was important for the calculation of inelastic interactions.

In the research on electronic excitations in cylindrical systems, analytic formulas were derived to deal with the DIIMFP and IIMFP for an electron moving parallel to the axis of a (clad) cylindrical structure based on the dielectric response theory. The dependences of the DIIMFP and IIMFP on the electron position and energy have been analyzed. All relevant inelastic interactions including volume, surface and interface excitations were considered. Information on electron inelastic interactions with cylindrical structures is essential in the applications of electron surface spectroscopies, involving nanowires and microcapillaries.



REFERENCES

- Arista N. R., *Phys. Rev. A* **49** (1994) 1885.
- Arista N. R., Fuentes M. A., *Phys. Rev. B* **63** (2001) 165401.
- Brockt G., Lakner H., *Micron* **31** (2000) 435.
- Chen Y. F., Kwei C. M., *Surf. Sci.* **364** (1996) 131.
- Chiarello G., Colavita E., De Cresenzi M., Nannarone S., *Phys. Rev. B* **29** (1984) 4878.
- Chu Y. T., Warmack R. J., Ritchie R. H., Little J. W., Becker R. S., Ferrel T. L., *Part. Accel.* **16** (1984) 13.
- Daniels J., Festenberg C. V., Raether H., Zeppenfeld K., *Optical Constants of Solids by Electron Spectroscopy*, Vol. 54 of Springer Tracts in Modern Physics, Springer, New York (1970).
- de Abajo F. J. G., Echenique P. M., *Phys. Rev. B* **46** (1992) 2663.
- de Abajo F. J. G., Echenique P. M., *Phys. Rev. B* **48** (1993) 13399.
- Ding Z. J., *J. Phys.: Condens. Matter* **10** (1998) 1753.
- Festenberg C. V., *Z. Phys.* **227** (1969) 453.
- Flores F., Garcia-Moliner F., *J. Phys. C* **12** (1979) 907.
- Gergely G., Menyhard M., Gurban S., Sulyok A., Toth J., Varga D., Tougaard S., *Surf.*

- Interf. Anal.* **33** (2002) 410.
- Gervasoni J. L., Arista N. R., *Phys. Rev. B* **68** (2003) 235302.
- Hoskins R. F., *Delta Functions: An Introduction To Generalised Functions, Horwood series in mathematics & applications*, Horwood, England (1999).
- Ingham J. C., Nebesny K. W., Peemberton J. E., *Appl. Surf. Sci.* **44** (1990) 279.
- Jablonski A., *Surf. Interface Anal.* **29** (2000) 582.
- Jablonski A., *Prog. Surf. Sci.* **79** (2005) 3.
- Jackson J. D., *Classical Electrodynamics*, Wiley, New York (1975).
- Kwei C. M., Tung C. J., *J. Phys. D: Appl. Phys.* **19** (1986) 255.
- Kwei C. M., Chen Y. F., Tung C. J., Wang J. P., *Surf. Sci.* **293** (1993) 202.
- Kwei C. M., Wang C. Y., Tung C. J., *Surf. Interface Anal.* **26** (1998) 682.
- Kwei C. M., Chiou S. Y., Li Y. C., *J. Appl. Phys.* **85** (1999) 8247.
- Kwei C. M., Hwang S. J., Li Y. C., Tung C. J., *J. Appl. Phys.* **93** (2003) 9130.
- Kwei C. M., Li Y. C., *Appl. Surf. Sci.* **238** (2004) 151.
- Kwei C. M., Li Y. C., Tung C. J., *Surf. Sci.* (2006) in press.
- Ohno Y., *Phys. Rev. B* **39** (1989) 8209.
- Orosz G. T., Gergely G., Gurban S., Menyhard M., Toth J., Varga D., Tougaard S.,
Vacuum **71** (2003) 147.
- Oswald R., Ph. D. Thesis, Eberhard-Karls-Universität, Tübingen, (1992).

Palik E. D. ed., *Handbook of Optical Constants of Solids*, Academic Press, New York (1985).

Palik E. D. ed., *Handbook of Optical Constants of Solids II*, Academic Press, New York (1991).

Palik E. D. ed., *Handbook of Optical Constants of Solids III*, Academic Press, New York (1998).

Raether H., *Excitations of Plasmons and Interband Transitions by Electrons*, Vol. 88 of Springer Tracts in Modern Physics, Springer, New York (1980).

Ritchie R. H., *Phys. Rev.* **106** (1957) 874.

Ritchie R. H., Howie A., *Phyl. Mag.* **36** (1977) 463.

Ritchie R. H., Hamm R. N., Turner J. E., Wright H. A., Bolch W. E., *Physical and Chemical Mechanisms in Molecular Radiation Biology*, Plenum, New York (1991).

Rivacoba A., Apell P., Zabala N., *Nucl. Instrum. Methods B* **96** (1995) 465.

Smith D. Y., Shiles E., *Phys. Rev. B* **17** (1978) 4689.

Tanuma S., Powell C. J., Penn D. R., *Surf. Interface Anal.* **17** (1991) 927.

Tökési K., Wirtz L., Burgdörfer J., *Nucl. Instrum. Methods B* **154** (1999) 307.

Tökési K., Burgdörfer J., *Surf. Sci.* **454-456** (2000) 1038.

Tougaard S., Chorkendorff I., *Phys. Rev. B* **35** (1987) 6570.

Tougaard S., Kraaer J., *Phys. Rev. B* **43** (1991) 1651.

Vicanek M., *Surf. Sci.* **400** (1999) 1.

Walsh C. A., *Philos. Mag. A* **59** (1989) 227.

Werner W. S. M., Smekal W., Tomastik C., Störi H., *Surf. Sci.* **486** (2001) L461.

Werner W. S. M., *Phys. Rev. B* **71** (2005) 115415.

Yubero F., Sanz J. M., Elizalde E., Galan L., *Surf. Sci.* **237** (1990) 173.

Yubero F., Tougaard S., *Phys. Rev. B* **46** (1992) 2486.

Yubero F., Sanz J. M., Ramskov B., Tougaard S., *Phys. Rev. B* **53** (1996) 9719.

Zabala N., Rivacoba A., Echenique P. M., *Surf. Sci.* **209** (1989) 465.

Zabala N., Ogando E., Rivacoba A., de Abajo F. J. G., *Phys. Rev. B* **64** (2001) 205410.



簡 歷

姓 名：杜宇軒

性 別：男

學 歷：

國立交通大學電子工程學系 (87年9月~91年1月)

國立交通大學電子研究所碩士班 (91年2月~92年1月)

國立交通大學電子研究所博士班 (92年2月~95年6月)



PUBLICATION LIST

Refereed Journal Papers:

1. Y. H. Tu, C. M. Kwei, C. J. Tung, “Angular and energy dependences of surface excitation parameter for semiconducting III-V compounds”, *Surf. Sci.*, (submitted).
2. Y. C. Li, Y. H. Tu, C. M. Kwei, C. J. Tung, “Retardation effect on energy losses of electrons moving parallel to solid surfaces”, *J. Appl. Phys.*, (submitted).
3. Y. H. Tu, C. M. Kwei, Y. C. Li, C. J. Tung, “Dielectric response theory for electron energy loss in clad cylindrical systems”, *Phys. Rev. B*, (accepted).
4. Y. H. Tu, C. M. Kwei, C. J. Tung, “Inelastic interactions of electrons with cylindrical interfaces”, *Surf. Sci.*, **600**, 820-824 (2006). (SCI)
5. C. M. Kwei, Y. H. Tu, Y. H. Hsu, C. J. Tung, “Memory effect on energy losses of charged particles moving parallel to solid surface”, *Nucl. Instr. and Meth. B*, **243**, 293-298 (2006). (SCI)
6. C. M. Kwei, Y. H. Hsu, Y. H. Tu, C. J. Tung, “Memory effect on the inelastic interaction of electrons moving parallel to a solid surface”, *Surf. Interf. Anal.*, **38**, 84-87 (2006). (SCI)

7. Y. C. Li, Y. H. Tu, C. M. Kwei, C. J. Tung, “Influence of the direction of motion on the inelastic interaction between electrons and solid surfaces”, *Surf. Sci.*, **589**, 67-76 (2005). (SCI)
8. C. M. Kwei, Y. H. Tu, C. J. Tung, “Surface excitation parameter for semiconducting III-V compounds”, *Nucl. Instr. and Meth. B*, **230**, 125-128 (2005). (SCI)

International Conference Papers:

1. C. M. Kwei, Y. H. Tu, C. J. Tung, “Calculation of surface excitation parameter for AlN”, *11th Joint Vacuum Conference (JVC 11)*, Prague, Czech, September 24-28, 2006. (submitted)
2. C. J. Tung, W. T. Chan, Y. H. Tu, C. M. Kwei, “Inelastic interactions of low energy electrons with biological media”, *10th International Symposium on Radiation Physics (ISRP-10)*, Coimbra, Portugal, September 17-22, 2006. (accepted)
3. C. M. Kwei, Y. H. Hsu, Y. H. Tu, C. J. Tung, “Memory effect on the inelastic interaction of electrons moving parallel to a solid surface”, *Electron Scattering in Solids - From Fundamental Concepts to Practical Applications 2004 (ESS '04)*,

Debrecen, Hungary, July 4-8, 2004.

4. C. M. Kwei, Y. H. Tu, C. J. Tung, “Surface excitation parameters for semiconducting III-V compounds”, *21st International Conference on Atomic Collisions in Solids (ICACS 21)*, Genova, Italy, July 3-9, 2004.
5. C. M. Kwei, Y. H. Hsu, Y. H. Tu, C. J. Tung, “Memory effect on the inelastic interaction of electrons moving parallel to a solid surface”, *21st International Conference on Atomic Collisions in Solids (ICACS 21)*, Genova, Italy, July 3-9, 2004.

